Dosimetric verification of intensity modulated radiation therapy

Alison Chapman
University of Wollongong

DOSIMETRIC VERIFICATION OF INTENSITY MODULATED RADIATION THERAPY

A thesis submitted in fulfilment of the requirements for the award of the degree

Master of Science - Research

from

University of Wollongong

by

Alison Chapman, B Med Rad Phys (Honours)

Department of Engineering Physics

2005

Certification

I, Alison Chapman, declare that this thesis, submitted in fulfilment of the requirements for the award of Master of Science - Research, in the Department of Engineering Physics, University of Wollongong, is wholly my own work unless otherwise referenced or acknowledged. The document has not been submitted for qualifications at any other academic institution.

Alison Chapman
22/05/06

Acknowledgement

I would like to thank many people who have helped with this project, including my supervisors Prof Peter Metcalfe and Prof Anatoly Rosenfeld, the staff at the Illawarra Cancer Care Centre, the physics staff at St George Cancer Care Centre, my parents Ken and Judy Chapman, and Mark Bradley for their constant support and commitment.

Abstract

Intensity modulated radiation therapy (IMRT) is a relatively new treatment planning and delivery technique. The complex multiple-segment nature of an IMRT plan makes it difficult to verify using traditional look-up tables and hand calculations.

The purpose of this project was to develop an effective and time-efficient plan checking procedure using a combination of ionisation chambers and film. The dosimeters available were 0.03 cc volume and 0.6 cc volume thimble ionisation chambers, Kodak X-Omat V (XV) film and Kodak Extended Dose Range (EDR2) film. First the dosimeters were tested for accuracy in terms of their dose response in the clinical range required (up to about 200 cGy). All were found to be suitable for further investigation for use in IMRT plan checking.

One non-IMRT and six IMRT plans were validated. The plans were transferred from the patient geometry to a 30 cm x 30 cm x 30 cm cubic phantom made up of slabs of solid water. The ionisation chambers and films were calibrated and used to measure the dose delivered to the phantom at the isocentre for each beam and for an entire IMRT treatment. The film was also used to provide axial and planar dose distribution maps for comparison with the predicted distributions. Time restraints meant that not every type of dosimeter was used for every beam and treatment plan.

It was found that the isocentric 0.6 cc volume ionisation chamber provided a suitably accurate dose check, with an average difference between predicted and measured full treatment doses of 2.0 cGy with a standard deviation of 2.7 cGy and 1.5% with a standard deviation of 2.1%. The film was less successful, with the EDR2 film (digitised and analysed using ImageJ software) giving an average difference between predicted and measured full treatment doses of 5.4 cGy with a standard deviation of 4.0 cGy and 4.0%

with a standard deviation of 3.1%. The film was very useful for obtaining qualitative dose distribution maps, which could be used as surrogates to verify that the radiotherapy treatment planning system's co-ordinate information was being transferred correctly.

Following the results of the test cases a procedure was established for all future IMRT plans. The procedure can easily be varied to include further measurements if necessary, and consists of measuring the dose at isocentre from each beam and the whole treatment using the 0.6 cc ionisation chamber. EDR2 film is to be used to visually verify the axial dose distribution, and XV film to verify planar dose distributions for each beam.

Contents

List of Figures

List of Tables

Abbreviations

%dd - percentage depth dose

3DRTP - three dimensional radiation treatment planning

3DCRTP - three dimensional conformal radiation treatment planning

AAPM - American Association of Physicists in Medicine

AHTAC - Australian Health Technology Advisory Committee

AP - anteroposterior

BEV - beam's eye view

CT - computed tomography

dMLC - dynamic multileaf collimator

DVH - dose volume histogram

EDR2 - Kodak Extended Dose Range [film]

FF - field factor

Gy - gray

IAEA - International Atomic Energy Agency

ICCC - Illawarra Cancer Care Centre

ICRU - International Commission on Radiation Units and Measurements

IMRT - intensity modulated radiation therapy

MLC - multileaf collimator

MU - monitor unit

OD - optical density

PA – posteroanterior

QA - quality assurance

relOD - relative optical density

ROI - region of interest

SAD - source-to-axis distance

SSD - source-to-surface distance

STF - step test film

TLD - thermoluminescent dosimeter

WHO - World Health Organisation

XV - Kodak X-Omat V [film]

Z - atomic number

Chapter 1: Introduction

1.1 Project Aims

Treating cancer patients with intensity modulated radiation therapy (IMRT) at the Illawarra Cancer Care Centre (ICCC) required independent validation of the radiotherapy treatment plans generated for these treatments. The multiple segment nature of IMRT treatment fields made it difficult to use look-up tables and a simple calculation check.

The purpose of this project was to investigate possible plan checking methods using physical dosimetry techniques. The new plans were checked with ionisation chambers and radiographic film dosimeters. Each technique used was examined in terms of practicality, reliability, speed and accuracy.

One forward-planned three-segment antero-posterior (AP) field and two-segment postero-anterior (PA) field plan was used to trial the dosimetry methods. Then six IMRT plans were validated with the said dosimetry. All aspects of the dosimetry and checking of the IMRT plans were examined and recorded in an attempt to create a viable process for independent validation of IMRT patient plans.

1.2 Cancer and Radiotherapy

1.2.1 Cancer

The word cancer is used to describe a type of disease that consists of damaged, malignant cells in the body. These damaged cells can reproduce faster than normal cells, and have no cohesion abilities so they can spread quickly and in an uncoordinated fashion throughout the body. There are many different types of cancer, which can vary greatly in severity and structure and occur in different parts of the body[76]. Some abnormal cells do not spread beyond the connective tissue capsule of the primary tumour itself (known as benign tumours), so the tumour simply distorts the surrounding tissue without altering the basic tissue organisation (Figure 1.1). Malignant, or cancerous, types of abnormal cells can eventually break away from the primary tumour and begin to invade surrounding tissue. If they reach nearby blood vessels they can travel throughout the body and eventually leave the circulatory system again to create secondary tumours, or metastases.

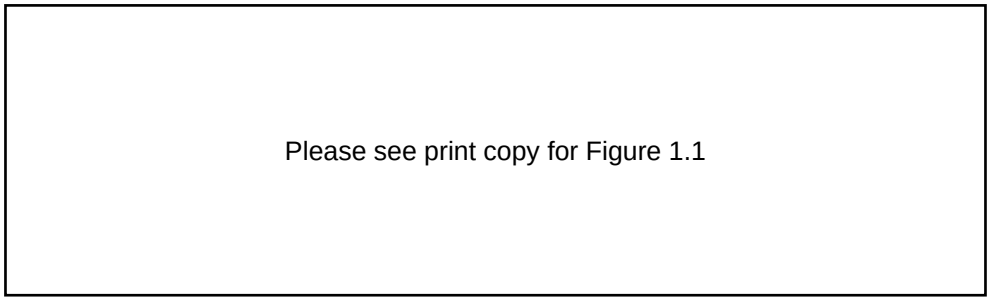

Figure 1.1. Normal cell structure compared to cancer formation, which is forcing normal cells out of the way[16].

The ways by which cancer can cause death are: because the tumour or tumours have compressed vital organs to a point where they can no longer function; because cancer cells have replaced functional normal cells in vital organs[76]; or because the cancer cells have competed so strongly for space and nutrients that they have crowded out normal cells[104]. When malignant cells, which cannot become specialised like normal cells, take over the normal cells they are unable to carry on the functions of the original cells, so there reaches a point where the vital organ is unable to continue its own function. Although

some types of cancers have known common causes or risk factors, most are initiated by a unique set of causes[5].

The treatment and prevention of cancer has become a major issue in society, and as a result treatment techniques continue to improve rapidly. Radiotherapy uses ionising radiation to destroy the cancer cells by damaging or completely breaking DNA strands, hence stopping the cancer cell from reproducing. The two chief forms of radiotherapy are external irradiation, and intracavity and interstitial irradiation, or brachytherapy[5].

Radiotherapy is most often used as a treatment by itself, or in combination with surgical removal of the cancer or with chemotherapy; it provides advantages in organ preservation, quality of life, palliation of symptoms, and survival rates. Many curable cancers that consist of solid tumours are still treated surgically, however unlike in the past the tendency is not to attempt to remove the entire tumour and surrounding tissue, but to remove a large portion in less radical surgery (for example, by performing a lumpectomy as opposed to removing the entire breast in a mastectomy) and use radiotherapy or chemotherapy to treat or 'clean up' surrounding areas. If the probability of cure from either surgery or radiotherapy is equal, the choice of treatment depends on the preference and knowledge of the prescribing doctor, the availability of either treatment, and the relative risk of morbidity or adverse effects[5].

The exact form of radiation treatment – even the precise dose of radiation to be delivered to a particular tumour – is not a set prescription because every cancer has its own pattern of local behaviour, metastasis, and response to prevention and treatment[5].

In the year 2000 cancer was the leading cause of death in Australia, at 30% of male deaths and 25% of female deaths[6]. Although the overall cancer death

rate has begun to fall from previous years, the incidence of cancer is increasing, with 88 000 new cases diagnosed each year, and the death rate from many of the most common cancers is increasing[5]. The most common cancers diagnosed in Australia in 2000 were bowel cancer, breast, prostate, melanoma, and lung cancer, which together accounted for 60% of registered cancers[6].

1.2.2 Radiotherapy

The main processes involved in the radiotherapy treatment of cancer are[80]: locating and defining the treatable tumour; defining the position of the patient, tumour, and important structures in relation to each other and to the treatment machine; deciding on a treatment plan; predicting the resultant dose distribution; and creating detailed instructions for the treatment.

X-rays are the most commonly used beams in radiotherapy. The important factor is the amount of energy that the radiation deposits. This is known as the absorbed dose, measured in Grays (Gy), which corresponds to joules absorbed per kilogram.

ICRU 50[48] formalised the following treatment volumes. The sites to be treated are defined by the treatment volume (TV), which is the area that needs to be treated in order to cover the known tumours and to account for surrounding microscopic malignancies (known as the clinical target volume or CTV) and to allow for movement and variations such as breathing. Because the collimation of the treatment beam is not perfect, but consists of a penumbra, an extra margin must be added to ensure that full dose is delivered to the treatment volume, without compromising the protection of critical structures and surrounding tissue[125]. ICRU 62[49] introduced the concept of the internal margin and the set-up margin. The CTV, internal margin, and set-up margin define the planning target volume (PTV). The irradiated volume (IV) is the volume that actually receives treatment.

The goal of radiotherapy is to treat the CTV to destroy the cancer, while minimising the size and dose to the surrounding areas of the IV. Obviously a radiotherapy beam shaped more exactly to the shape of the CTV would help to accomplish both of these objectives. The relationship between the clinical volumes is shown in Figure 1.2.

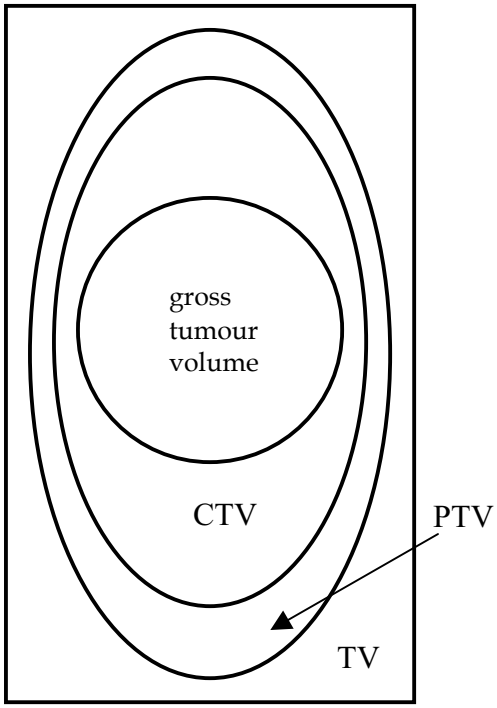

Figure 1.2. The defined treatment volume. The IV would surround the TV.

Where the energy from the x-rays is deposited, the aim is to maximise the effect on cancer cells but to minimise the effect on normal cells, especially in more radiosensitive tissues such as the heart. For example, too small a dose might not destroy the cancer cells effectively, whereas too large a dose would be more effective on the cancer cells, but might also kill too many healthy cells. IMRT presents the option to give a higher dose to the tumour and less to normal tissue.

To evaluate the dose delivered to the tumour it is important to predict and check the planned amount and distribution of absorbed dose. As well as the resultant dose being calculated or modelled on a planning computer, physical and mathematical verification can be carried out on both the plan and *in vivo*.

1.3 Radiation Interactions – Clinical IMRT Sites

IMRT is currently being used to treat tumours of the prostate, breast, head and neck, central nervous system, lung and liver. Successful results have been reported, with a decrease in complications from conventional treatment, as well as a good response in the treatment of metastases[9]. The main success has been with tumours of the head and neck, which tend to have stable (or easy to stabilise) target locations, highly sensitive surrounding structures, and a relatively high response to increases in radiation dose[50].

Two sites that are often of concern in the treatment of head and neck cancers are the lacrimal and parotid glands. IMRT offers the ability to minimise the doses that are delivered to these sensitive structures.

1.3.1 Lacrimal Gland

The eye (Figure 1.3) is an important structure that is made up of many sensitive components, all of which may be affected by radiation in different ways. Some susceptible parts include, for example[85]:

- The eyelashes, which serve as touch sensors, protect the eye from tiny particles by causing the eye to blink when contact is made. Radiation destroys the lashes, sometimes permanently.
- The eyelid is covered by the thinnest skin on the body and a very delicate mucosa both of which, when irradiated, are affected to the point where flexibility and therefore effectiveness and comfort of the lid is decreased.
- The nasolacrimal duct and sac provide a drainage system for tears, and may become blocked following irradiation.
- The cornea does not contain blood vessels, so radiation does not produce vascular damage but disrupts the epithelial and connective tissue layers of the cornea. With irradiation the corneal surface thins and can develop tiny ulcers (keratitis); these usually clear up after treatment, but sometimes lead to corneal ulcers.

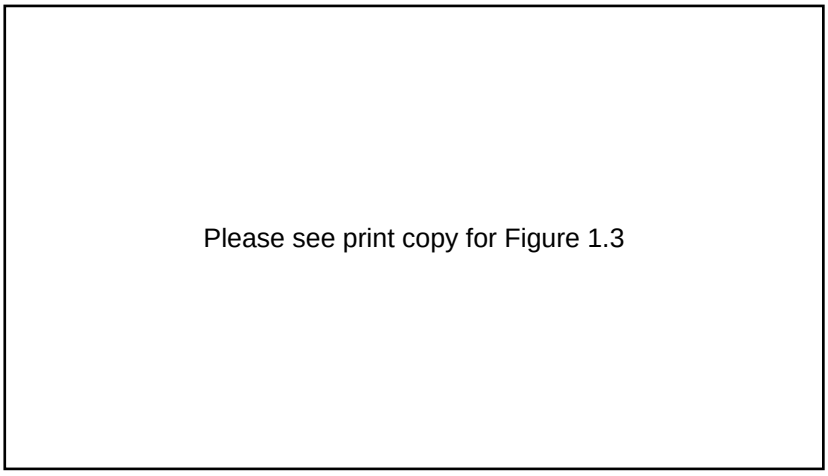

Figure 1.3. Diagram of the eye showing the position of the lacrimal gland[96].

The almond-shaped lacrimal gland, otherwise known as the tear gland, lies in the upper lateral corner under the eyelid. It provides the main ingredients

and most of the volume - about 1 mL per day - of the tears that bathe the surface of the eye. The secretion also contains lysozyme, an enzyme that attacks micro-organisms[76].

Radiation can suppress the productions of the lacrimal gland, leading to 'dry eye'[85]. This condition can be very painful, and can result in fast deterioration of the cornea by constant irritation. Treatment may involve constant use of eye drops, called 'artificial tears', or even surgery[76].

According to Moss[85], if a fractionated dose of 32 to 45 Gy is delivered to the lacrimal glands and eye, then slow changes tend to occur over 4 to 8 years, and approximately a quarter of patients lose that eye. Fractionated doses of 54 Gy have been found to result in severe dry eye in all patients.

The lacrimal gland was spared in the first two patients treated at ICCC. For the second IMRT treatment at ICCC a conventional plan was prepared with a planned dose of 63 Gy to the lacrimal gland, which is a very damaging dose. When the treatment was replanned for IMRT the planned dose to the lacrimal gland was 12 Gy[79].

1.3.2 Parotid

The parotid salivary glands (Figure 1.4) produce approximately 25% of the saliva found in the mouth. The secretion from the parotid salivary glands consists of a large amount of salivary amylas, a digestive enzyme that begins the chemical breakdown of food. Saliva is necessary when eating to lubricate the mouth and to dissolve chemicals that stimulate the tastebuds. When not eating the saliva flushes oral surfaces and helps to control oral bacteria[76].

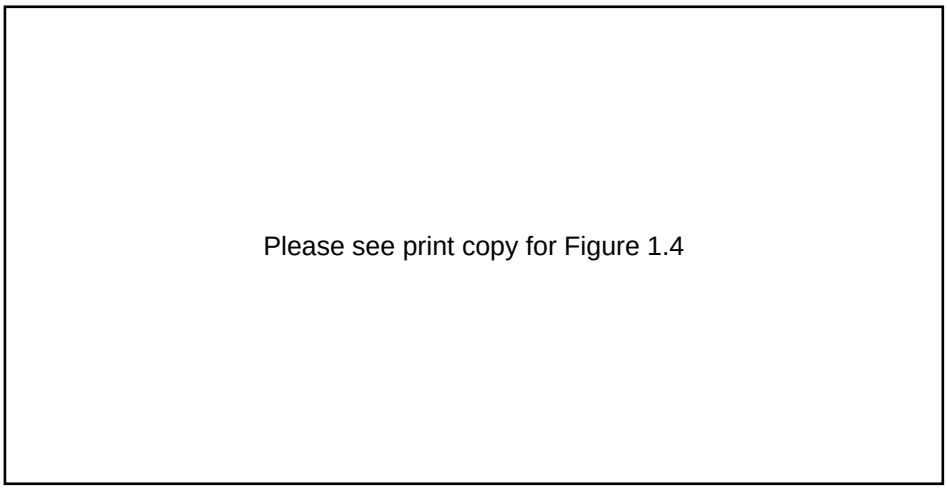

Figure 1.4. Diagram showing the position of the parotid glands[96].

If the amount of saliva is reduced, which happens when the parotid salivary glans are affected by radiation therapy, a condition known as xerostomia occurs. Then not only can the dryness of the mouth become very uncomfortable but the subsequent increase in bacterial populations can quickly lead to recurring infections and the erosion of teeth and gums.

The University of Michigan has studied the use of 3DCRT and IMRT in parotid-sparing radiation treatment, and found that IMRT plans, in comparison to conventional treatment plans, showed better target conformity, and reduced the dose to the parotid by about two-thirds. As a result salivary flow was conserved in the majority of IMRT cases[50]. However, it has been found that care must be taken when using IMRT to reduce the dose to the

parotid as a consequence may be to increase the dose to the oral cavity and the submandibular glands[121].

The University of California, San Francisco (UCSF) has also treated a large number of patients for nasopharyngeal carcinoma since 1995, and reported success in comparison with conventional treatments[112].

IMRT treatment represents a high cost due to increased planning, treatment time and equipment requirements, which is currently not reimbursed in Australia. Head and neck cancers are well suited to IMRT because of better target fixation, and it is this clinical site that has aroused most interest in Australia. Several other centres have reported good results with successful sparing of the parotid, such as the Peter MacCallum Cancer Centre, Melbourne, which has treated at least 14 head and neck patients since November 2000[95]. Three IMRT treatments at ICCC have involved sparing the parotid glands, and typically doses below 20 Gy to the glands of these patients have been achieved.

1.4 Dosimetry Validation

1.4.1 Quality Assurance

The World Health Organisation (WHO) in 1988 stated that it was necessary for all radiotherapy centres to implement quality assurance (QA), defining it as "all those procedures that ensure consistency of the medical prescription and the safe fulfilment of that prescription as regards dose to the target volume, together with minimal dose to normal tissue, minimal exposure of personnel, and adequate patient monitoring aimed at determining the end results of treatment"[5]. Quality assurance should combine routine machine QA with patient-specific QA (such as the taking of port films) to provide sufficient confidence that treatment dose distributions are delivered as planned[64].

In 1996 Australia had no formal policy on QA[5], although the ACPSEM (Australasian College of Physical Scientists and Engineers in Medicine) Position Paper[82] outlines recommended QA procedures, and this paper is currently being updated by a college committee. Most centres routinely carry out such procedures including physical evaluations of beam outputs, recording and verifying treatment procedures, taking port films during treatments, and informal chart reviews throughout the treatment period.

QA includes the checking of all patient treatment plans to ensure they have been calculated, transferred and generally planned correctly. There is evidence that differences as small as 5 to 10% in the absorbed dose that is delivered to a target might result in significant differences in the local control of tumours for some types of treatment, which indicates the necessity for accurate dose delivery[86]. Additional errors in the treatment delivered may result from patient movement during treatment (external and internal, such as breathing), and incorrectly setting the controls of the treatment machine.

Linear accelerators require regular QA checks to ensure everything is working correctly and the machine dose output is accurate. Beam characteristics are also measured, as linear accelerators do not produce exactly the same beam characteristics as each other. Some of the most important measurements and checks include[36]:

- Flatness and symmetry of the beam.
- Central axis percentage depth doses and tissue maximum ratios.
- Penumbra.
- Field-size dependent output factors.
- Wedge transmission factors.
- Block tray transmission factors.
- Transmission through tertiary block materials such as fixed blocks or multileaf collimators (MLCs).

QA of MLC systems should include the standard tests applicable to conventional secondary collimator systems, such as light and x-ray field coincidence, interlocks, and collimator rotation. It should also involve tests on[84]:

- Leaf position compared to the position readout.
- Width of the penumbra as a function of the leaf position.
- Leakage between leaves and through back-up collimators.
- Systems for shaping MLC leaves and transferring of leaf files.
- Dose distribution at the stepped edge.
- For MLCs that are to be used for dynamic deliveries, leaf speed control.

Regular QA checking of the output of each energy on a linear accelerator is usually limited to one field size – conventionally 10 cm × 10 cm – and involves one set of standard measurements – around 100 MU. Step-and-shoot IMRT can involve very short beam-on times (less than 10 MU), small segment field sizes (less than 3 cm, which is the minimum field size usually prescribed in conventional treatment), and segments that are completely offset from the

axis of the collimator[103]. As traditional QA practices do not usually test such conditions they may not be sufficiently verified as accurate for use in IMRT. For example standard QA procedures do not usually take into account the delivery of small quantities of MUs, but when planning IMRT the output of the linear accelerator for small deliveries of MUs should be considered[39]. In addition, regular dosimeters may not be suited to such conditions – an ionisation chamber that is well suited to a field size of 10 cm × 10 cm might be too large to provide sufficient spatial resolution in a smaller field size. Commissioning tests of the linear accelerator that should be carried out specific to IMRT conditions include dose rate stability, stability of beam flatness and symmetry, and relative output factors[103].

Mageras *et al.*[75] provides a list of safety objectives for when conformal treatment is being planned and carried out. These include ensuring that: settings during verification and treatment are to the exact specifications of the plan, including verification of patient and data; the set-up is properly verified before treatment; and potential hazards such as equipment collisions are prevented, minimised, and checked for.

Because IMRT dose verification techniques are still developing there is debate about whether plan checking should include pre-checking the MLC system itself, versus patient-by-patient plan checks[100]. Pre-checking involves rigorous dosimetric and QA procedures on the entire system, largely eliminating individual patient plan checks. Clearly this becomes more of an issue as the number of patients being treated with IMRT increases.

Chapter 2: Literature Review

2.1 IMRT Delivery Methods

Intensity modulated radiation therapy (IMRT) is a relatively new treatment planning and delivery technique that can greatly improve the process of conformal radiotherapy[88]. Conformal radiotherapy refers to the process of blocking a beam with irregularly shaped beam portals so that the dose delivered corresponds more closely to the tumour whilst reducing the dose to healthy tissue[99]. In practice IMRT plans nearly always involve more field angles than competing conformal non-IMRT plans. More beams with optimised weights allows for the dose distribution to conform better to the target, although a drawback is that an increased volume of normal tissue is irradiated at low dose[141].

Three-dimensional conformal radiation treatment planning (3DCRTP) involves a number of beams of uniform intensity (or simply modified with a wedge or compensator), which are shaped to fit the target from multiple set beam directions. In addition IMRT provides varying intensity across the field in order to account for the tumour shape in the third dimension. This allows for a higher dose to be delivered to the tumour whilst sparing of critical sensitive structures is maintained.

According to Purdy[99], as of 1st April 1996 just 124 patients at seven institutions around the world had been treated using the technology. Now nine years later about 300 clinical sites in the USA have treated patients using IMRT[59], and several (at least six) centres in Australia. At the Memorial Sloan Kettering Cancer Centre, New York, USA – one of the first centres to implement IMRT – the treatment of several thousand patients has been reported, with about 200 treatments carried out a day[63].

Although IMRT is actually just one of the various techniques that allow complex dose planning and delivery, it utilises dose objective planning and

calculation to more effectively conform dose to three-dimensional volumes. This method is often referred to as 'inverse planning'.

Delivery of MLC IMRT treatments may be dynamic, where irradiation continues while the necessary components of the treatment machine are in motion, the most common being 'dynamic sliding window' delivery, where each MLC leaf pair moves independently but in the same direction across the target volume, effectively sweeping variable leaf widths across the field and leaf separation determines the dose. Or MLC IMRT treatments may be static, in which a number of fixed segmented fields in each beam are set up and treated automatically, with the treatment beam pausing while segments are repositioned[75]. This is commonly known as step-and-shoot treatment, and is the style of delivery used in this project. Static step-and-shoot delivery is more like multiple discreet fields, but is more easily verifiable than dynamic delivery and requires less quality assurance because the speed of the MLC leaves does not need to be verified[24]. According to a study by Chui *et al.*[24] a dynamic sliding window dose delivery requires approximately 20% more beam-on time in monitor units (MUs) than most static step-and-shoot MLC deliveries, however static delivery requires a little more actual treatment time per MU because there is beam hold-off as the leaves move from segment to segment.

Conventional treatment plans deliver higher doses to the main tumour, and lower doses to smaller subclinical regions usually following the main treatment (called a boost treatment)[50]. In head and neck cancers especially a treatment program often consists of several successively shrinking treatment volumes. Treatments tend to show an improved response if treatment courses are shortened, sometimes to even two treatments a day. With IMRT it has been shown that if a treatment is delivered as a concurrent or concomitant boost – large enough to cover the main tumour and the boost region – the dose delivery to both regions may be more efficient, as fractionation to the

tumour boost region is sped up[136], and the dose distribution is likely to be more conformal because the multiple dose regions, being delivered together, do not accidentally overlap[50].

To create fields wider than the limitations set by the Varian MLC leaf extension and over travel, beams can be split into asymmetrical overlapping fields with variable intensity in the overlapping region. This is probably more effective and less prone to error than trying to align two (or more) non-overlapping abutted field edges[136].

One potential problem that occurs with IMRT is that the IMRT field may consist of many segments. Multiple segment treatments lead to a relatively higher ratio of MUs to dose than single segment treatments. As a result of this the total leakage of dose through the leaves (i.e. transmission) increases in proportion to the MUs delivered, although this can be minimised by using the secondary collimator jaws as back-up shields.

IMRT treatments are more susceptible to certain errors than conventional treatments. According to Papatheodorou *et al.*[89] (in 1999) the implementation of IMRT has been held back because of problems relating to practical delivery and verification tools, and quality assurance procedures. For example, according to LoSasso *et al.*[64] a 1 mm error in the calibration of the jaws and leaves is normally considered tolerable for non-IMRT dose delivery. However, the leaf error tolerance is reduced to a much more precise 0.2 mm for a dynamic IMRT dose delivery.

Inaccuracies or uncertainties in the treatment set-up or fluence profiles that may be relatively insignificant in conventional treatment planning can produce large inhomogeneities in the overall dose distribution, resulting in significant hot or cold spots[26]. Convery *et al.*[26] found that inaccuracies in gantry angle have little impact on the dose delivered.

The intensity modulated beam profiles may include very sharp dose gradients compared to standard plan beam profiles, both within and at the boundaries of the target area, which means that accurate knowledge of patient position is very important, and also that patient movement during dose delivery can have much more effect on the precision of the treatment than it would have for normal unmodulated static fields[61]. Although there are no published standards for the dosimetry of IMRT, for standard radiation therapy the ICRU 42[46] recommends a dose accuracy of ±2% or ±2 mm in very steep dose gradients where there is a change of greater than 1% of average intensity per mm.

Gamma analysis is a mathematical method that searches for regions that do not meet one of the above constraints. Because most dose measurements in this report were positioned in low dose gradient regions, at least for combined fields, percentage differences are quoted in the results sections. Positional tolerances (mm) in high dose gradient regions were not examined.

IMRT beams often involve many fields that are smaller than those used in conventional treatments (where a 3 cm x 3 cm field is generally accepted as the smallest that can be reliably verified). For Varian linear accelerators an increase in backscatter to the monitor ionisation chambers from smaller fields can cause the chambers to accumulate dose sooner, which results in a decrease in dose. Approximately a 2 to 3% increase in backscatter has been found for a field size of 0.5 cm x 0.5 cm compared to a field size of 40 cm x 40 cm[121]. As the MLCs are pre-mounted they are lower in the treatment head, further away from the monitor chambers. This is the main contributor to the difference between output factors for MLC and jaw-defined fields. At very small fields approaching 1 cm x 1 cm the spatial resolution of the detector also becomes an issue.

2.1.1 Matchlines

When radiation fields are abutting, precise and accurate placement of the radiation fields is required[144]. If the two fields are not matched exactly, the region where they meet could receive too little or too much dose (known as a cold or hot spot respectively). This dose zone is known as a matchline. It becomes especially important in IMRT because of the number of MLC segments present in one beam.

The Varian MLC has a rounded leaf end. Partial transmission through the leaf end causes a slight penumbra that contributes to the matchline effect. To avoid this the leaves can be deliberately offset a certain distance[115].

2.1.2 Tongue and Groove Effect

Each MLC has a tongue and groove designed to minimise interleaf leakage. When either the leaf or its adjoining pair is left out for a significant amount of time in a segment arrangement this can lead to an under-dose shadow in the exposed part of IMRT segments. This is because the tongues of the leaf pair cause a dose shadow. The effect is shown in Figure 2.1; a three-segment sequence is shown, where the cold dose region equates to a 20% dose shadow.

Deng *et al.*[28] found that the tongue-and-groove effect for a single IMRT field produced an effect of up to 10% of the maximum dose. However, for an IMRT treatment using more than five gantry angles the effect averaged out to just 1.6%.

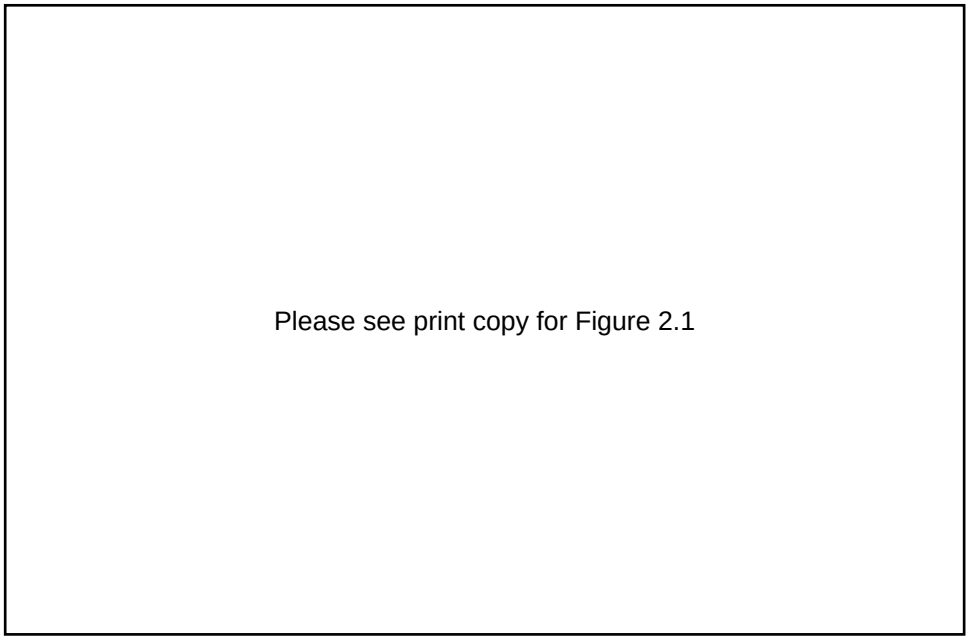

Figure 2.1. The tongue and groove underdose effect from a three-segment IMRT sequence. The line indicates the regions of underdosage (courtesy of Peter Hoban and Peter Metcalfe, private communication, 2004).

2.2 Planning

2.2.1 Radiotherapy Planning Computer

Computers have been used in planning radiation therapy for around 40 years[99]. Today nearly all radiotherapy treatments are planned on a radiotherapy treatment-planning computer. Computers allow for better optimisation of the dose, and provide detailed instructions for the setting up and treatment of the patient, including maps of the planned dose distribution. The planner enters and manipulates patient information such as CT scan data, and inputs instructions such as the dose required to the target volume. In order to use information from various sources, which likely have different data parameters such as pixel size and different conventions for labelling and sequencing data, the treatment planning system must be able to accept and assimilate a range of data types, as well as account for variations in patient orientation and position[129].

The central basis of an IMRT calculation, the 'inverse method', is that a computer is used to calculate physically deliverable modulated beam fluence profiles that will give the best possible dose distribution to the defined target volume and critical structures. Previously, radiation treatment planning computers did not actually design the planned treatment distribution as such, but were more commonly used to recalculate treatments using beam weights and wedge modulators based on the experience of the planners. IMRT planning allows for a much greater degree of freedom in designing the treatment, which in turn means a lot more information must be processed[108]. Because the process of creating complex intensity maps followed by an associated leaf sequence is generally too complex for humans, computers have been developed to calculate appropriate beam modulation from a series of dose objectives. Today, technology has advanced enough for computers to handle the large amounts of data necessary and to solve such complex inverse planning problems as are necessary for IMRT plans to be processed.

Computer-generated plans are usually represented graphically as a series of relatively simple two-dimensional isodose distributions overlayed on CT slices (Figure 2.2), often with colourwash overlays to make high and low doses more easily distinguishable. Using a computer it is possible to view the beam positions and dose distribution three-dimensionally from any angle. A quantitative measure known as the dose-volume histogram (DVH) can show the cumulative fraction of dose received by each specified volume[129] (Figure 2.3). This has developed as probably the most useful three-dimensional analysis tool for comparing and reviewing plans.

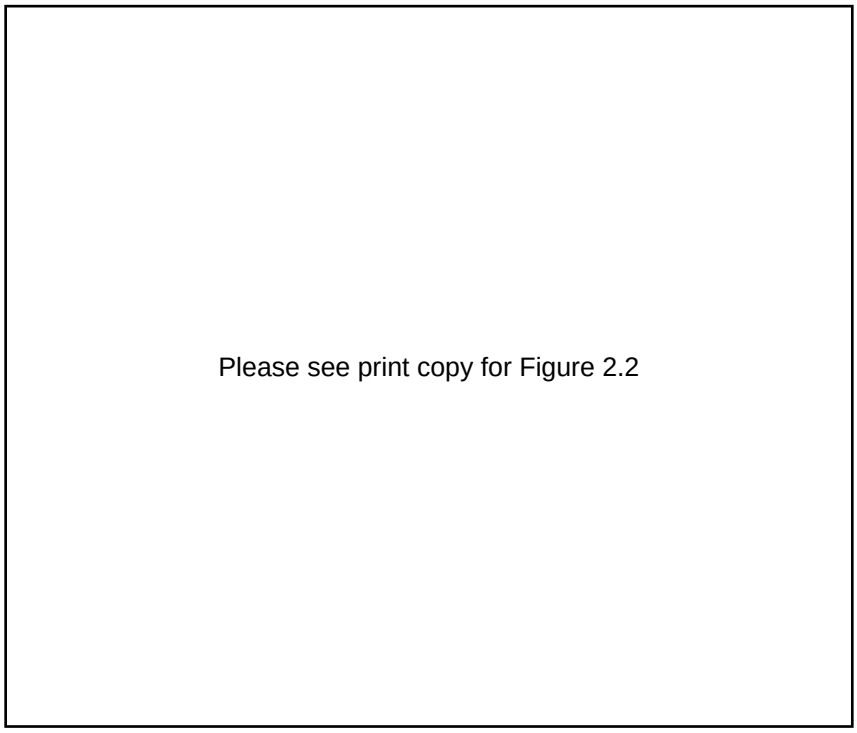

Figure 2.2. Example of isodose curves in a depth dose distribution[78].

The dose delivered to a patient must agree with the prescription to assure the outcome of the treatment[59], so the dose output per MU from the machine must be accurately calculated by the planning system. Beam data, which provides the unique characteristics of each beam from each linear accelerator, is acquired, or commissioned, correctly, and the dose calculation algorithm used by the planning computer needs to be accurate. This is best achieved by

having a model that closely mimics the physics of the interaction and dose deposition processes.

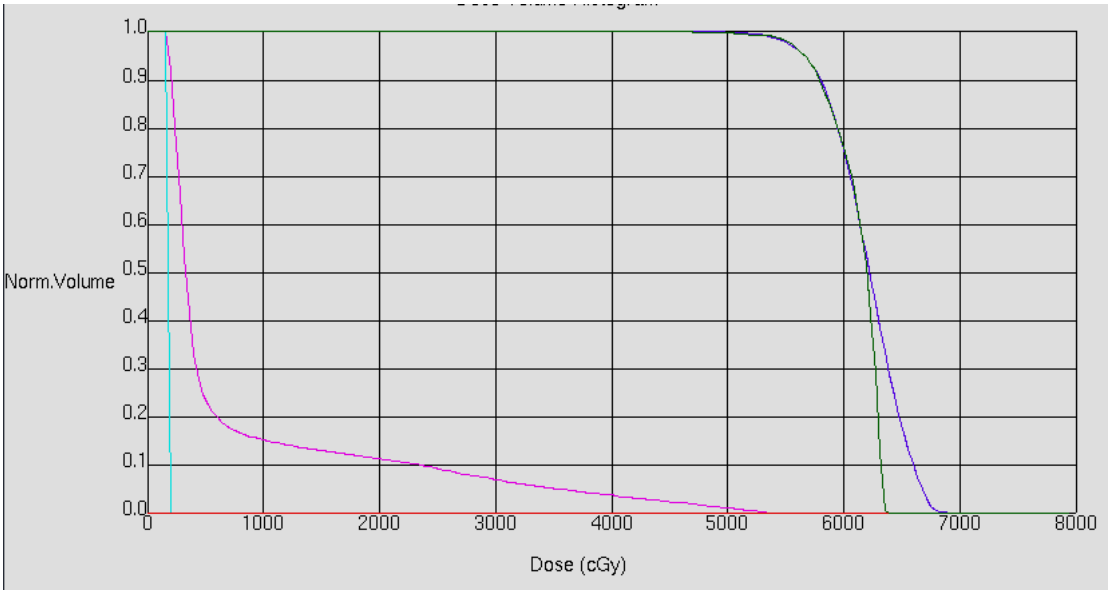

Figure 2.3. An example of the DVH that was created to evaluate Case 2 plan. The y-axis indicates the percentage of each volume that receives the dose indicated on the x-axis. The blue and green lines represent dose to target volumes, to which the majority of dose is desired to most of the volume, and the aqua and pink lines represent critical structures, where minimal dose is desired to most of the volume.

2.2.2 Conventional Planning

Traditionally, dose-planning calculations whether manual or computed have involved simple corrections based on measured dose distributions, such as jaw-dependent output factors and depth dose factors. According to Mackie *et al*.[74] the three basic steps in correction-based algorithms are:

- Using generating functions to characterise the dose in a homogeneous medium (such as collected in a water phantom);
- Reconstructing the generating functions to account for the treatment field (this involves summing up small contributions from discrete beam elements). Included in this step are corrections for all beam modifiers and shapers.
- Correcting for patient anatomy, including contours and heterogeneities (such as lung, air cavities and bone).

More advanced dose calculation engines are usually based on radiation transport models to predict the dose from first principles[74]. Model-based algorithms include convolution methods and Monte Carlo methods. Mackie[73] has grouped all the methods into two main types; corrections-based and model-based.

2.2.3 Convolution Calculations

The Monte Carlo method is especially popular with researchers when accurate benchmarks in inhomogeneous media need to be established. However, for everyday radiotherapy planning it is currently considered to be too slow as it involves tracking many millions of individual photon histories to achieve high statistical accuracy. Instead, the current standard technique is a convolution calculation. For the planning involved in this project the method used was collapsed cone convolution (first described by Ahnesjo[3]).

In general, convolution methods involve the superposition integral of a primary interaction array (fluence or TERMA) with a dose spread array kernel. Kernel values are obtained by recording the energy deposited in the voxels that make up the kernel, from the total energy delivered by the primary photons to an interaction voxel. A fractional energy component in each voxel is calculated by dividing the energy in each voxel by the total energy. Monte Carlo methods have been used to generate first scatter and multiple scatter kernels, or an analytical function can be used to model the dose-spread kernel. Convolution methods approximate the effects of electron ranging, allowing a faster calculation of the dose at every point in the target volume than Monte Carlo methods.

2.2.4 Inverse Planning

The inverse technique is often used for calculating intensity-modulated distributions. It is so named because the method used to solve the optimisation problem inverts the known desired dose distribution to obtain the unknown intensity modulation[124]. When Monte Carlo generation is used to predict conventional dose distributions, the error involved arises from the statistical nature of the Monte Carlo process. If Monte Carlo is used to generate dose distributions for inverse treatment planning, an additional error arises called 'noise convergence error'. This is a result of the optimisation converging to the optimal solution for noisy dose calculations, which is different to the optimal solution for noise-free dose calculations. This error should be present in any inverse treatment plan that uses either inaccurate or imprecise dose calculation, such as pencil beam or Monte Carlo methods, respectively[51].

IMRT planning involves computer optimisation of treatment plans. Biological optimisation can be used, but dose optimisation is an alternative when minimal radiobiological data for the tumour and normal tissue is available[60]. Biological optimisation methods are preferable because the precise reactions of the individual tumour and the surrounding normal tissues can be predicted. However this can be very difficult as obtaining individual radiobiological response information is not feasible for each unique patient and tumour. Dose-based optimisation methods are more common because they are more straightforward and the majority of radiotherapy planning experience is based on dose prescription. In the same way IMRT uses dose as a substitute for biological effect[52]. First, optimal dose criteria are specified. Next a complex optimisation, or search, algorithm is used to find the best plan based on a score ranking for each possible plan[99].

Specifying the optimal criteria for a treatment plan involves giving a value and weighting to each factor. For example, the minimum and maximum

doses to be delivered to the tumour might be stipulated and given an importance weighting. Similarly, the maximum doses allowed to critical structures can be given weightings. The treatment planner can identify the various structures on a patient data image by programming in optimal isodose contours[84]. The weighting denotes the importance of each given criteria; allowing the computer to find the closest match to the plan, rather than trying to perfectly satisfy all conditions.

Once the criteria have been specified as objective functions the computer uses an optimisation algorithm to carry out an iterative search to find the best beam fluence pattern. The proposed treatment plan is assigned a score based on its suitability to the objective functions, which can be used to compare subsequent plans. To calculate a plan the CT image of a patient is divided into voxels, which are small volume elements of density information for dose calculation. The beams for an initial plan are also divided into smaller rays, known as beamlets or pencil beams. The contribution of each pencil beam to the target and to normal tissue is calculated, and the projected dose to each voxel is determined. In order to improve the plan the weighting of each pencil beam is adjusted and the overall result re-evaluated. When the proposed plan is deemed acceptable the pencil beams are converted into instructions for the linear accelerator[50].

It is possible for the computer software system to deliver clinically impractical solutions, for example the computer may come up with a plan that requires negative beam weights to be delivered. Obviously, although this may be mathematically feasible, it is not realistically possible to deliver negative doses. Many software systems are programmed to automatically discard such unfeasible plans.

2.2.5 Plan Verification

When the planner has finished simulating and planning a standard treatment plan it is passed on to a physicist and/or a therapist to be checked with an independent manual or computer calculation of monitor units based on specific beam data. In addition to the calculation checks for the regular plans, a highly blocked or irregular field may require an output factor. This simply involves measuring with an ionisation chamber the actual output through shaping devices in comparison with a standard known field.

Checking IMRT plans is more complex than for regular plans. Manual calculations are generally not feasible as each field usually consists of more than ten or so segments, and many segment shapes are too small and/or irregular – including being positioned completely off centre – for reasonable dose estimates to be calculated manually. Therefore, other forms of plan checking such as traditional physical dosimetry in a surrogate phantom are considered as an option.

Zhu *et al.*[145] suggests three types of measurements for IMRT dose verification in phantoms. These are:

- Absolute point dose measurements using detectors such as ionisation chambers or thermoluminescent dosimeters (TLDs).
- Relative two-dimensional dose distribution measurements using detectors such as film or electronic portal imaging.
- Three-dimensional measurements using polymer gels.

The choice of dosimeter depends to some degree on the equipment available and the expertise within the radiotherapy centre concerned – some may have a quality film dosimetry set-up, but a poor TLD system, whereas others may have more reliable TLDs and prefer to use them more often than film. For example Pasma *et al.*[91] developed a dose verification method that uses an amorphous-silicon electronic portal imaging device (EPID), and Ploeger *et al.*[93] mentions the use of a charge-coupled device camera-based fluoroscopic

EPID, a liquid-filled ionisation chamber EPID for off-line verification, and a Gd_2O_2S scintillation screen. At the time of this research the expertise at the ICCC was with the use of ion chambers and film dosimetry. The centre is slowly moving to replacing some of the film planar dose map validation with amorphous-silicon EPID-collected images, which are then converted to dose maps[81].

An important consideration in IMRT is that as each beam consists of many segments, some of them deliver very low doses. It has been shown that the dose delivered is less than expected when a radiation field delivers less than three MUs[29]. Olch[87] found that some linear accelerator's dose output delivery is unstable when delivering less than two MUs.

Further to this, if the original MUs for an IMRT treatment were reduced, for example to fit a single fraction dose to the range of a dosimeter, the MUs for some segments may be reduced to less than one, in which case they might 'disappear' because some machines are incapable of delivering non-integer MUs. This highlights the need to find a dosimeter that can read accurately within the dose range of the IMRT treatment, rather than fitting the IMRT treatment to the dosimeter.

During any radiotherapy treatment, usually with the first fraction delivered, a port film is taken to verify the position of the delivered beam in relation to the patient. This provides an x-ray showing the dose distribution of each field in relation to the patient. With IMRT, this is impractical for each segment – and certainly not for dynamic IMRT[64]. Usually a portal image of the largest segment is adequate.

Chapter 3: Materials and Methods

3.1 Planning Computer

The planning computer used was a Philips (Adac) Pinnacle Radiation Therapy Planning (RTP) computer with software version 6.2b (Adac Laboratories, Milpetas, CA, USA). It runs the P^{3}IMRT inverse planning program, referred to as Pinnacle inverse planning software, and uses the collapsed cone convolution method for dose calculations.

To reduce the number of variables the computer must deal with, beam energy and gantry angles are still defined by the user. Objective goals are assigned with a weighted importance or as a percentage volume of the relevant structure. The computer then iteratively adjusts the parameters of each beam to reach an optimum solution incorporating each of the objective goals, assessing the results by using a cost function test that incorporates a least squares test between doses required and doses calculated.

The optimisation engine used is called the weighted gradient method, and belongs to a group defined by Webb[126] as deterministic, where variables are changed systematically, as opposed to stochastic methods where variables are changed randomly.

The beam parameters are adjusted by changing the intensity distribution, which is physically achieved by creating a series of MLC field segments and assigning an MU weighting to each. The series of field segments that make up a beam are called a leaf sequence. To convert the intensity distributions to a usable step-and-shoot leaf sequence Pinnacle uses a K-means clustering algorithm and extraction method to approximate the dose variation with a series of dose levels. To control this conversion process the acceptable percentage difference between the desired and the actual dose distribution can be specified. Currently a 2% match is specified, and this typically leads to the generation of 10 to 20 segments per field. The minimum segment MUs

and field size can also be specified. A minimum of 1 MU and an equivalent square of 1 cm^2 per segment was set.

3.2 Treatment Delivery

3.2.1 Linear Accelerators

Linear accelerators (Figure 3.1) are often used in radiotherapy departments, although they are not the only machines capable of delivering radiation. They usually have the advantage of being able to produce beams of several electron energies and two different megavoltage photon energies. The beams produced have high dose rates (up to 600 cGy per minute), small penumbras (an 80% to 20% penumbra of 6 mm for 6 MV beams), and minimal field edge divergence at 100 cm source-to-surface distance (SSD)[80].

Figure 3.1. A linear accelerator similar to that used for the IMRT deliveries, showing the treatment couch in the bottom left corner, the rotating gantry, and the stand behind.

The Varian Clinac 2100C linear accelerator used for this project is a dual-photon energy (6 MV and 10 MV), multiple electron energy machine fitted with a Varian Millennium MLC. Only the 6 MV photons have been used for IMRT treatments.

The whole treatment machine system consists of a stand, a rotating gantry housing the accelerator itself, a modulator, and a treatment couch.

The modulator contains the major electrical components of the linear accelerator, and provides the short-pulse-high-voltages used by the klystron.

The patient treatment couch can be moved in three linear directions (up and down, left and right, to and from the gantry) and rotated horizontally. These motions, and the vertical rotation ability of the gantry and treatment head (aligned with the gantry), can be manipulated from the external control room, which contains all of the monitors and control consoles and computers necessary to deliver the treatment (Figure 3.2).

Figure 3.2. A control room at ICCC, showing the various monitors, computers, and keyboards necessary to control the linear accelerator.

Figure 3.3 shows a diagram of the major components of the linear accelerator stand and gantry. Within the stand is a klystron, to magnify microwaves from a small microwave generator, a waveguide transports the microwaves to the accelerator, and a circulator ensures any reflected microwaves are absorbed in a water load. A vacuum system provides the low pressure needed for the electron gun, accelerator waveguide structure, and bending magnet – to stop electrons from colliding with air molecules. The transmission waveguide

transfers microwaves from the klystron to the accelerator waveguide. It is filled with pressurised sulphur hexafluoride (SF_6) gas to prevent electrical breakdown that can be caused by the high power microwave electric fields. An auxiliary cooling system delivers temperature-controlled water to sensitive parts such as the bending magnet and also cools the target.

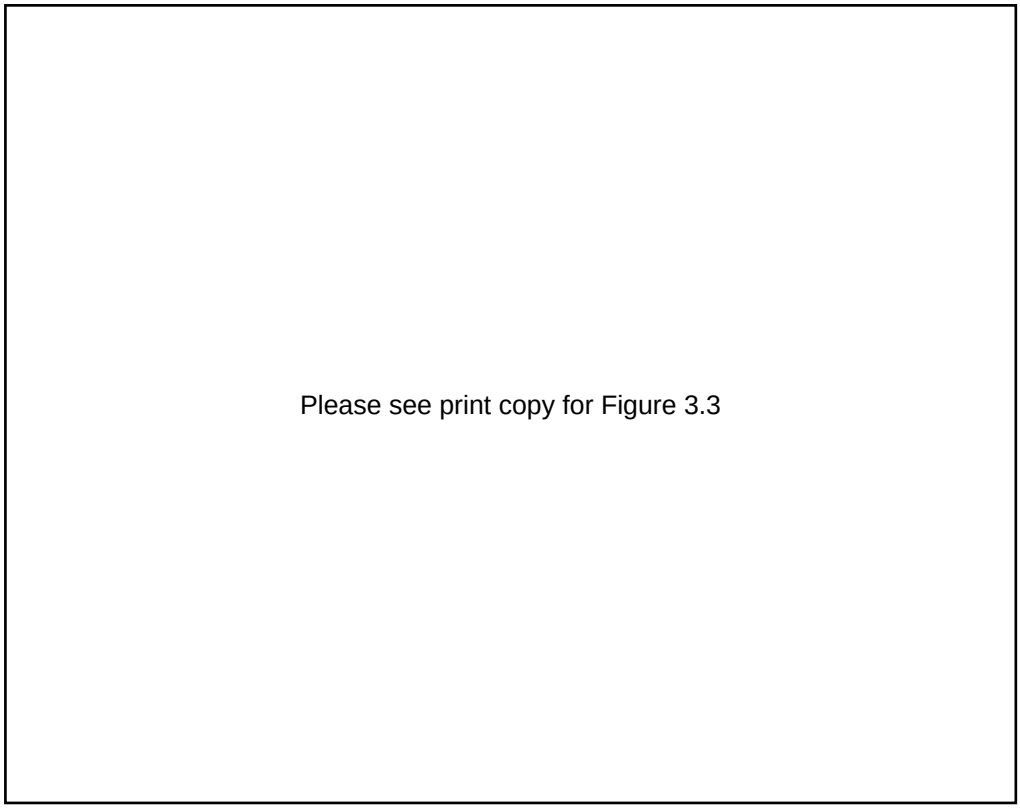

Figure 3.3. The major components of a linear accelerator[80].

Inside the gantry is the accelerator structure, which includes an electron gun to supply the electrons. As most high-energy linear accelerators are too long to be positioned vertically, in order to direct the beams at the treatment couch a bending magnet in the treatment head uses magnets to turn the horizontal electron beam through a loop of 270°. A diagram of the beam control components of the treatment head is shown in Figure 3.4.

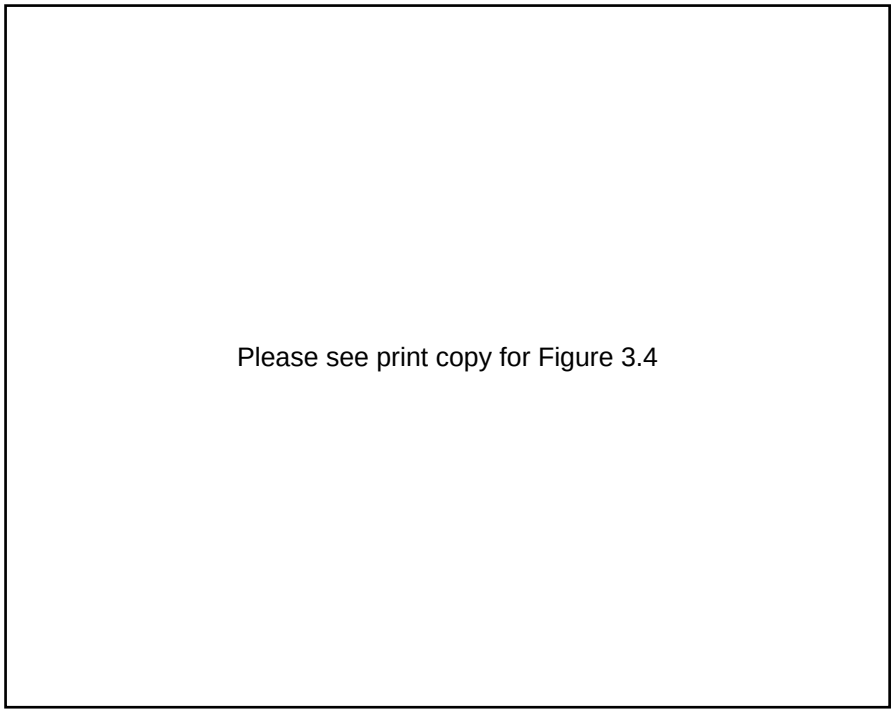

Figure 3.4. The bending magnet and beam shaping components of a linear accelerator[77].

To convert the electrons to x-rays and evenly distribute the beam a target and conical flattening filter are used in combination.

To provide the therapist with a virtual beams-eye-view (BEV) of the treatment field borders, a light source projects an image of the field onto the patient on the treatment couch. A numerical scale can also be projected onto the patient in order to check the SSD. A cross-hair shadow indicates the field centre and there are patient-alignment lasers mounted on the wall, which all aim at the isocentre of the rotating gantry.

The main field-shaping devices are contained within the treatment head, these being the primary and secondary collimators to define the rectangular shape and size of the beam, and possibly the MLCs to provide additional shaping.

The primary fixed collimator is usually made of tungsten and sits between the target and the flattening filter. It has a set size and shape like an open and

slightly diverging cone, and its main purpose is to prevent leakage from the treatment head.

The secondary collimators are made of 8 cm thick tungsten – enough to absorb at least 98% of the primary beam[84]. These collimators consist of four blocks, or jaws, set in perpendicular opposing pairs called the x-jaws and the y-jaws (one pair is positioned above the other). The jaws can be adjusted individually to create any size of rectangular fields, up to a 40 cm x 40 cm projected field size at isocentre. The collimators reduce the penumbra of the beam to a minimum by being as far from the beam source as possible, and by matching the jaw edge to the divergence of the beam[84], which helps to minimise partial transmissions through the jaw. The beam divergence for different field sizes is matched by running the jaws along a slightly arced line to keep the block edge flat to the diverging beam. This can be achieved by having a physical wedge ramp and jaws on a pivot, which means the jaws gently slope up as they drive out.

When field sizes are given for beams from a linear accelerator it is important to remember that this is not necessarily the size of separation of the secondary jaws, but the size of the beam that they produce at a given SSD, this conventionally being 100 cm.

Extra modulation of the x-ray beam may be provided via external attachments such as wedges and cutout blocks (which are not usually necessary when an MLC is installed) or longer collimators (cones) for electrons.

Internal monitoring of the linear accelerator is achieved via two sets of ionisation chambers, usually made from kapton filled with oxygen-enriched air and sealed to avoid the effects of changes in temperature and pressure[80]. The chambers are positioned one beneath the other at a 90^{o} angle as shown in

Figure 3.5. The inner chambers of each set are used for beam angle steering, the outer two chambers are used for beam position steering, and all of the chambers are used to obtain a total symmetry reading. If the incident beam is positioned or angled incorrectly one half of the chamber will receive a higher dose than the other, and this information can be fed back to the beam steering controls in the bending magnet to correct the direction of the beam[80]. The first set of monitor ionisation chambers is also used to automatically turn the beam off after the set amount of MUs has been detected. The second set of monitor ionisation chambers is a failsafe to backup the first chamber. A timer can turn the beam off after a set period of time, in case both the ionisation chambers should fail. The radiotherapist delivering the treatment can also terminate the beam from the external control room at any time.

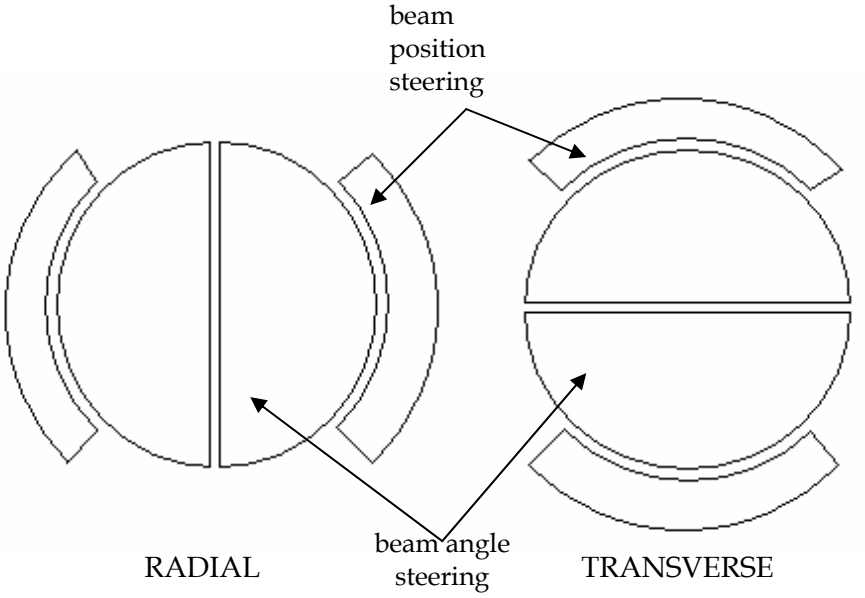

Figure 3.5. A schematic diagram of linear accelerator monitor ionisation chambers, the second chamber set at right angles to the first.

Record and verify computer systems check the parameters of the treatment setup and delivery for the particular patient, such as ensuring the jaws are in the specified position and the correct amount of MUs has been selected. The system also serves as a record of patient treatments, and a planning tool for organising treatment times.

3.2.2 Radiation Interactions from Linear Accelerators

The two forms of radiation generally used in radiotherapy are: gamma rays, or x-rays, which have both wave and particle characteristics; and electron beams, which display particle characteristics. An incident radiation beam on a material is attenuated via interactions that result in scattering or absorption.

Gamma beam energy spectrums may consist of discreet monoenergetic lines from a radionuclide source. From a linear accelerator the energy is actually made up of a continuous spectrum of energies caused by bremsstrahlung radiation, possibly with some monoenergetic characteristic lines[86]. Traditionally the peak energy is used to describe the energy of the beam – for example a '6 MeV beam' refers to the maximum energy, the average energy is about 2 MeV.

Photons, which make up x-ray beams, are primarily attenuated by:

- The transfer of energy to electrons.
- Photons escaping from the beam.
- A decrease in intensity due to the inverse square law effect.

Electrons are a form of directly ionising radiation, which means they deliver energy directly to matter, as opposed to photons, which rely on the transfer of energy to electrons that will then perform the same function of depositing energy in matter. The main form of energy loss of a photon beam in materials with a low atomic number, like human tissue, is the ionisation of atomic electrons.

The three main types of photon interactions follow.

- The photoelectric effect (Figure 3.6) is dominant at photon energies up to 50 kV[54]. A photon transfers its energy to an inner, or bound, electron, knocking it out of its orbit. An outer electron moves in to take its place, emitting another photon, and so on until all the inner shells have been refilled.

- Compton scattering (Figure 3.7) is dominant at photon energies between 200 kV and 2 MV. It occurs when the photon knocks an outer electron out of its orbit, resulting in the recoil electron and scattered photons. Compton scattering is the dominant interaction for most radiotherapy beam energies.
- Pair production (Figure 3.8) is only possible at energies of 1.022 MV and above, and dominant at more than 30 MV. The photon interacts with the nucleus to form an electron-positron pair; the electron travels away and the positron goes on to recombine with a free electron, which creates more photons.

Triplet production is a less common interaction that can occur with energies of 2.04 MV or above, where the photon interacts with an electron to eject the electron and form an electron-positron pair.

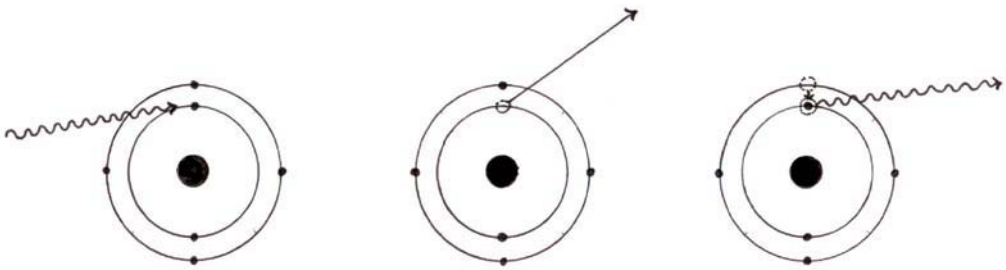

Figure 3.6. Schematic of the photoelectric effect.

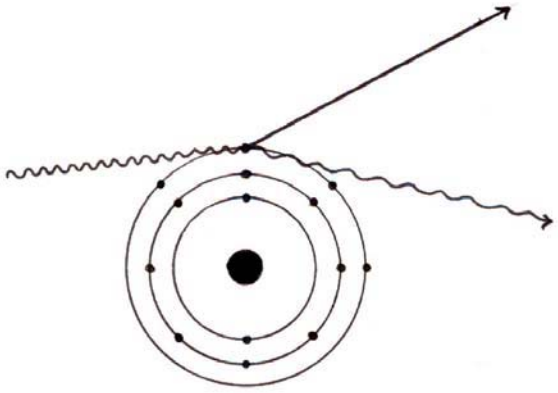

Figure 3.7. Schematic of Compton scattering.

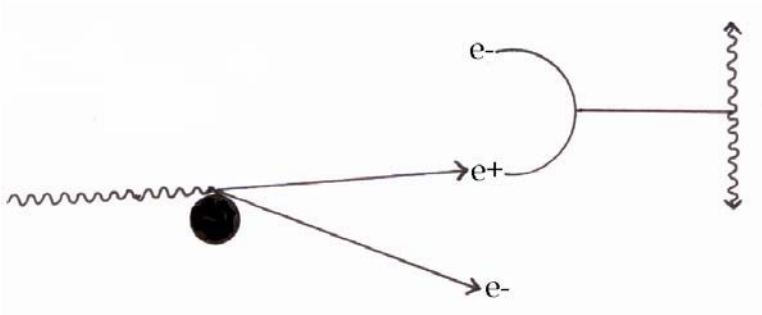

Figure 3.8. Schematic of pair production.

3.2.3 Conversion of Monitor Units

Monitor units are arbitrary values that correspond to a specific dose under certain conditions, and are used to calibrate the preset dose received by the linear accelerator's monitor ionisation chambers in the treatment beam. The specific conditions under which the calibration dose is set include the position of the source and the depth of measurement in the material irradiated, the type of material used, and the field size of the beam.

The monitor ionisation chambers in a linear accelerator are calibrated to give a known output for a set conversion. There are two main ways of calibrating the dose per MU; the linear accelerator used for this project was calibrated using IAEA TRS-277[44] (it has since been recalibrated using IAEA TRS-398[45]):

$(D/MU)_{std,SSD,water}$ = 1 cGy/MU at 100 cm SSD for a 10 cm × 10 cm field in a water phantom at d_{max}.

This means that one MU is equal to a dose of 1 cGy when delivered to the depth of maximum dose (d_{max}) in a water phantom at 100 cm SSD. Another common method is to calibrate at 100 cm source-to-axis distance (SAD).

For manual calculations of dose, or for checking the dose calculated by a planning computer, several factors become important. The jaw dependent field factor (FF) is equivalent to a value of one for a 10 cm × 10 cm field size, and increases with field size. Because the MU chambers reside above the jaws their response is only slightly affected by jaw opening. The ionisation chamber measurements in the phantom/patient position are affected (due to scatter), hence the need for field factors.

Percentage depth dose (%dd) is a function of both depth and equivalent field size, and is independently evaluated for an individual machine. It can be calculated using the following equation:

$$\%dd = \left(\frac{R_{depth}}{R_{d\max}} \right) \times 100$$

where R is the relative electrometer reading after delivering a standard dose (100 MU for example) to an ionisation chamber at the required depth and at d_{max} in a solid water phantom at 100 cm SSD.

Using the above factors, the MUs required to deliver a particular dose can be calculated using:

$$MU = \frac{D}{\%dd \times FF}$$

where D is the dose in cGy. The equation can be reversed when checking a plan to ensure that the MUs calculated will deliver the desired dose. Additional factors such as an off-axis factor and a wedge factor may be involved in the calculation, but were not applicable in this project.

3.2.4 Multileaf Collimator

Devices such as wedges and compensators have been used for many years to provide a very basic form of beam intensity modification, as have methods for blocking various parts of the beam in order to shape it more closely to the desired treatment field. For the purposes of complex intensity modulation wedges are too basic. Compensators are capable of more complex modulation of the beam, but their production is labour-intensive, treatment time can be significantly increased because they need to be changed by therapists between each field, and considerable scattering and beam hardening caused by the compensators must be taken into account when calculating dose[120]. Low melting point materials such as cerrobend can be used to block and shape the beam, but it is time consuming to create special blocks for each treatment field. These blocks in turn have to be changed manually between each field. Compensators and cerrobend blocks are very heavy, which can present an accidental injury risk to both patient and therapist. Cerrobend is a toxic material, which can present an exposure risk if the vaporisation temperature is unintentionally exceeded, as can the accidental melting of the Styrofoam™ used in shaping the blocks[117].

A multileaf collimator (MLC) (Figure 3.9) is made up of two opposing rows of closely spaced narrow leaves, each of which can be moved separately to create an overall conformal shape to block the beam. As the collimators can be controlled via computer, the MLC can be shaped from the control room during and in between treatment doses, allowing for more complex treatment routines. Therefore the MLC allows for fast, automated treatment field shaping, reducing the need to spend time and money on cerrobend blocking.

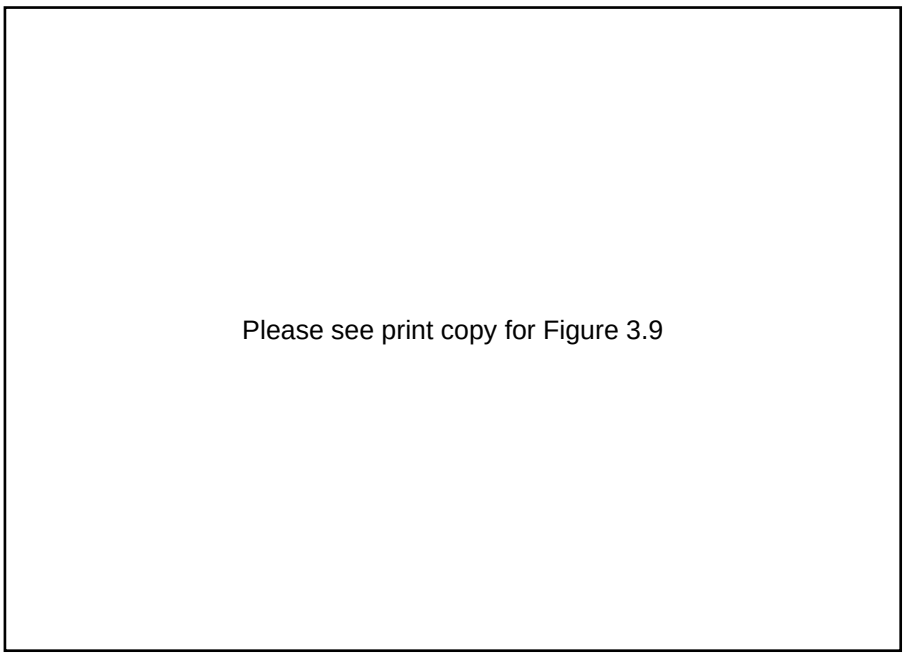

Figure 3.9. The treatment head of a linear accelerator, showing the MLC[94].

To accurately move the MLC leaves to the desired positions, three factors must be taken into account by the manufacturer. These are the detection of the position of the leaf in real-time, the precise control of the movements of the leaf, and the mechanism that actually moves the leaf[117].

The Varian Millennium MLC is fitted below both sets of secondary jaws, as opposed to replacing one pair, making it a tertiary collimation system[117]. It consists of 120 leaves, or 60 opposing pairs. The central 80 are 5 mm wide, and the outer 40 are 10 mm wide, with a leaf height of 60 mm. The leaves are made from a tungsten alloy because it has a high density, is hard, cost-effective, and does not readily expand, so the leaves can be fitted together very closely. The addition of various mixtures of nickel, iron and copper to pure tungsten improve the machinability of the brittle material[117]. The MLC is made so that the leaves can pass the centre of the radiation field. Using an 'over-running' MLC has the advantage that the treatment field can be conformed to target volumes through which the central axis of the source does not pass[129].

Tertiary collimation can reduce the clearance distance between the patient and the treatment head, but also allows for the lower jaws to act as a back-up

block behind the MLC to reduce leakage between the leaves. Another advantage is that the further the leaves are from the beam source, the larger the physical width of the leaves can be. A further advantage is that in the case of a malfunction, the leaves can be manually moved out of the field and the linear accelerator can still be run with normal blocking methods, thus eliminating possible major downtimes. When the MLC is used as a tertiary collimator, with both sets of secondary collimator jaws backing it up, it only needs to attenuate the beam to the same extent as would a customised block, rather than having to act as a secondary collimator. However, the increased transmission that comes from between the leaves means compensation must be made in the leaves to reduce the overall transmission[117].

Leakage can occur between the leaves of the MLC, and between the opposing banks of leaves when fully closed. To reduce leakage between the leaves they are formed with a tongue-and-groove arrangement. This can lead to serious under-dosages in static intensity-modulated beams, because the beam can be partially absorbed by the tongue of a leaf that is extended past neighbouring leaves, resulting in an under-dosage of up to 10 to 15%[124].

When leaves from opposite sides share the same position in different segments, the leaf end transmission can lead to horns or matchlines in the measured dose profile, which can be improved by reducing the MLC leaf gap[15] (see '2.1.1 Matchlines').

An obvious difficulty with MLCs is that the stepped edge of the leaf banks results in the curved section of the field boundary within each leaf width being approximated by a straight line[142]. Therefore the accuracy of the shape formed by the MLC compared to the shape desired is limited by the width of each leaf, leading to a distinct stepped, rather than a smooth, edge to the shape that may not provide enough discrimination between the normal tissue outside the target volume and the tissue within the target volume to be

irradiated[11]. It is possible to set the leaf positions so that the under-blocked areas equal the over-blocked areas[142], in an attempt to compensate for the lack of smoothness of the MLC shape.

A potential disadvantage in treatment delivery using an MLC is the slightly wider penumbra compared to divergent blocks and jaws because of the finite width of the MLC leaves, which are not divergent along their length[21]. Wang *et al.*[124] estimates the difference between predicted and measured dose outside the beam boundary to be up to 10%. The increased penumbra should only prove a problem when treating very limited areas, such as a tumour that is very close to a critical structure. Limiting the displacement between leaf ends (so that no single leaf is positioned significantly further from the surrounding leaves) can reduce the penumbra effect by reducing the partial transmission through the tongue-and-groove edges. The Varian MLC is provided with rounded leaf ends so that the penumbra can be kept relatively constant over the range of leave travel, and the partial transmission through the ends offsets the penumbra to a point within the leaf end position, effectively widening the MLC leaf opening[15].

A matchline effect problem encountered by Cadman et al.[15] when validating MLC leaf modelling for a treatment planning system was that the rounded leaf ends were not modelled in the planning computer, compromising the shape of the beam profile in the vicinity of the leaf ends. This can be corrected by reducing the leaf gap by a small amount, equivalent to the effective leaf gap widening resultant from the modelling of non-rounded leaf ends. This is determined as the difference between the 50% points of the measured and calculated profiles.

When calculating the MUs for a dose to be delivered with an MLC the main difference in the calculation is in the collimator scatter factor (S_c)[117]. Also known as the in-air output ratio, S_c arises partly from collimators, but mostly

from other parts in the treatment head (also known as 'extra focal scatter', contributors include the flattening filter and monitor ionisation chambers) and varies with field size and shape. However, if the treatment field is blocked to more than 50% of the secondary collimator-defined field, which occurs quite often with IMRT fields, the radiation output falls below that predicted[117]. The estimation of S_c is made more difficult by the irregularity of MLC-shaped fields, which makes the estimation of the equivalent square size of the field difficult. As the Varian Millenium MLC is installed as a tertiary collimator it has little effect on S_c unless the field it shapes is substantially smaller than that produced by the secondary collimators, so MU calculations can be carried out with the MLC-shaped field treated in a similar way to a cerrobend block-shaped field. It is recognised that the small blocked areas produced by the IMRT segments will impact more on the extra focal scatter (i.e. S_c) than would larger conformal single-segment portals. This is one of the main calculation challenges for monitor unit checks, which often rely on an equivalent square method for field factor calculations.

3.3 Verification Dosimetry

Ideally a radiation detector used in radiotherapy would be able to directly measure absorbed dose (that is, energy absorbed) – calorimetry is capable of this, where small changes in water temperature are measured. However such a method is awkward and inconvenient. Other detectors indirectly measure radiation via, for example, ionisation or chemical changes.

A suitable dosimeter for radiotherapy measurements should be carefully considered for each application in terms of its[80]: accuracy; precision and reproducibility; range of measurement; linearity of dose response; independence from the dose rate and radiation type and energy; and high spatial resolution.

3.3.1 Ionisation Chambers

Ionisation detectors measure the ionisation produced by a particle (in this case an electron from a photon) in a gas medium. They are reliable, and well understood from a long history of use, and can be attached to an electrometer to measure charge in real time (Figure 3.10).

Figure 3.10. The electrometer and small ionisation chamber used for the dose measurements.

When electrons and positive ions are produced in a medium during an ionisation event they recombine very quickly, making the ionisation event undetectable. A high potential difference set up across the ionisation detector medium draws the ions to either electrode before they can recombine. When this occurs they create small currents that pass through a resistor, leading to a voltage drop that can be amplified and measured. Due to the now low recombination rate the measured voltage drop can be linked to the ionisation events, which in turn can be related to the amount of energy, or dose, actually deposited in the medium. The medium used for the detector must be one that is easily ionised but chemically inert so that ionisation electrons are not recaptured by the medium; for example, simply air is commonly used.

An ionisation chamber is amongst the most commonly used type of ionisation detectors in radiotherapy. Ionisation chambers operate at lower voltages, and although this means they produce smaller signals when detecting low-

ionisation particles, they can produce quite strong and linear results when used in high flux fields (such as in radiotherapy), and need a relatively short recovery time.

Both of the chambers used for this project were thimble-type ionisation chambers, which are enclosed cavity cylindrical ionisation chambers. The thimble chambers can absorb dose from any direction, except through the stem by which the chamber is attached to the electrometer[4].

Figure 3.11. The 'regular' NE 2571 Farmer ionisation chamber used for dose measurements.

The thimble chamber used in this project is shown in Figure 3.11. The NE 2571 Farmer chamber (NE Technology Ltd., Reading, UK) has a 0.6 cc capacity cavity volume, which is 24.0 mm long and 3.2 mm in radius. The wall is made of 0.065 g/cm^2 thick conductive graphite, to connect to the stem. A thin aluminium wire, insulated from the thimble and the stem, runs down the centre and together with the wall forms a capacitor in which to store electric charge. The stem is also a capacitor.

The IC 10 chamber (Scanditronix-Wellhöfer) (Figure 3.12) has a 0.14 cc capacity cavity volume, which is 6.3 mm long and 3.0 mm in radius. The wall is made of an air-equivalent plastic called C-552, 0.068 g/cm^2 thick, and the central electrode is also made of C-552.

Figure 3.12. The 'small' IC 10 ionisation chamber used for dose measurements.

Typical issues concerning an ionisation chamber include electrical leakage, reproducibility of readings, stem blockage (radiation incident on the stem can also increase the reading[86], energy dependence, angular dependence, polarity effect, efficiency of charge collection, and atmospheric communication (how fast the chamber adjusts to the surrounding environment)[41].

Ma *et al.*[69] refers to a potential problem with the central aluminium electrode in an ionisation chamber, which is that a chamber with this type of electrode can over-respond when being used for dosimetry. The increase in dose response has been found to increase with the diameter of the electrode, given as approximately 0.6% for an electrode with 1 mm diameter in a ^{60}Co beam. Due to the small difference and the difficulty in quantifying it, this factor is often given a value of one[44].

When an ionisation chamber is used for radiation dosimetry, corrections must be made for the temperature and atmospheric pressure surrounding the chamber, as they affect the number of gas molecules available to be ionised in the fixed volume of the ionisation chamber, and therefore the sensitivity[86].

The volume of the ionisation chamber can also affect measurements in what is known as the volume averaging effect – because the ionisation chamber is a finite volume it measures an average of the dose passing through it, without

any way of telling the actual distribution of the dose in that region. A 0.6 cm^3 Farmer chamber, which is the main chamber used at ICCC, has been found to give difference of up to 6% between calculated and measured doses in an IMRT treatment, whereas a 0.015 cm^3 pinpoint chamber can give a maximum difference of 2%[57].

3.3.2 Electrometers

The electrometer used for this project was a Farmer 2570/1 electrometer from NE Technology.

An electrometer is a device used to collect the charge created by an ionisation chamber. The electrometer must be very accurate and sensitive, as well as stable over time. A diagram of an electrometer is shown in Figure 3.13. The energy E collected by the ionisation chamber is the product of the dose D accumulated and the sensitive volume m of the chamber, represented by[80]:

$$E = D \cdot m$$

This creates a charge Q given by:

$$Q = \frac{E}{(W/e)}$$

where W/e is a constant 33.97 J/C per ion pair, independent of the initial beam energy. The resultant current I:

$$I = \frac{Q}{t}$$

is gathered by the electrometer, where t is the time over which the dose is delivered.

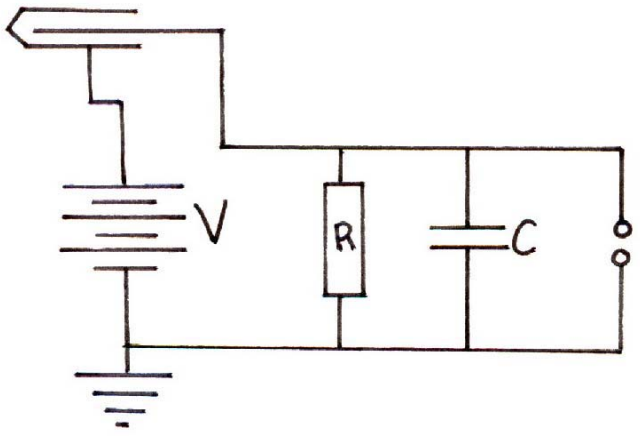

Figure 3.13. A schematic of an electrometer.

A voltage proportional to the charge in the ionisation chamber is collected across a capacitor. A resistor provides a very high resistance to prevent

leakage. Considering that the given parameters are all relatively small, the electrometer has to be accurate to within less than one pico-amp ($A \times 10^{-12}$).

An electrometer should have: a stable voltage; the capacity for polarity charge in order to measure polarity effects; the ability to supply fractional values of the voltage; a minimum number of connections in order to prevent leakage; a short warm-up time; a small background current; a linear scale; and a sensitivity that is independent of surrounding environmental conditions. Further features might include an internal timer, and the ability to display in multiple units to account for the different sensitivities of different ionisation chamber[41].

3.3.3 Film

X-ray film consists of an emulsion suspended in a gelatin matrix and coated onto glass or cellulose acetate film, with a thin subbing layer to maximise the adhesion between the two layers (Figure 3.14). The emulsion is typically 40% silver halide (usually bromide), 10 to 20 μm thick with grains 0.2 to 2 μm in diameter. For increased sensitivity the emulsion is often coated onto both sides of the film.

Figure 3.14. The layers of film: protective coating A; film emulsion B; subbing layer C; film base D.

Any incident photons (including light) that interact with the film cause a secondary electron to be created, which in turn converts a silver ion to a neutral particle. If any silver ions in a grain have reacted, then when the film is developed the entire grain will turn black. The term optical density (OD) refers to the level of transmission of light through the film - a darker film absorbs more light and has a higher OD. The OD is proportional to the number of silver interactions in the film, which in turn can be related to the number of x-rays incident on that section of the film whether they interact or not.

When the film is put through a temperature-controlled automatic processor it feeds through a roller system, which takes the film through various stages. First, the film is immersed in developer, an alkaline solution that reduces the silver ions affected by radiation to silver atoms. The next stage is an acidic

solution called fixer that controls further development of the image, and dissolves any unexposed silver bromides out of the film. Finally, the film is washed to remove leftover chemicals, and dried to make handling it easier[84]. According to Suchowerska[110] a typical automated processor in a radiotherapy department can manage reproducibility in OD over one day of about 3.3%.

The light transmission through a point in the developed film is inversely proportional to the amount of metallic silver present, which is a direct but non-linear function of the dose deposited at that point. To measure the relative optical density (relOD) of the film a light densitometer, or film scanner, can be used. The spatial resolution of the film depends on the size of the grains, and the aperture size of the light-collecting device in the densitometer, the resulting trade-off is a reduction in the amount of light collected, which means an increase in the signal-to-noise ratio.

Optical density is given by:

$$OD = \log\left(\frac{I_0}{I_t}\right)$$

where I_0 is the intensity of the incident light and I_t is the intensity of the transmitted light. This is the most common form of measuring intensity as it corresponds to the way in which the eye also sees light intensity in logarithmic form. It is important to remember when analysing film that the relOD results given by a densitometry scanner may not be the actual OD. To find this, films with several known real ODs must be scanned, and related to the exposed film to comparatively calculate the real OD. A 'step film' (Figure 3.15) was used in this project, which is a strip of film with twenty-one stripes, or steps, of known OD, allowing a comparative plot to be made of relOD against real OD.

Figure 3.15. A digitised section of the step film used.

One of the greatest advantages of film is that it provides a good two-dimensional spatial map of the shape and intensity of all incident radiation. Ionisation chambers or TLDs, for example, can only provide measurements of dose points, which are often relatively time consuming to position and collect. This spatial characteristic makes film particularly useful for qualitative analysis.

Within certain limits of exposure (which varies between different types of film) the OD of exposed film has a fairly linear relationship with the amount of dose it has been exposed to, making calibration and analysis relatively straightforward. This linearity also means that the relative net ODs of two separate films can simply be added together (integrated) to provide a total, or the film can be exposed several times to give a cumulative result.

A further advantage of film as a dosimeter is that it can be kept as a permanent record for future reference, comparison and measurement.

The ideal film for quality assurance of IMRT should: be able to measure absolute dose with accuracy better than 2%; give results that are independent of photon energy; respond linearly to doses between 5 and 250 cGy; and be minimally responsive to variations in film processing[87].

Using film as a dosimeter has disadvantages. For example: the probability of a Compton x-ray interacting in the emulsion is quite low, meaning the sensitivity of film is low; film is prone to under- and overexposure; unexposed film contains noise (which can be reduced with superior instruments); and film is produced in sheets, which can make it difficult to use for irregular surfaces. Radiographic film does not respond immediately, meaning results must be delayed until the film can be developed[129]. Film can be very sensitive to external conditions, especially in the developing phase. These conditions include temperature, the exact mix of developer fluids used, and even small exposures to light. Sheets of film that are made in different batches are variable, for example in the thickness of the gelatin matrix. So each set of x-ray films used for dosimetry, including all calibration films, should come from the same box. They should also be developed at the same time, to minimise variations in environmental factors.

Although the film could be cut to fit a particular two-dimensional shape or size (for example, to fit the film into a space in a phantom), the film edges must be taped securely with black electrical tape or similar, or otherwise protected from the light, which can increase the chance of accidental exposure of the film. According to Dogan *et al.*[29], film also tends to show a considerable response to depth, energy and field size, which could affect the accuracy of measurements. Childress *et al.*[22] found that multiple measurements taken over a period of time showed a fairly constant dose for regions not blocked by a collimator, but a slightly higher standard deviation for areas receiving large amounts of MLC scatter.

Film can over-respond to low doses because the large amount of high-Z silver halides in the film have increased photoelectric attenuation values in comparison to biological tissue. This can be a particular disadvantage in IMRT because the multiple low-dose fields can potentially compound the over-response[22] as the penumbral tails of many segments are included in the fields. These regions may contain more low energy scatter at depth. The over-response of film increases with depth because of changes in the photon energy, and is dependent on whether the plane of the film is aligned perpendicular or parallel to the beam axis. Film that is exposed perpendicular to the beam has been found to have less dependence on this effect than parallel film, which shows an over-response of up to 14% at 25 cm depth[111].

Various methods can be employed to reduce the depth dependence of film. Two of these are[138]: to sandwich the film between thin sheets of lead in order to block the softer photon beams; and sandwiching the film between organic plastic scintillators that convert the energy deposited by upstream electrons to a relatively large amount of lower energy visible light photons. The enhanced response of the film to visible photons can suppress its over-response to the lower energy photons. However these specialised lead-lined cassettes were not available for this project.

The over-sensitivity to low doses results in an even greater over-response when film is irradiated in the parallel plane (to the beam axis), because scatter contribution increases with depth[15] and the photon energy spectrum softens, or tends towards lower energies[138]. Due to this limitation one suggestion is to calibrate in the same orientation the film is to be irradiated in - that is, if the dosimetry film is to be irradiated in the parallel plane, the calibration films should also be irradiated in the parallel plane. This can present a particular difficulty in IMRT where some treatment beams tend to be non-coplanar, so the film would have to be calibrated for each orientation.

According to Childress *et al.*[22], reasonable estimates of film non-reproducibility due to variations in the film uniformity and response, processor, and densitometer would be 6 to 15% if there was no method used to compensate for standard film over-response, and 3 to 8% if there were.

3.3.4 Kodak X-Omat V

One of the most commonly used dosimetry films in radiotherapy departments is the Kodak X-Omat V (Eastman Kodak Company, New York, USA), commonly known as XV film, which is designed to have a range of about zero to 100 cGy. According to El-Khatib *et al.*[32] the film consists of a gelatin emulsion layer 10 to 25 μm thick that contains 30% to 40% silver bromide (AgBr) grains by weight.

As a result of the relatively low saturation dose XV film has a fairly short linear dose-response region of up to 80 cGy[29]. This is rarely a disadvantage in regular quality assurance and dosimetry procedures, where low doses are used or where higher doses can be reduced to an appropriate level. However, if the number of MUs in an IMRT treatment is reduced for the delivery of a beam, inaccuracies can occur in the delivery of segments with lower MUs, affecting the overall dose delivered.

According to Olch[87] a limitation of XV film for photon dosimetry lies in an overestimation of percentage depth doses, especially at depths greater than 10 cm and for field sizes larger than 7 cm × 7 cm. This is due to the silver content in the film causing an increase in photoelectric interactions for the scattered low energy photons in the film.

When measuring electrons, a difference in OD of up to 6% has been found between XV films that remained in the pre-packaged form and film that had been removed from the pack. However, the normalised ODs were found to be identical[32]. Olch[87] claims that reports are conflicting as to whether XV film can be used for absolute dose measurements with an accuracy better than 5%. The accuracy of XV film in dosimetry is in large part dependent on the stability of the film processor used[87]. The standard of quality assurance that may be necessary in order to run the processor at the accuracy required to improve that of the film itself is unfeasible at many centres.

3.3.5 Kodak EDR2

A film released recently (in the first half of 2001) is the Kodak Extended Dose Range (EDR2) (Eastman Kodak Company, New York, USA), which has a much larger dose range than XV film; according to Kodak the range is zero to 600 cGy. The linear response of the film apparently applies from about zero to 500 cGy[15]. The film consists of silver bromide grains that are one-tenth the size and more uniformly shaped than the grains of the XV film[87]. EDR2 is a slow speed film with double emulsion layers coated into a 0.18 μm Edtar base[145]. A halved silver content[87] and the smaller size of the grains results in lower sensitivity than the XV film, and the increased uniformity of the grains leads to higher contrast and hence less noise in readings[145].

According to a study by Dogan *et al.*[29] the EDR2 shows less energy dependence, similar field size dependence, and generally less depth dose dependence than the XV film. The EDR2 film also showed an improved match between measured and calculated isodose lines, and between measured and calculated maximum doses. Comparisons have found that the EDR2 film responds to variations in dose rate with accuracy within 0.5%[145].

Although the increased range of the EDR2 film provides an advantage over the XV film when irradiating with large doses, the relative insensitivity that allows this advantage may become a disadvantage when measuring lower doses, as the film is less responsive and this will result in a higher signal-to-noise ratio[87]. The EDR2 film has been found to require approximately quadruple the dose of the XV film in order to obtain accurate measurements. At least one study has also found that EDR2 film gives OD results 5 to 10% higher when irradiated parallel to a radiation beam than when it is irradiated perpendicular to the beam[29].

When developing EDR2 film Dogan *et al.*[29] found that films irradiated on the same day and developed over different days were reproducible to within

1.5%, but if developed on the same day were reproducible to within 0.5%, which indicates the need to develop each set of films in the one session.

3.3.6 Dosimetry Phantoms

According to Woodard *et al.*[135], "The need for reliable composition and density data of body tissues is a prerequisite in theoretical dosimetry involving radiation interactions in humans." This includes reliable information on the structure and composition of the individual patient, as well as the interactions of x-rays in such materials.

An analogue material is used to approximate the characteristics of some component of the human body. A phantom is a body substitute made up of tissue analogue materials that is used to predict the effects of incident radiation by modelling radiation transport properties. Phantoms can be created in various forms ranging from basic homogeneous geometric blocks to more complex anthropomorphic shapes. The most important properties are the mass stopping power, the mass attenuation coefficient and scattering. It follows that the material's equivalent atomic number, electron density and physical density should closely match the material it is substituting.

More than 80 different tissue substitutes are known to have been created in the past, including water and wax[132]. Water is often used as an analogue because it's mean atomic number of $Z = 6.6$ and physical density of $\rho = 1$ g/cm^3 approximate human muscle, and water is simple to acquire and use.

Solid water is a very common alternative to water, being a plastic material with an equivalent electron density to water, in order that the transmission of x-rays through the two materials is equivalent, although its mass density is slightly higher. The solid water phantom used in this project was constructed from RMI-457 (Gammex RMI, Wisconsin, USA). Elementally it consists of, by weight, carbon (67.22%), oxygen (19.84%), hydrogen (8.09%), nitrogen (2.40%), calcium (2.32%), and chlorine (0.13%), with a density of 1.030 g/cm^3 and an effective atomic number of $Z = 5.96$. The solid water phantom (shown in Figure 3.16) was a 30 cm × 30 cm × 30 cm cube made up of slabs of solid

water, which range in thickness from 0.2 to 4.0 cm. The slabs were stacked or lined up together, and carefully aligned to make the edges of all the slabs as level with each other as possible.

Figure 3.16. The cubic solid water phantom used in this project.

According to Tailor *et al.*[114] errors between temperature measurements of air and of the actual temperature of the phantom material - and hence the ionisation chambers that are used with them - can easily range up to ±2°C. One reason for this error is taking temperature readings at the wrong position - for example, if the temperature is measured at a point in the treatment room directly under an air-conditioning vent the temperature read would be different to the real temperature near the beam isocentre, where the measurement should be taken. If the phantom material is taken from a different environment and not allowed enough time to reach thermal equilibrium with the surrounding air - which may take several hours[114] - the temperature of the ionisation chamber positioned inside the phantom will also be different to the reading taken in air. As the ionisation chamber is affected by temperature, incorrect temperature measurements can affect the final corrected measurements taken by the chamber.

According to Constantinou *et al.*[25], a notable source of uncertainty when measuring radiotherapy photon doses in a phantom comes from the ionisation chamber having walls and/or a buildup cap that are of a different composition to the surrounding phantom material. When this is the case, a part of the total ionisation in the chamber is produced by secondary electrons from the chamber wall.

3.3.7 Vidar Film Scanner

The processed film was scanned into a computer using a Vidar VXR-12 plus film digitiser (VIDAR Systems Corporation, Hendon, VA, USA), shown in Figure 3.17, with Osiris imaging software (Digital Imaging Unit, University Hospital of Geneva, Switzerland). The VXR-12 can produce images with 256 or 4096 levels of grey (known as 8-bit or 12-bit depth), with four pixel sizes from 85 to 423 microns (equivalent to 300 to 60 dots-per-inch respectively)[122].

Figure 3.17. The Vidar VXR-12 film scanner.

To scan an image into the computer the film is placed into a roller mechanism, which pulls the film over a fluorescent lamp. A fixed focus, fixed aperture lens on the other side of the film focuses the light that has been attenuated by the film onto a 5000-element charge-coupled detector (CCD) array. Each element in the array produces an electric charge that is proportional to the amount of light striking it, so the charges generated can be converted to represent the OD of the image as digital greyscale data.

At ODs above 2, a 12-bit CCD-based commercial film digitiser may be limited in accuracy by noise. XV film has been found to produce an OD of approximately 2 when irradiated with 85 cGy of 6 MV x-rays, which is just half of a typical daily fraction dose[145].

Various options are available for adjusting the settings of the scanner, using the Osiris software. Resolution refers to the detail that can be captured in the film. A higher resolution results in finer detail than a lower resolution, however it also produces a bigger file size and requires more memory[122]. So the level of resolution selected may depend on the accuracy desired in a trade-off with the capabilities of available disc storage space and the computer monitor. Mersseman *et al.*[78] found that the optimum scanning resolution for a Vidar VXR-12 film scanner is 75 dots-per-inch.

According to the Vidar User's Manual[122], "depth refers to the number of data bits the film digitiser captures per pixel." This in turn determines the number of greyscale levels that can be distinguished. A 12-bit depth scan, with 4096 levels of grey, produces a much large image than an 8-bit depth scan with 256 levels of grey, resulting in a similar accuracy-to-size trade-off as the resolution options.

'Exposure' refers to the amount of time that light strikes the CCD array for each line section of the scan. The higher the exposure level, which ranges from 10 to 40 milliseconds on the VXR-12, the more light passes through the film, and so the lighter the image that results. The choice of exposure depends on how light the final image is desired, and whether too high an exposure will cause detail to be lost in the lighter regions of the film[122].

'Dark Enhance' can be used to lighten the image further or to increase the contrast in dark regions of the film image. 'Line Averaging' can increase the

signal-to-noise ratio, improving the greyscale accuracy, which results in better image clarity[122].

The digitiser can be calibrated, in which the white and black levels are calibrated and pixel-to-pixel variations in either end of the greyscale are compensated for, to produce an even scan[122].

Once the image is stored digitally, the Osiris software can be used to manipulate and measure the data. The software was used in this project to measure the relOD in specific areas of interest (usually the isocentre of treatment) on the films. New software called ImageJ, which is a Java-based program that has been designed to offer more versatility than the rather basic Osiris software, was also used for the analysis of the film.

Chapter 4: Ionisation Chamber Tests

4.1 Aim - Ionisation Chamber Tests

The aim of testing the ionisation chambers and electrometer was to evaluate their response to dose distributions typical of those delivered in an IMRT treatment. Most ionisation chamber use in dosimetry has been with standard open fields, or larger modified fields with gradual gradients (such as those created by wedges), and a standard dosimetry delivery of around 100 to 200 cGy. IMRT fields tend to be smaller, more irregular with steep dose gradients, and may deliver a very small dose.

A particular disadvantage of using an ionisation chamber to measure IMRT fields is the volume averaging effect (see '3.3.1 Ionisation Chambers'). This means that if the ionisation chamber is placed in a high dose gradient region, or at a dose junction, there is no way of telling the actual makeup of the measured region. The small IC 10 (0.14 cc capacity) chamber was to be tested in small fields, in comparison with a chamber of less volume and with an XV film, in order to quantify the volume effect.

The direction of the incident beam can affect the ionisation chamber because it's shape means it does not collect dose uniformly. Normally the ionisation chamber would be positioned so that the axis of the beam is incident perpendicular to the axis of the ionisation chamber. However the first IMRT treatment planned, which was for clinical 'Case 2' (see '6.4 Case 2 Dosimetry'), had one non-coplanar beam where the couch was set to 90° so that the axis of the beam was angled perpendicular to the other nine beams. Without changing the position of the ionisation chamber during treatment it would not be possible to direct all of the beams perpendicular to the axis of the chamber. It is anticipated that future IMRT treatments will involve more non-coplanar beams, so it was very important to establish the effect of the orientation of the beam in relation to the ionisation chamber. The ionisation

chambers were to be tested for dose response to various orientations in relation to the incident radiation beam.

Ionisation chambers should give a nearly perfect linear dose response, so that several dose calibrations can be interpolated to give a complete calibration scale. Ionisation chambers do not save the charge they collect from incident radiation so they have no theoretical saturation limit. Electrometers do have a limit in terms of charge collected, but this should not be reached during normal dosimetry use.

Two thimble ionisation chambers were to be evaluated – a 0.03 cc volume Scanditronix-Wellhöfer IC 10 chamber called the 'small' chamber, and a 0.6 cc volume NE 2571 chamber called the 'regular' chamber (details for these are outlined in '3.3.1 Ionisation Chambers'). Theoretically the smaller ionisation chamber should have the advantage of a decreased volume averaging effect. The larger ionisation chamber should have the advantage of a higher dose collection capacity.

The most commonly used chamber orientation, with the axis of the beam perpendicular to the axis of the chamber, was subsequently selected for use in IMRT dose calibrations. In this orientation the ionisation chambers were to be tested for linearity of dose response, including response to low doses, depth dependence, and what differences existed between the two chamber volumes.

When measuring the absorbed dose to water at a point of interest in an ionisation chamber a correction must be made for the perturbation of the beam in the air cavity. The effective point of measurement is displaced from the centre of the chamber, which effectively changes the depth of measurement. The effective point of measurement for an ionisation chamber with radius r is $0.75r$[44]. In practice this results in an effective point of

measurement of zero for the small chamber and approximately 2 mm for the regular chamber. It is not always possible to add an extra 2 mm of solid water to all of the sides of a cubic phantom, so the effect of not accounting for the effective point of measurement was to be measured for the regular ionisation chamber.

4.2 Method - Ionisation Chamber Tests

4.2.1 Method - Ionisation Chamber Set-Up

Because of the cylindrical shape of the ionisation chamber it must be positioned inside a specially drilled solid water slab. The space in the solid water fits the ionisation chamber neatly, with the physical centre of the chamber volume at the exact centre of the solid water (therefore, a separately machined piece of solid water is required for each type and size of chamber). Because the chamber itself is larger in diameter than the attached cord, the space where the cord follows the chamber into the solid water necessarily has an air gap around it. However, this is far enough from the measuring point of the ionisation chamber to be considered to have a negligible effect on measurements. The chamber was always set up so that the incident beam would not have to pass through the stem of the chamber.

Solid water can be placed on top of the holding slab to effectively position the ionisation chamber at any depth desired, within 1 mm. The holding slab itself is 2 cm thick, and contributes a fixed 1 cm of depth. The dimensions of the holding slab limit the depth of ionisation chamber measurement. In this case, because the length and width dimensions of the solid water blocks are 30 cm × 30 cm, the only depth at which measurements through the length of the ionisation chamber can be made is 15 cm.

A cubic phantom with dimensions 30 cm × 30 cm × 30 cm was made up from the solid water. The ionisation chamber was positioned inside the phantom and micropore tape used to hold it in place.

To perform calibration measurements perpendicular to the axis of the chamber the gantry and collimator were positioned at zero degrees, which means the gantry was upright. The ionisation chamber in the phantom was positioned at the centre of the field and the appropriate depth of solid water

added on top. A diagram of the ionisation chamber in the solid water phantom positioned perpendicular to the beam axis is shown in Figure 4.1. The surface of the phantom was set to 100 cm SSD using the optical distance indicator (ODI), physical front pointer and lasers. Measurements were performed primarily at 1.5 cm depth and 15 cm depth (hereafter designated as 'perpendicular-1.5cm' and 'perpendicular-15cm' set-ups respectively) and at various other depths to test the depth dependence of the chamber.

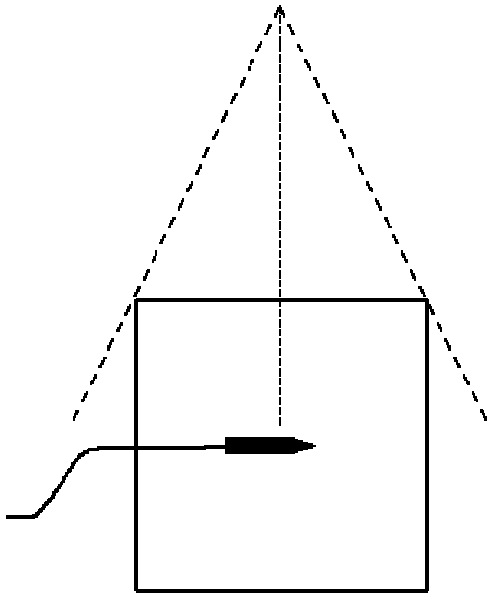

Figure 4.1. The set-up of the ionisation chamber in the solid water phantom with the beam incident perpendicular to the axis of the chamber.

To perform measurements parallel to the axis of the ionisation chamber the gantry was rotated to 90°. The phantom was repositioned so that the axis of the ionisation chamber would be aligned parallel to the axis of the beam, with the end of the chamber facing the beam output, and so that the side surface of the phantom was now at 100 cm SSD. A diagram of the ionisation chamber in the solid water phantom positioned parallel to the beam axis is shown in Figure 4.2. Due to the physical restriction of placing the chambers

inside solid water slabs, the parallel measurements could only be performed at 15 cm depth, and are hereafter designated as the 'parallel-15cm' set-up.

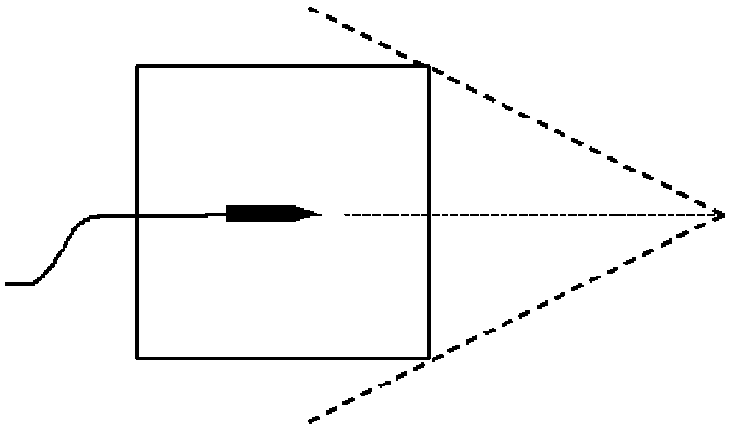

Figure 4.2. The set-up of the ionisation chamber in the solid water phantom with the beam incident parallel to the axis of the chamber.

4.2.2 Method - Ionisation Chamber Dose Measurements

The ionisation chamber was attached to an electrometer outside the treatment bunker so that measurements could be collected from the control room. 6 MV photons were used for all measurements, as this is the only energy that was used for the IMRT plans. As a minimal warm-up for the ionisation chamber and electrometer the chamber was exposed to approximately 500 MUs before any measurements were taken. In an attempt to keep the temperature of the solid water as regular as possible so that discrepancies between the measured air temperature and the actual temperature of the ionisation chamber in the solid water were minimised, the solid water was stored inside the treatment room whenever possible.

The ionisation chamber was exposed to the designated dose with the appropriate field size in the appropriate orientation. For calibration purposes the field size was set to 10 cm × 10 cm, which is the field size at which the linac is calibrated to give 1 cGy per MU at d_{max}. There was no need to enter the treatment room during the measurements unless the set-up itself needed changing, and the charge measurements could be collected in real time. Each charge measurement was taken three times and averaged. To obtain a dose delivery of 100 cGy nominally 100 MU was delivered for each charge but this was tailored to the dose per MU, which changes with depth, using data from percentage depth dose tables.

To assess the magnitude of the difference between the effective and the physical point of measurement 100 MU was delivered to the regular ionisation chamber at 1.5 cm physical depth, which is an effective depth of 1.3 cm, and at 1.7 cm physical depth, which is an effective depth of 1.5 cm, which is d_{max}. The measurements were repeated with physical depths of 5.0, 10.0 and 15.0 cm, and with the 2 mm added to each depth. For all

measurements the SSD was set to 100 cm, and percentage depth dose tables used to calculate the dose delivered to 1.5, 5, 10 and 15 cm depth.

To create a calibration curve the results collected were plotted against the dose delivered using Microsoft Excel and an equation formed relating them. In order to form comparisons between the ionisation chambers the results were normalised to a maximum value of one.

Testing the difference between orientations was a very important test, and discrepancies likely to be small in any case. To establish whether a difference occurred, when performing measurements for the comparison of the orientations of the ionisation chamber all of the readings were taken on the same day so as to avoid errors caused by fluctuations of pressure and temperature.

To qualify the volume effect on the small chamber, a dose profile scan of a 3 cm x 3 cm field was performed in a water tank. Measurements were taken at d_{max} of 1.5 cm, 10 cm, and 20 cm depths. The results were compared to those for a smaller chamber - a Scanditronix-Wellhöfer CC01 chamber, with a 0.01 cc effective volume and an inner radius of 1.0 mm. XV film was also exposed at d_{max} in solid water and digitised on the Vidar VXR-12 film scanner. A dose profile was measured across the centre of the field and the results compared to those of the ionisation chambers.

4.3 Results - Ionisation Chamber Tests

Although there is not room to show this in the tables, it should be noted that when each measurement was carried out three times and averaged, each time all of the readings were very close together, indicating a good daily reproducibility of ionisation chamber results. The tables and plots referred to in each section are shown following that particular section.

4.3.1 Results - Effective Point of Measurement

Table 4.1 gives the results of testing the effective point of measurement of the regular ionisation chamber. It shows the measurements for a 10 cm x 10 cm field at the depths desired, and the depths with the 2 mm of solid water added to account for the effective point of measurement. The dose delivered was calculated from beam data tables for the desired depth of measurement, and the charge readings were all averaged from three measurements each. The difference between the two measurements at each 'depth' was calculated as a percentage value.

The results measured at d_{max} are very close together. The difference between the measurements made with and without the effective point of measurement is 0.1, which is -0.13%. 0.1 represents the limit of reading of the electrometer, so the difference is practically negligible. The difference increases with depth, up to a charge reading of -0.7 or -1.34% at 15 cm, which is the depth at which the chamber would have to be calibrated in the parallel set-up. This is still a fairly good result, and overall the results show that if necessary the effective point of measurement can be disregarded when performing measurements on the cubic phantom. Since the closest results were for measurements performed at 1.5 cm and 1.7 cm depth, if the effective point of measurement is to be ignored, preferably calibrations should be performed at 1.5 cm depth.

The assumption that the effective depth is equivalent to the physical depth causes no more than a 1.34% difference at 15 cm depth. The actual difference will depend on field size, segment size etc. and will vary. This correction was not applied to the reported readings in this thesis.

Table 4.1. Effect of effective point of measurement on regular ionisation chamber.

Depth (cm)	Dose Delivered (cGy)	Charge Reading	Reading Difference (%)
1.5	100.0	103.2	
1.7	100.0	103.1	-0.13
5.0	85.9	89.1	
5.2	85.9	88.0	-1.26
10.0	66.8	68.4	
10.2	66.8	67.5	-1.25
15.0	51.5	51.6	
15.2	51.5	50.9	-1.34

4.3.2 Results - Regular Ionisation Chamber Calibration

Tables 4.2, 4.3 and 4.4 and Figure 4.3 give the experimental results for the calibration of the regular ionisation chamber in different set-ups. Table 4.5 compares the results for the perpendicular-15cm and parallel-15cm set-ups. The plot in Figure 4.3 is a plot of the uncorrected readings versus dose delivered for each chamber set-up. Lines of fit were added using Microsoft Excel, with a set intercept of zero, and the corresponding equations are given in the appropriate tables.

From the plot it appears that the response of the regular ionisation chamber is very linear in relation to the dose delivered. The orientation and depth of measurement of the ionisation chamber also does not appear to significantly affect the results.

The tables of calibration results for each of the set-ups show the dose delivered and average uncorrected charge reading for each dose point of the ionisation chamber. A line of fit was used to create an equation for calculating the dose from a given charge reading; this is shown at the bottom of the table. Using this equation a dose value was calculated from the measured charge readings. The dose delivered was compared to the dose calculated in order to evaluate the closeness of the line of fit. This is presented as a dose difference and a percentage difference.

As can be seen from Table 4.2 for the perpendicular-1.5cm set-up, the deviations of the measured values from the lines of fit are very small. The largest dose difference is ±0.1 cGy for the 150, 175, 200, 250 and 600 cGy dose points. The largest percentage difference is 0.1%, for just three points of measurement (25 cGy, 50 cGy and 250 cGy). Where the dose difference is zero even though a percentage difference is not, and vice versa, this is because the results shown have been rounded down to one decimal place.

For the perpendicular-15cm set-up (Table 4.3) the largest dose difference is ±0.2 for many dose points, and the largest percentage difference is ±0.3% for the 50 cGy and 75 cGy dose points. The highest difference for the parallel-15cm set-up (Table 4.4) is 0.3 cGy or 0.6% for the 50 cGy dose point, and 0.1 cGy or 0.4% for the 25 cGy dose point. It should be noted that the higher percentage deviations are all around the lower dose points, which means that a difference of just 0.3 cGy between the reading and the calculated fit resulted in a percentage deviation of 0.6% at the 50 cGy dose point for the parallel orientation at 15 cm depth. Towards the higher dose points the percentage differences are either zero or a negligible 0.1%, and the maximum difference between the delivered and calculated doses is 0.2.

The low deviations of the measurements from the line of fit indicate that the dose response of the ionisation chamber is very linear, making direct interpolation of results, and calculation of relative doses, a straightforward matter.

Table 4.5 shows the uncorrected charge readings for the measurements made at 15 cm depth in the perpendicular and parallel orientations. The differences between the set-ups are given as charge readings and percentage values. The charge differences increase as the dose increases, reaching a maximum of -0.018 for the 500 and 600 cGy dose points. The maximum percentage difference between the two orientations is -0.3% for most points, which is very acceptable. In fact, the difference between the two equations from the lines of fit is insignificant, with a difference between them of less than 0.5%, indicating that the ionisation chamber can be reliably used in either orientation to produce similar readout results.

Table 4.2. Results for calibration of regular ionisation chamber, perpendicular orientation, 1.5 cm depth.

Perpendicular-1.5cm				
Dose Delivered (cGy)	**Uncorrected Charge Reading**	**Dose Calculated from Line of Fit**	**Dose Difference (cGy)**	**Percentage Difference (%)**
0	0.000	0.0	0.0	
25	0.261	25.0	0.0	0.1
50	0.521	50.0	0.0	-0.1
75	0.781	75.0	0.0	0.0
100	1.042	100.0	0.0	0.0
125	1.302	125.0	0.0	0.0
150	1.562	149.9	-0.1	0.0
175	1.824	175.1	0.1	0.0
200	2.083	199.9	-0.1	0.0
225	2.344	225.0	0.0	0.0
250	2.603	249.9	-0.1	-0.1
300	3.126	300.0	0.0	0.0
400	4.167	400.0	0.0	0.0
500	5.209	500.0	0.0	0.0
600	6.251	600.1	0.1	0.0

Equation for line of fit: D = R/0.010418

Table 4.3. Results for calibration of regular ionisation chamber, perpendicular orientation, 15 cm depth.

Perpendicular-15cm				
Dose Delivered (cGy)	**Uncorrected Charge Reading**	**Dose Calculated from Line of Fit**	**Dose Difference (cGy)**	**Percentage Difference (%)**
0	0.000	0.0	0.0	
25	0.262	25.1	0.1	0.2
50	0.525	50.2	0.2	0.3
75	0.783	74.8	-0.2	-0.3
100	1.046	99.9	-0.1	-0.1
125	1.309	125.0	0.0	0.0
150	1.571	150.1	0.1	0.1
175	1.830	174.8	-0.2	-0.1
200	2.092	199.8	-0.2	-0.1
225	2.355	225.0	0.0	0.0
250	2.618	250.1	0.1	0.0
300	3.140	300.0	0.0	0.0
400	4.189	400.2	0.2	0.0
500	5.234	500.0	0.0	0.0
600	6.280	599.9	-0.1	0.0

Equation for line of fit: D = R/0.010468

Table 4.4. Results for calibration of regular ionisation chamber, parallel orientation, 15 cm depth.

Parallel-15cm				
Dose Delivered (cGy)	**Uncorrected Charge Reading**	**Dose Calculated from Line of Fit**	**Dose Difference (cGy)**	**Percentage Difference (%)**
0	0.000	0.0	0.0	
25	0.262	25.1	0.1	0.4
50	0.525	50.3	0.3	0.6
75	0.781	74.9	-0.1	-0.2
100	1.044	100.0	0.0	0.0
125	1.305	125.0	0.0	0.0
150	1.567	150.2	0.2	0.1
175	1.825	174.9	-0.1	-0.1
200	2.085	199.8	-0.2	-0.1
225	2.349	225.0	0.0	0.0
250	2.610	250.1	0.1	0.0
300	3.131	300.0	0.0	0.0
400	4.175	400.1	0.1	0.0
500	5.216	499.8	-0.2	0.0
600	6.262	600.0	0.0	0.0

Equation for line of fit: D = R/0.010436

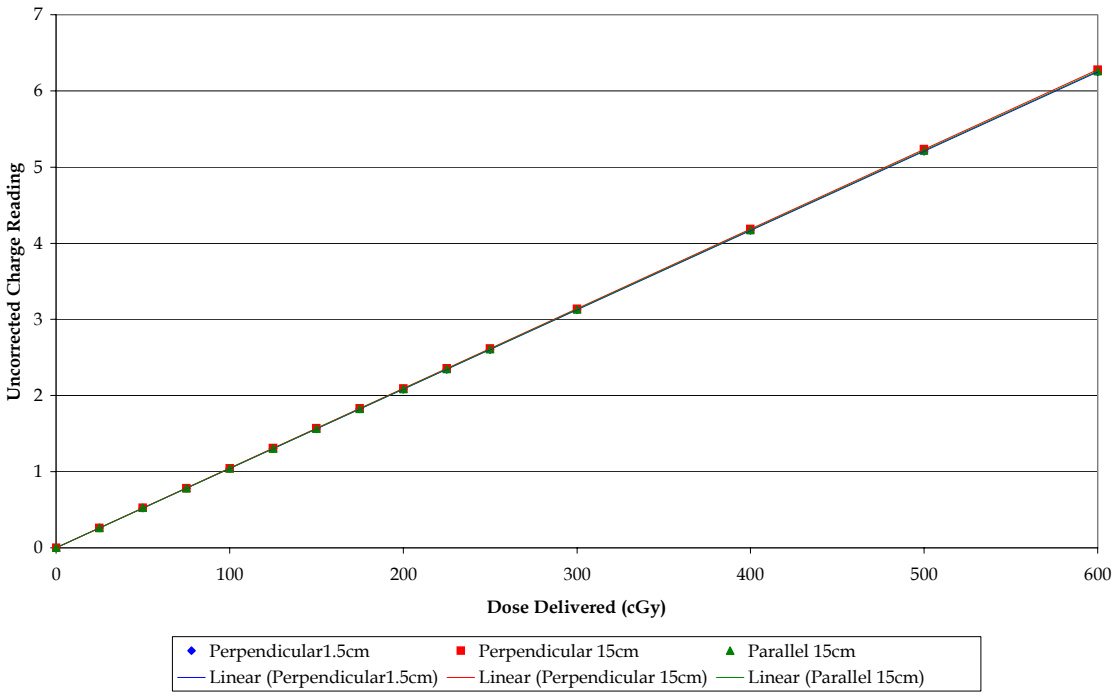

Figure 4.3. Results for calibration of the regular ionisation chamber in all set-ups.

Table 4.5. Comparison of results for calibration of regular ionisation chamber, perpendicular and parallel orientations, 15 cm depth.

Dose Delivered (cGy)	Perpendicular Charge Reading	Parallel Charge Reading	Charge Reading Difference	Percentage Difference (%)
0	0.000	0.000	0.000	
25	0.262	0.262	0.000	-0.1
50	0.525	0.525	0.000	0.0
75	0.783	0.781	-0.001	-0.2
100	1.046	1.044	-0.002	-0.2
125	1.309	1.305	-0.004	-0.3
150	1.571	1.567	-0.004	-0.3
175	1.830	1.825	-0.005	-0.3
200	2.092	2.085	-0.007	-0.3
225	2.355	2.349	-0.006	-0.3
250	2.618	2.610	-0.008	-0.3
300	3.140	3.131	-0.009	-0.3
400	4.189	4.175	-0.014	-0.3
500	5.234	5.216	-0.018	-0.3
600	6.280	6.262	-0.018	-0.3

4.3.3 Results - Small Ionisation Chamber Calibration

Tables 4.6, 4.7 and 4.8 and Figure 4.4 give the experimental results for the calibration of the small ionisation chamber in different set-ups. Table 4.9 compares the results for the perpendicular-15cm and parallel-15cm setups. The plot in Figure 4.4 is a plot of the uncorrected readings versus dose delivered for each chamber set-up. Lines of fit were added using Microsoft Excel, with a set intercept of zero, and the corresponding equations are given in the appropriate tables.

From the plot the response of the small ionisation chamber to dose appears to be very linear. This is further shown in Table 4.6, where it can be seen that the largest deviation for the perpendicular-1.5cm set-up is -0.2 cGy for the 150, 500 and 500 cGy dose points. The highest percentage deviation is -0.5% for the 25 cGy dose point. The largest deviations for the perpendicular-15cm set-up are 0.6 cGy or 1.2% for the 50 cGy dose point, and 0.4 cGy or 1.6% for the 25 cGy dose point. The largest deviations for the parallel-15cm set-up are -0.5 gy or -0.6% for the 75 cGy dose point, and -0.4 cGy for the 175, 500 and 600 cGy dose points.

These discrepancies tend to be slightly higher than for the regular ionisation chamber. As explained for the regular ionisation chamber previously, the higher percentage differences at lower dose points – i.e. at lower readings – would be inflated by the fact that very low readings tend to result in higher percentage differences, and because the limit of reading of the electrometer affects the accuracy of the reading. Hence, at lower dose points, the small chamber would give more variable results because it does not collect as much charge as the regular chamber, so its readings are closer to the limit of reading of the electrometer.

Similar to the regular ionisation chamber, the acceptably low deviations of the measurements from the normal line of fit indicate that the small

ionisation chamber can be reliably used as a dosimeter in either orientation, and easily calibrated.

Table 4.9 shows the uncorrected charge readings for the measurements made at 15 cm depth in the perpendicular and parallel orientations. The differences between the two orientations are quite large, ranging from -1.0% at the 600 cGy dose point, to -2.4% at the 25 cGy dose point. These differences are relatively higher than the same calculations for the regular ionisation chamber, possibly due to the reduced collection efficiency of the smaller chamber. Although the differences are not unacceptably large, some care must be taken when using the small ionisation chamber to measure in both parallel and perpendicular orientations.

Table 4.6. Results for calibration of small ionisation chamber, perpendicular orientation, 1.5 cm depth.

Perpendicular 1.5cm				
Dose Delivered (cGy)	**Uncorrected Charge Reading**	**Dose Calculated from Line of Fit**	**Dose Difference (cGy)**	**Percentage Difference (%)**
0	0.000	0.0	0.0	
25	0.013	24.9	-0.1	-0.5
50	0.025	49.9	-0.1	-0.2
75	0.038	75.0	0.0	0.1
100	0.051	100.0	0.0	0.0
125	0.063	124.9	-0.1	-0.1
150	0.076	149.8	-0.2	-0.2
175	0.088	174.9	-0.1	-0.1
200	0.101	200.0	0.0	0.0
225	0.114	225.1	0.1	0.1
250	0.126	249.9	-0.1	0.0
300	0.152	300.0	0.0	0.0
400	0.202	400.0	0.0	0.0
500	0.252	499.8	-0.2	0.0
600	0.303	599.8	-0.2	0.0

Equation for line of fit: D = R/0.000505

Table 4.7. Results for calibration of small ionisation chamber, perpendicular orientation, 15 cm depth.

Perpendicular 15cm				
Dose Delivered (cGy)	**Uncorrected Charge Reading**	**Dose Calculated from Line of Fit**	**Dose Difference (cGy)**	**Percentage Difference (%)**
0	0.000	0.0	0.0	
25	0.013	25.4	0.4	1.6
50	0.026	50.6	0.6	1.2
75	0.038	75.2	0.2	0.3
100	0.051	100.2	0.2	0.2
125	0.063	125.4	0.4	0.3
150	0.076	150.4	0.4	0.3
175	0.088	175.0	0.0	0.0
200	0.101	200.4	0.4	0.2
225	0.114	225.2	0.2	0.1
250	0.126	250.4	0.4	0.2
300	0.151	300.2	0.2	0.1
400	0.202	400.1	0.1	0.0
500	0.252	499.9	-0.1	0.0
600	0.302	599.6	-0.4	-0.1

Equation for line of fit: D = R/0.000504

Table 4.8. Results for calibration of small ionisation chamber, parallel orientation, 15 cm depth.

Parallel 15cm				
Dose Delivered (cGy)	**Uncorrected Charge Reading**	**Dose Calculated from Line of Fit**	**Dose Difference (cGy)**	**Percentage Difference (%)**
0	0.000	0.0	0.0	
25	0.013	25.1	0.1	0.2
50	0.025	50.1	0.1	0.2
75	0.037	74.5	-0.5	-0.6
100	0.050	99.8	-0.2	-0.2
125	0.062	124.8	-0.2	-0.1
150	0.075	150.3	0.3	0.2
175	0.087	174.6	-0.4	-0.2
200	0.100	199.8	-0.2	-0.1
225	0.112	224.8	-0.2	-0.1
250	0.125	249.9	-0.1	0.0
300	0.150	299.7	-0.3	-0.1
400	0.200	399.8	-0.2	-0.1
500	0.249	499.6	-0.4	-0.1
600	0.299	599.6	-0.4	-0.1

Equation for line of fit: D = R/0.000499

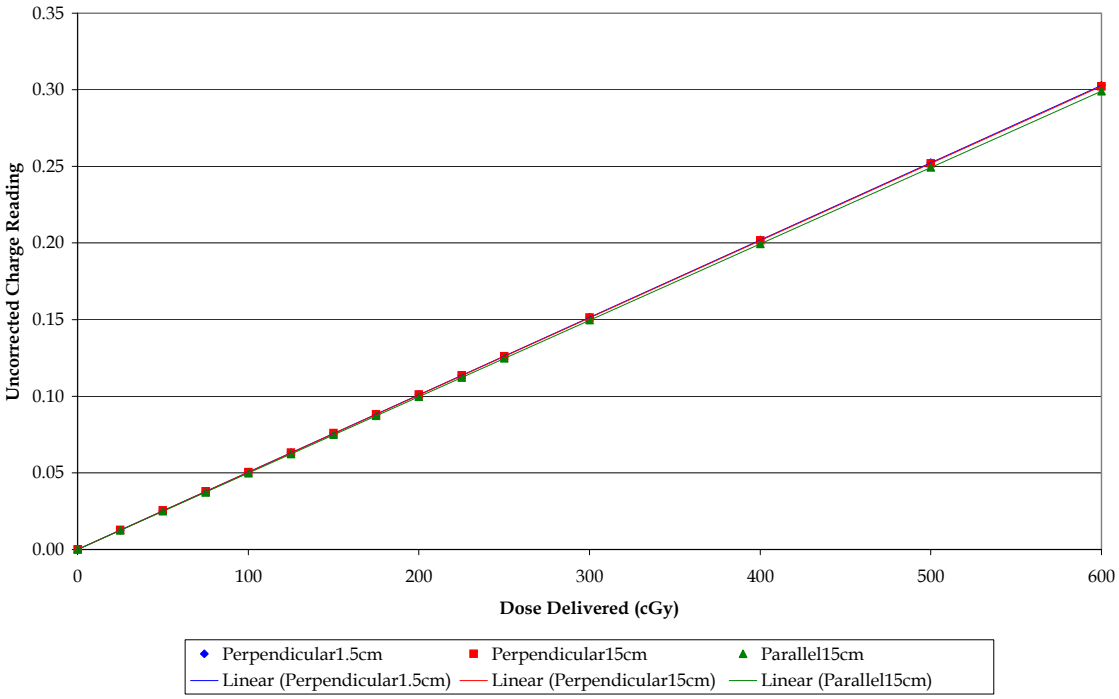

Figure 4.4. Results for calibration of the small ionisation chamber in all set-ups.

Table 4.9. Comparison of results for calibration of small ionisation chamber, perpendicular and parallel orientations, 15 cm depth.

Dose Delivered (cGy)	Perpendicular Charge Reading	Parallel Charge Reading	Charge Reading Difference	Percentage Difference (%)
0	0.000	0.000	0.000	
25	0.013	0.013	0.000	-2.4
50	0.026	0.025	0.000	-2.0
75	0.038	0.037	-0.001	-1.9
100	0.051	0.050	-0.001	-1.4
125	0.063	0.062	-0.001	-1.4
150	0.076	0.075	-0.001	-1.1
175	0.088	0.087	-0.001	-1.2
200	0.101	0.100	-0.001	-1.3
225	0.114	0.112	-0.001	-1.2
250	0.126	0.125	-0.002	-1.2
300	0.151	0.150	-0.002	-1.2
400	0.202	0.200	-0.002	-1.1
500	0.252	0.249	-0.003	-1.1
600	0.302	0.299	-0.003	-1.0

4.3.4 Results - Ionisation Chamber Volume Comparison

Table 4.10 shows the combined results for the regular and small ionisation chambers in the perpendicular orientation at 15 cm depth, with the doses measured normalised to a maximum of one for the purposes of comparison. The measurements in each orientation are compared as a percentage difference. Figure 4.5 shows a plot of the normalised results of the small ionisation chamber and the regular ionisation chamber versus dose. Lines of fit have been added to each plot, with the intercept set to zero.

Looking at Figure 4.5 little difference can be distinguished between the small and the regular ionisation chamber. According to Table 4.10, the largest difference between the small and the regular ionisation chambers is -0.4% for the 75 cGy dose point. The next highest discrepancy is -0.3% for the 50 cGy dose point. The very low differences between corrected readings for the small ionisation chamber and the regular ionisation chamber indicate a good reproducibility of results, and mean that the chambers could be comparatively interchanged for measurements without affecting corrected results, and that either chamber should be suitable for reliably measuring doses delivered.

Table 4.10. Comparison of results for calibration of regular and small ionisation chambers, perpendicular orientation, 15 cm depth.

Dose Delivered (cGy)	Normalised Regular Chamber Charge Reading	Normalised Small Chamber Charge Reading	Percentage Difference (%)
0	0.000	0.000	
25	0.042	0.042	-0.1
50	0.084	0.084	-0.3
75	0.125	0.124	-0.4
100	0.167	0.166	-0.2
125	0.208	0.208	-0.1
150	0.250	0.251	0.2
175	0.291	0.291	-0.1
200	0.333	0.333	0.1
225	0.375	0.375	0.0
250	0.417	0.417	0.0
300	0.500	0.500	0.0
400	0.667	0.667	0.0
500	0.833	0.833	0.0
600	1.000	1.000	0.0

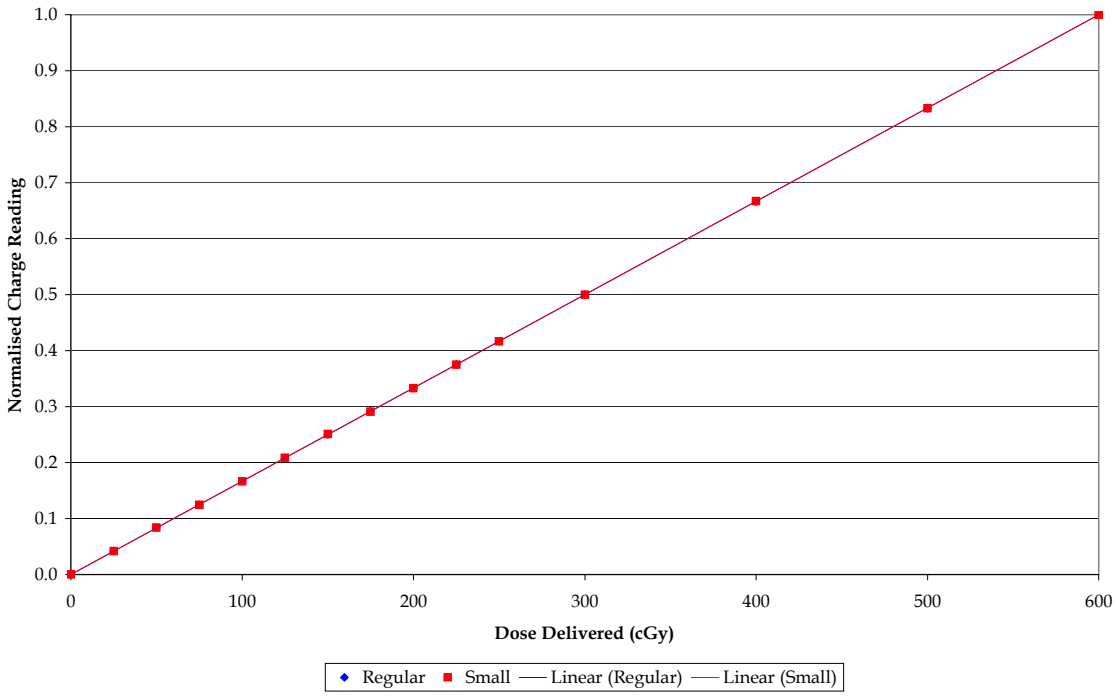

Figure 4.5. Results for the regular and small ionisation chambers, normalised to 1.0, perpendicular orientation at 15 cm depth.

4.3.5 Results - Small Field Dose Profiles

Figures 4.6 and 4.7 and 4.8 give the experimental results for the small field dose profile scans using the small chamber, the 0.01 cc (CC 01) chamber, and the XV film at depths of 1.5 cm (d_{max}), and the small chamber and the CC 01 chamber at depths of 10 cm and 20 cm.

The figures show that the XV film at 1.5 cm depth measures a steeper drop-off in dose towards the edges of the field than the small chamber does. This is to be expected as the film has a much higher spatial resolution capability than the ionisation chambers used (see '3.3.3 Film').

The smaller 0.01 cc chamber in turn measures a steeper drop-off dose than the small IC 10 chamber. This indicates that the volume of the ionisation chamber will have an effect on measurements at the edges of small fields. This effect remains at all depths measured.

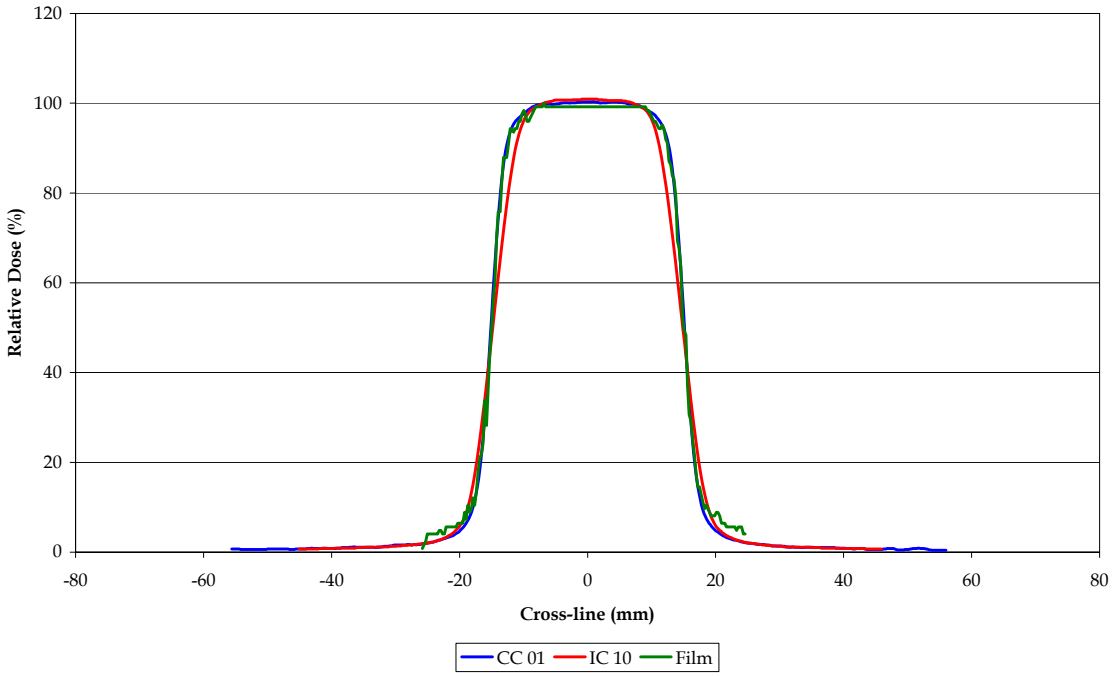

Figure 4.6. Results for the small chamber, CC 01 chamber and XV film dose profile measurements at 1.5 cm depth.

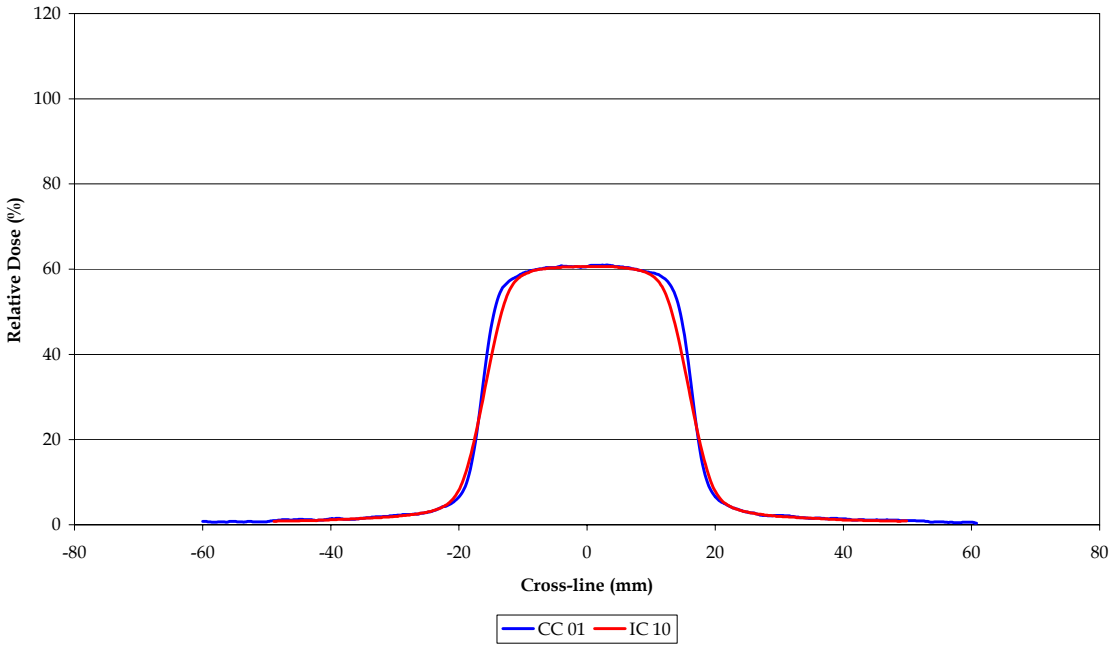

Figure 4.7. Results for the small chamber and CC 01 chamber dose profile measurements at 10 cm depth.

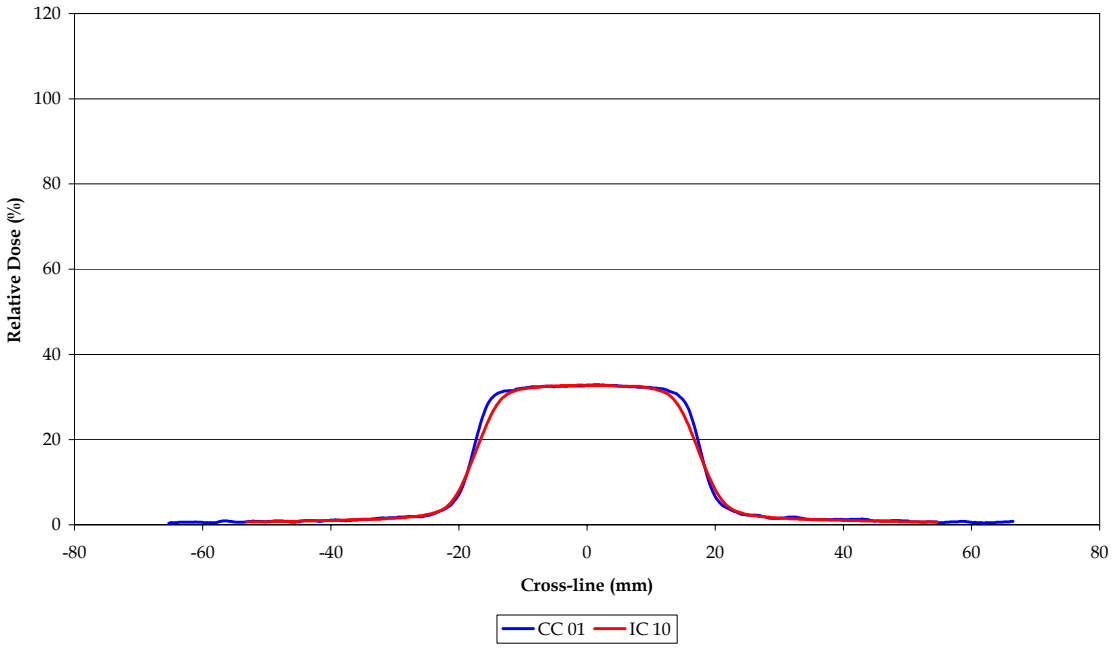

Figure 4.8. Results for the small chamber and CC 01 chamber dose profile measurements at 20 cm depth.

4.4 Conclusion - Ionisation Chamber Tests

Based on the results the ionisation chamber has been shown to be a very reliable dosimeter, with reproducible results and a linear dose response so that dose values can be easily calculated from relatively few dose points.

Disregarding the effective point of measurement for the regular ionisation chamber is not ideal, but it will be done for the IMRT checks in order to avoid the difficulty of adding 2 mm to each side of the phantom.

Although the set-up of the ionisation chamber in the solid water limits positioning, this should not be a problem for IMRT checks as any plan can be easily adjusted to calculate the dose at the centre of a block of solid water, or if necessary at variable depths. The parallel set-up showed little variation in results compared to the perpendicular set-up, which means that measurements can be translated between the two.

The two different ionisation chambers produced very similar results. The difference is that the smaller dimensions of the small ionisation chamber makes it easier to avoid the high dose gradient regions that contribute to dose measurement uncertainties. However, the small ionisation chamber does not have the dose collection efficiency of the regular ionisation chamber, so it will not be suitable for the small dose outputs that are common with single IMRT fields.

The volume averaging effect evident in the small chamber dose profile measurements indicates that the regular chamber will be less accurate measuring dose in a small field or at the edge of a field than measurements taken using the small chamber.

Therefore the choice of which ionisation chamber to use for IMRT dosimetry will depend on the more important aspects of the dose being measured – if a

plan consists of high dose gradients from individual beams at isocentre, the small ionisation chamber should be best for measuring a whole fraction of treatment. Because of its larger collection volume and hence higher sensitivity, the regular ionisation chamber should be suitable for measuring individual beams if small doses per field are being delivered where the dose gradient does not tend to be so pronounced. Laub *et al*.[57] found differences of more than 6% between measured and calculated values of IMRT fields measured with a 0.6 cm^3 Farmer ionisation chamber. The difference was reduced to 2% when measured with a 0.015 cm^3 pinpoint ionisation chamber. Low *et al*.[67] found errors of up to 10% for a 0.6 cm^3 Farmer ionisation chamber, indicating that the smaller chamber is more suitable for small fields, or that a correction factor should be introduced when using the larger chamber. Because it is difficult to know the proportion of the chamber that was on the edge of a leaf or in a dose gradient no volume averaging correction methods were employed.

Chapter 5: Film Tests

5.1 Aim - Film Tests

The purpose of the film tests was to evaluate the response of radiographic film to dose deliveries typical of an IMRT treatment. Film is often used in radiotherapy as a qualitative assessment tool – that is, as a tool for dose comparison and two-dimensional imaging, as opposed to dose measurement. Film is not widely regarded as an absolute dosimeter, and is limited by a saturation range. However, with the right processing and analysis equipment some centres do use film quantitatively.

Two types of film were to be tested. X-Omat V (XV) is the most common film normally used in radiotherapy, and is regularly used for port films, but it is traditionally limited by a dose saturation limit of about 100 cGy. The more recently developed EDR2 film is similar to XV film but has a higher saturation limit of about 600 cGy, which should make it more useful for measuring combined fields. However this may prove to be a disadvantage as the film might under-respond to low doses, which are generally characteristic of the individual beams in an IMRT plan.

XV film has been in use for longer than the EDR2 film, so its properties are better established (see '3.3.4 Kodak X-Omat V'). However, both types of film were to be tested for linearity of response, response to low doses, response to orientation relative to the beam axis, depth of exposure, and dose saturation limit.

5.1.1 Aim - Step Film Test

The 'Step Test Film' (STF) is a strip of film supplied by Kodak on which are marked 21 regular stripes, or steps, of known ODs. The ODs range from 0.05 to 3.05 in 0.15 increments. The idea of the STF is that it can be used to calibrate film digitisers to accurate ODs.

In this case the conversion test was to be carried out primarily in order to verify the regularity of the film digitiser and software. It was mentioned in '3.3.7 Vidar Film Scanner' that the Vidar VXR-12 scanner has been found to produce results that are too noisy to be accurate at ODs greater than 2.0, so this would also be looked at.

5.1.2 Aim - Film Orientation Tests

The simplest set-up for film was the perpendicular orientation, where the film was positioned with its surface perpendicular to the axis of the beam. A diagram of the film in the solid water phantom positioned perpendicular to the beam axis is shown in Figure 5.1. This set-up was useful for planar dose map measurements and dose profiles at a single depth because the full cross-section of the beam could reach the film, providing a relatively large area with which to analyse the beam.

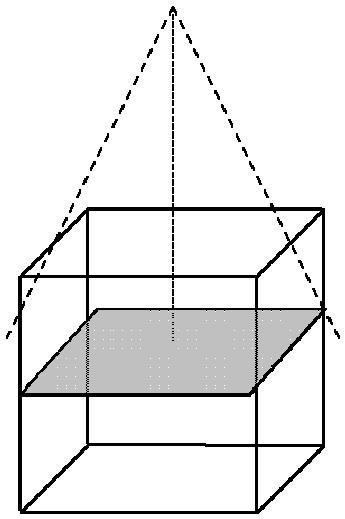

Figure 5.1. The set-up of the film in the solid water phantom with the beam incident perpendicular to the plane of the film.

The second type of orientation set-up to be used was parallel, where the film was positioned parallel to the axis of the beam. A diagram of the film in the solid water phantom positioned parallel to the beam axis is shown in Figure 5.2. Theoretically this technique was optimal because it was the same set-up as would have to be used to expose films to mimic axial isodose distributions. The parallel set-up could be delivered with a gantry angle of zero, with the cubic phantom set on end, and with the gantry angle at 90° or 270°, with the phantom set flat. A variation of the parallel set-up was also to

be tested where the film was aligned 2° off the parallel axis of the beam. Setting the film 2° off-axis is recommended[78] because the angle is not great enough to significantly affect the effective depth at which the film would be irradiated, but should be enough that along the central axis the x-ray beam was attenuated by mostly solid water (as it should be) rather than by the film itself, which does not have the same density as solid water. A discussion of this effect can be found in Suchowerska *et al.*[111].

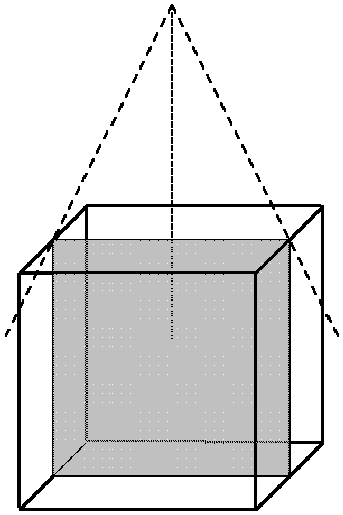

Figure 5.2. The set-up of the film in the solid water phantom with the beam incident parallel to the plane of the film.

5.1.3 Aim - Film Dose Response Tests

The dose response of the films was to be found by plotting the results of the relOD of the films against the dose delivered. Although the film does not have to provide linear dose plots, the important feature to be checked was that the results were regular relative to each other. Also it was desirable to find a dose response to which a simple curve and equation could be fitted, so that further translations between the relOD measured and the dose received could be calculated using a set equation for each calibration group, rather than attempting to manually match the dose on a plot.

The limits of exposure of the films refers to finding the maximum dose to which they can be irradiated before the film saturates, at which point a nominal plateau in film OD increase with dose is reached. The limit of exposure defines the useful dose range of the film.

Similarly, to study the low dose response, the films were to be exposed to a range of lower doses, and the relOD plotted against dose delivered. Finding the low dose response of the films was of particular importance in this project because of the very low doses produced by many of the beams in an IMRT plan, so it was important to ensure that the films did not under- or over-respond in these regions, or gave irregular responses.

5.1.4 Aim - Film Scanner Tests

The Vidar VXR-12 film scanner can digitise film with several different settings. Exposure, resolution and greyscale level (see '3.3.7 Vidar Film Scanner') can be manipulated to optimise the resultant image. In an attempt to find the best scanner settings the perpendicular EDR2 calibration films were digitised and analysed with different exposure, resolution and depth bit (greyscale) settings.

Scanning film with 8-bit depth limits the number of greyscale levels available in comparison to 12-bit depth, and might not provide sufficient dose contrast resolution for analysing the steep dose gradients present in IMRT dose distributions.

5.2 Method - Film Tests

5.2.1 Method - Film Preparation

The sheets of XV and EDR2 film come individually wrapped in protective packets designed to protect them from light, dust, and environmental factors. XV film is 34 cm × 43 cm, EDR2 film is 37 cm × 45 cm as measured by the outer packet. Because the size of the film makes it unnecessary and wasteful to perform one calibration per sheet, each sheet was cut to size before use.

To reduce discrepancies in results arising from variations in the film that occur during production (for example the thickness of the emulsion layer), the films to be used for the one set of calibrations and measurements were taken from the same batch.

The film was prepared in a dark room with a red light, as this is not supposed to affect film. For perpendicularly exposed film the film was cut into rectangles, approximately 12 cm × 12 cm, for parallel film it was cut into strips at least a few centimetres longer than the intended depth of measurements; approximately 7 cm × 22 cm.

As each cut was made in the film the two open sides of the film wrap were sealed using black electrical tape. It had to be carefully folded over the exposed side, with small tags left overlapping at the ends, to stop any light reaching the film. At the same time as much air as was possible was removed from the packets.

5.2.2 Method - Film Exposure

To expose the films in the perpendicular orientation the gantry was set to zero degrees (that is, in the upright position, so that the axis of the beam would be aiming vertically down). A rectangular piece of film was positioned in the centre of the cubic solid water phantom and of the beam (using the field light crosshairs), so that 15 cm of solid water was below the film to block scattered x-rays, and 15 cm was placed on top of the film to provide the appropriate attenuation. To irradiate the film at different depths the appropriate amount of solid water could be removed to provide the depth required. The surface of the top of the solid water was set to 100 cm SSD. The film was exposed at 15 cm depth, designated as the 'perpendicular-15cm' set-up.

Because not all of the air in the film packets could be removed during preparation the weight of the solid water helped to push out some of the bubbles. Some packets unavoidably had a relatively large amount of air in them, which affects the attenuation and scatter of the incident beam, and provides an uneven base on which to place the top portion of solid water. Packets like this were discarded, or if that was not possible, a tiny pin prick was made in one corner so that the air could be expelled without allowing light to be incident on the central part of the film.

For the parallel exposures three set-ups were used – designated 'vertical-parallel', 'horizontal-parallel' and '2degree-parallel'. To expose the parallel film horizontally, the solid water was set up in the same way as for the perpendicular exposures. The gantry was set to 90°, so that the axis of the beam would be parallel to the floor. Because the phantom is a cube shape, the dimensions of the phantom relative to the beam output did not change from the perpendicular set-up. The strip of film was placed between the slabs of solid water, but this time one end of the film was positioned flush with the

edge of the solid water facing the beam output. The solid water was positioned so that the long plane of the film was aligned with the axis of the beam output, with the near edge at 100 cm SSD. To perform parallel measurements with a 2° offset the solid water and the film remained in the same set-up, but the gantry was rotated slightly to 88° or 92° to provide the angular incidence required.

The vertical exposure of the parallel film required the gantry to be positioned upright at zero degrees, and the solid water phantom was set on end. The phantom was still at 100 cm SSD, but the slabs of solid water were positioned on their edge. The strip of film was taped flush with the top surface of the solid water phantom, and positioned so that the long plane of the film would be aligned with the axis of the beam.

The calibration films were exposed to the dose desired. 6 MV photons were used for all measurements, as this is the only energy that was used for the IMRT plans. Because the perpendicular set-up was the simplest it was used for all of the film tests and the scanner tests other than orientation, so the perpendicular EDR2 film was exposed to zero to 250 cGy in increments of 25 cGy and a further 300 to 600 cGy in increments of 100 cGy. The parallel EDR2 films were exposed to zero to 600 cGy in increments of 100 cGy only, which was sufficient for purposes of comparison with the perpendicular exposures. The XV films, with their known lower saturation limit, were exposed to zero to 200 cGy in 25 cGy increments in the perpendicular orientation only.

The films were developed as soon as possible after exposure, and where possible in a single session, to eliminate errors that might arise from changes in the chemical mix or temperature of the processor. The processor was located in a dark room, so the film could be unwrapped under a special red light. To warm up the processor and mix up the chemicals inside, two to

three waste films were processed first, followed by the calibration films. The packets were opened and fed into the machine one at a time, so that if something went wrong, such as the developer or fixer running out and needing replacement, the main light could be turned on without having to worry about protecting a large number of unwrapped, unexposed films.

The developed films were collected and returned to their respective packets to help protect them from dust, scratches and fingerprints. The grease from handling the film with unprotected hands can affect the optical characteristics of the film, so care had to be taken to only pick them up by their edges.

The developed films could be stored and used or referred to at a later date. They were digitised on the Vidar VXR-12 film scanner using Osiris or ImageJ software, and the resultant images analysed using the same software. The films were analysed at 15 cm depth, which was equivalent to 15 cm along the length of the film.

5.2.3 Method - Scanner Tests

The developed films were scanned into a computer using the VXR-12 digitiser and stored as image files. The film was placed in the top feed tray of the digitiser, from which it was automatically drawn through the roller mechanism to be read. Various scan options could be selected including 8-bit or 12-bit resolution (which refers to the number of greyscale levels used), resolution, exposure, and calibration. The film could be pre-scanned in order to select only a part of the film to be properly scanned. Once the desired combination of options was selected the film was scanned and automatically saved. The same process was followed with the ImageJ software.

Each film was scanned three times over a number of days, in order to produce an average value for each calibration film. This also allowed occasional errors in the scanning process to be picked up in the form of erroneous results.

Using either Osiris or ImageJ the image files could be opened and a rectangular ROI selected at the appropriate point on each film image. The software could provide an average relOD for that area. To correct the films for background OD the value of the relOD of the 0 cGy film (that is, unexposed film) was subtracted from all results. Other ROI data that was provided by the digitising software was the standard deviation of the average relOD, the minimum and maximum and total relODs in that region, the relative position on the ROI in the image, and the size of the ROI. A histogram of the distribution of relODs in the ROI could also be obtained. This information was used to provide an informal check of the variation in relOD across the ROI.

The average corrected relODs were plotted against the known doses delivered to produce dose versus corrected relOD calibration curves. Using

Microsoft Excel a curve could be fitted to the results to obtain a calibration equation relating the corrected relOD to the dose.

The film images could be manipulated visually in order to make them easier to interpret or to make qualitative judgments. The scanner produced black and white images that appear opposite to the actual distribution of light and dark on the film, like a photograph negative. This meant that the higher dose parts of the dose distribution appear as the darkest regions on the film, but as the lightest regions on the digitised computer image. Using image manipulation software such as Osiris and ImageJ, the digitised image could be inverted to appear more similar to the actual film. To allow for easier qualitative interpretation of the film, the darkness of the image could be adjusted to provide better contrast in various areas of the film, and colour washes could be laid over the image to provide a coloured isodose distribution.

5.2.4 Method - Step Film Tests

The STF was fed through the film digitiser and an image obtained. The image was analysed using the same software tools as for the calibration films in '5.2.3 Method - Scanner Tests'. The relOD of each step on the film was measured and compared to the known real OD of the film. Using this data a conversion table, a plot, and a related equation were created to convert relOD to real OD.

5.3 Results - Film Tests

5.3.1 Results - Osiris and ImageJ Software

The results for the measurements of relOD of the EDR2 film using Osiris software at 8-bit and 12-bit depth are given in Table 5.1 and Figure 5.3. The results for the measurements using ImageJ software are given in Table 5.2 and Figure 5.4. Because the 8-bit depth setting uses a smaller greyscale range, the values given for relOD are much smaller than for the 12-bit depth setting. For purposes of comparison the results have been normalised to a maximum value of one. The normalised relOD values have been compared as a percentage difference.

Figure 5.3 clearly shows that the 12-bit depth setting gives several erratic results, whereas the results measured with the 8-bit depth setting follow a much smoother curve. Osiris is a relatively basic program, and it appears that it cannot reliably handle the large amounts of information required to handle a 12-bit depth scan.

The ImageJ software was obtained later in the project. Table 5.2 and Figure 5.4 show no significant difference between the 8-bit and the 12-bit depth settings, and both appear to be appropriate for calibrating the film. ImageJ was easier to use and provided more analysis tools, so it became the preferred software for calibrating and calculating doses from film.

Comparisons between the set-up techniques are presented in '5.3.4 Results - EDR2 Film Set-Up Tests'. Results for the actual calibration curves measured using ImageJ with 12-bit depth are discussed in '5.3.5 Results - XV Film Calibration' and '5.3.6 Results - EDR2 Film Calibration'.

Table 5.1. Comparison of normalised results for measurements of EDR2 film with Osiris software at 8-bit and 12-bit depth.

Dose Delivered (cGy)	8D Normalised	12D Normalised	RelOD Difference	Percentage Difference (%)
0	0.000	0.000	0.000	
25	0.039	0.057	0.019	32.3
50	0.080	0.119	0.039	32.7
75	0.128	0.180	0.052	28.8
100	0.177	0.259	0.082	31.7
125	0.237	0.348	0.111	31.8
150	0.293	0.426	0.133	31.2
175	0.357	0.527	0.170	32.3
200	0.414	0.611	0.196	32.1
225	0.480	0.540	0.060	11.1
250	0.548	0.815	0.266	32.7
300	0.662	0.914	0.252	27.6
400	0.886	0.871	-0.015	-1.7
500	0.984	0.982	-0.002	-0.2
600	1.000	1.000	0.000	0.0

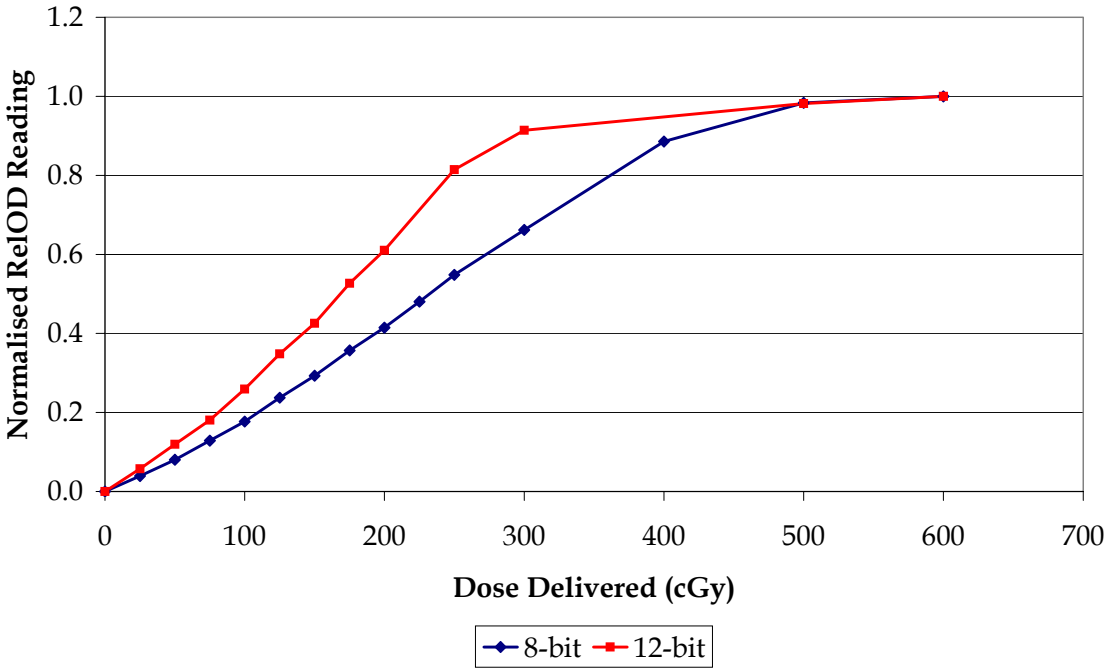

Figure 5.3. Plot of normalised results for measurements of EDR2 film with Osiris software at 8-bit and 12-bit depth.

Table 5.2. Comparison of normalised results for measurements of EDR2 film with ImageJ software at 8-bit and 12-bit depth.

Dose Delivered (cGy)	8D Normalised	12D Normalised	RelOD Difference	Percentage Difference (%)
0	0.000	0.000	0.000	
25	0.039	0.038	0.000	-0.6
50	0.080	0.079	0.000	-0.6
75	0.128	0.127	-0.001	-0.5
100	0.175	0.173	-0.002	-1.1
125	0.235	0.234	-0.002	-0.8
150	0.290	0.288	-0.002	-0.9
175	0.354	0.352	-0.002	-0.7
200	0.412	0.409	-0.003	-0.8
225	0.477	0.474	-0.003	-0.6
250	0.546	0.544	-0.002	-0.4
300	0.660	0.657	-0.003	-0.4
400	0.884	0.876	-0.008	-0.9
500	0.984	0.982	-0.002	-0.2
600	1.000	1.000	0.000	0.0

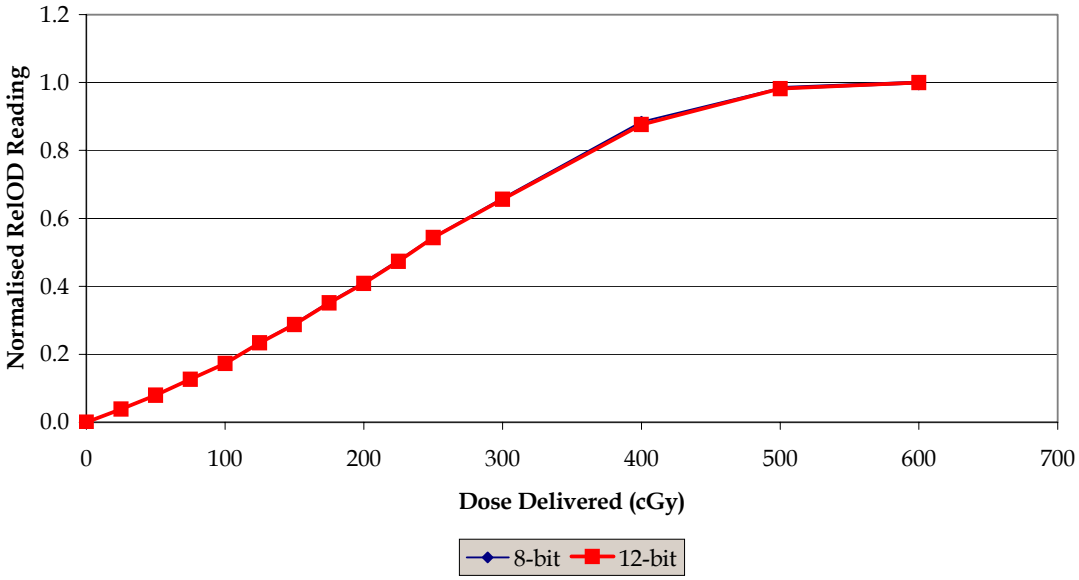

Figure 5.4. Plot of normalised results for measurements of EDR2 film with ImageJ software at 8-bit and 12-bit depth.

5.3.2 Results - Step Film Tests

The table and the plot of the result of scanning the Step Test Film (STF) with Osiris software with 12-bits depth are shown in Table 5.3 and Figure 5.5. The table provides the known real OD of each step in the film and the average relOD reading for each step, taken from three readings each. The computer was used to match a polynomial line of fit, and the equation for that is given in the table. The results have not been normalised or extrapolated to a zero value because there is no value for zero OD. The computer-fitted equation has been used to calculate the OD from the readings given, and this is compared to the known OD in order to provide a measure of the closeness of the line of fit.

Points 20 and 21, at real ODs 2.90 and 3.05, have been cut from the plot because it is at this point that the results start to curve downwards. From the plot it can be seen that the scan of the STF follows a fairly smooth curve with only slight deviations from the line of fit. The table similarly demonstrates this – the largest OD difference is -0.05 for the 2.75 OD point, followed by -0.04 and 0.04 for the 0.65 and 2.45 OD points. In general the percentage differences are also good, only increasing significantly for the lower dose points, which is due to the small values involved rather than large reading differences.

There were several problems with the STF. The main one was that the film was rather old and had not been well maintained. It has a crease in it and a stain on one section, both of which would contribute to inaccuracies in the reader, although all attempts were made to avoid making measurements in these sections. The other problem was that the STF was so narrow that scanning it lengthways was difficult. The film roller had trouble holding on to it so the strip often tilted, producing undesirable diagonal scans. When the STF was scanned widthways it was too narrow for the rollers to catch at all and would not go through the scanner. To get around this strips of normal

film were attached to either side of the STF, creating a bigger piece of film that could more easily be scanned.

Table 5.3. Results for calibration of step test film with ImageJ software at 12-bit depth.

Known Real OD	Measured RelOD	Real OD Calculated from Fit	Real OD Difference	Percentage Difference (%)
0.05	2279	0.07	0.02	27.3
0.20	4187	0.21	0.01	3.9
0.35	6079	0.35	0.00	0.5
0.50	7993	0.50	0.00	0.5
0.65	9286	0.61	-0.04	-7.0
0.80	11546	0.80	0.00	-0.3
0.95	13181	0.94	-0.01	-1.1
1.10	14904	1.09	-0.01	-0.6
1.25	16535	1.24	-0.01	-0.5
1.40	18228	1.40	0.00	0.3
1.55	19752	1.55	0.00	0.1
1.70	21283	1.70	0.00	0.2
1.85	22880	1.87	0.02	0.9
2.00	24204	2.00	0.00	0.2
2.15	25795	2.17	0.02	1.0
2.30	27177	2.32	0.02	1.0
2.45	28687	2.49	0.04	1.6
2.60	29409	2.57	-0.03	-1.2
2.75	30560	2.70	-0.05	-1.8

Equation for Line of Fit: $OD = 0.000\,018R^2 + 0.0076R - 0.052$

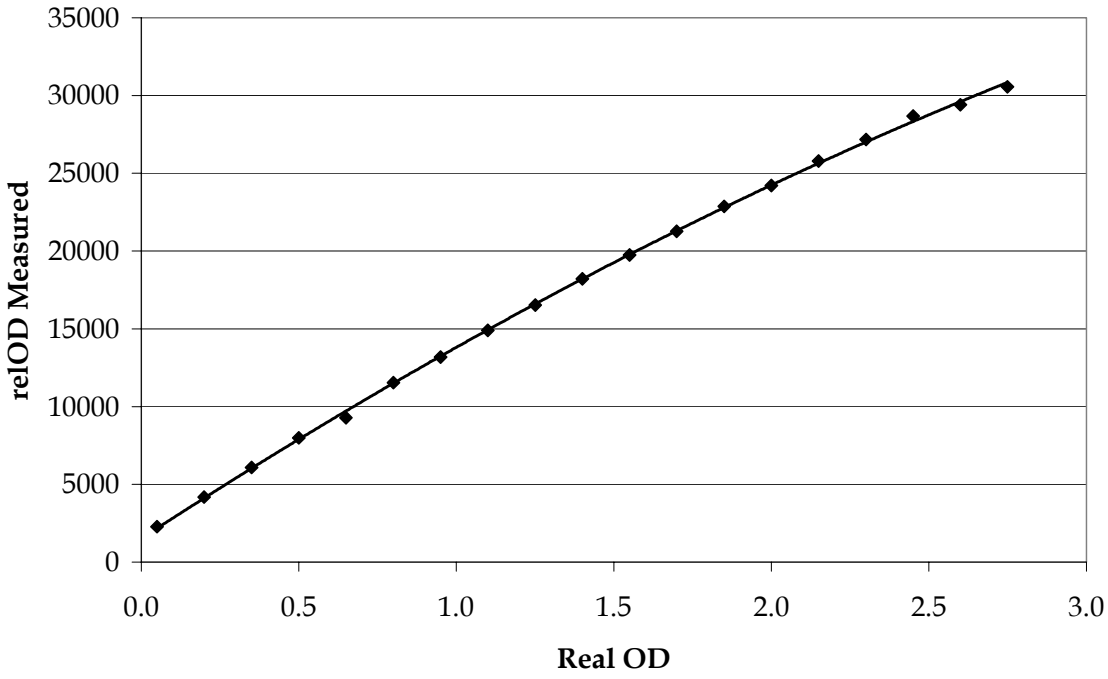

Figure 5.5. Plot of results for calibration for step test film with ImageJ software at 12-bit depth.

5.3.3 Results - Film Measurements

Tables 5.4, 5.5, 5.6, 5.7 and 5.8 and Figure 5.6 show the experimental results for the different orientations of the EDR2 film, and the perpendicular orientation of the XV film. The tables show the uncorrected relOD values ('Raw Reading RelOD') as scanned using ImageJ software on the 12-bit depth setting, alongside the same values corrected to give a value of zero for a zero dose ('Corrected Reading').

Figure 5.6 shows the plot for uncorrected relOD readings versus dose delivered. Clearly the XV readings cannot be directly compared to the EDR2 readings, as the range is much smaller, so it must be analysed separately.

The XV plot begins to flatten out at around the 125 cGy dose point. This means that 125 cGy is the dose at which the XV film begins to saturate, and hence is no longer a reliable indicator of dose. '5.3.5 Results - XV Film Calibration' discusses the usable part of the XV plot in greater detail.

The EDR2 plots appear to flatten at around the 300 to 400 cGy point. '5.3.6 Results - EDR2 Film Calibration' discusses the portion of the plot up to 300 cGy in greater detail.

5.3.4 Results - EDR2 Film Set-Up Tests

Figure 5.6 shows that within the different set-ups of the EDR2 film, the plots all follow approximately the same path. However, it is clear that the measurements for each orientation do not follow those of the others exactly. This is shown in Tables 5.4 to 5.7, which indicates each orientation's deviation from the perpendicular-15cm set-up, using the corrected relODs. At the 100 cGy point, the measurements do not correspond very closely at all, with 14.0% difference for the horizontal-parallel-15cm set-up, and 25.0% difference for the vertical-parallel-15cm set-up. The 2degree-parallel set-up is relatively close to the perpendicular set-up, with 3.4% difference. As with the discrepancies between ion chamber readings, this could be exaggerated by the much lower readings at this dose level. The differences improve markedly as the dose increases, with the horizontal-parallel-15cm and vertical-parallel-15cm set-up results deviating from the perpendicular-15cm set-up measurements by just 9.9% and 7.6% at the 200 cGy point, and the 2degree-parallel set-up by 0.6%.

Overall, the 2degree-parallel-15cm set-up gives the closest results to the perpendicular orientation. This was the expected result, because shifting the axis of the solid water 2° away from the axis of the beam resulted in the beam being attenuated almost entirely by the solid water, rather than by the film (and some air, especially in the case of the vertical set-up, where the solid water had a tendency to 'fan out'), with a minimal increase or decrease in effective pathlength.

In future measurements where it is not possible to set the film perpendicular to the beam, the film should be aligned 2° off the parallel axis of the beam. This would be difficult to do for an IMRT plan with multiple incident fields because the phantom would have to be shifted and sometimes wedged up to

align the film at 2° to each gantry angle. The phantom is heavy and shifting it each time whilst maintaining the position of the isocentre is not feasible.

Table 5.4. Results for measurements of EDR2 film, perpendicular orientation, 15 cm depth.

Perpendicular-15cm		
Dose Delivered (cGy)	**Raw Reading RelOD**	**Corrected Reading**
0	2551.0	0.0
25	4276.8	1725.8
50	6120.1	3569.1
75	8247.9	5697.0
100	10305.2	7754.2
125	13039.4	10488.4
150	15468.6	12917.7
175	18341.8	15790.8
200	20901.9	18350.9
225	23832.3	21281.3
250	26961.5	24410.5
300	32040.4	29489.4
400	41900.1	39349.1
500	46662.2	44111.2
600	47457.3	44906.3

Table 5.5. Results for measurements of EDR2 film, horizontal-parallel orientation, 15 cm depth.

Horizontal-Parallel-15cm			
Dose Delivered (cGy)	**Raw Reading RelOD**	**Corrected Reading**	**Difference from Perpendicular (%)**
0	2543.5	0.0	
25			
50			
75			
100	11556.1	9012.6	14.0
125			
150			
175			
200	22913.6	20370.1	9.9
225			
250			
300	34540.6	31997.1	7.8
400	44021.7	41478.2	5.1
500	46646.1	44102.6	0.0
600	47097.3	44553.8	-0.8

Table 5.6. Results for measurements of EDR2 film, vertical-parallel orientation, 15 cm depth.

Vertical-Parallel-15cm			
Dose Delivered (cGy)	**Raw Reading RelOD**	**Corrected Reading**	**Difference from Perpendicular (%)**
0	2543.5	0.0	
25			
50			
75			
100	12876.5	10333.0	25.0
125			
150			
175			
200	22398.5	19855.0	7.6
225			
250			
300	34250.4	31707.0	7.0
400	43601.7	41058.2	4.2
500	46621.7	44078.3	-0.1
600	47135.1	44591.6	-0.7

Table 5.7. Results for measurements of EDR2 film, 2-degree-parallel orientation, 15 cm depth.

2Degrees-Parallel-15cm			
Dose Delivered (cGy)	**Raw Reading RelOD**	**Corrected Reading**	**Difference from Perpendicular (%)**
0	2543.5	0.0	
25			
50			
75			
100	10574.3	8030.8	3.4
125			
150			
175			
200	21010.8	18467.3	0.6
225			
250			
300	32165.3	29621.8	0.4
400	41979.9	39436.5	0.2
500	46055.8	43512.3	-1.4
600	47146.6	44603.2	-0.7

Table 5.8. Results for measurements of XV film, perpendicular orientation, 15 cm depth.

X-Omat V		
Dose Delivered (cGy)	**Raw Reading RelOD**	**Corrected Reading**
0	2165.3	0.0
25	18011.1	15845.8
50	29205.7	27040.4
75	37170.4	35005.2
100	43571.4	41406.1
125	46532.3	44367.0
150	47393.7	45228.4
175	47635.1	45469.8
200	47745.2	45580.0

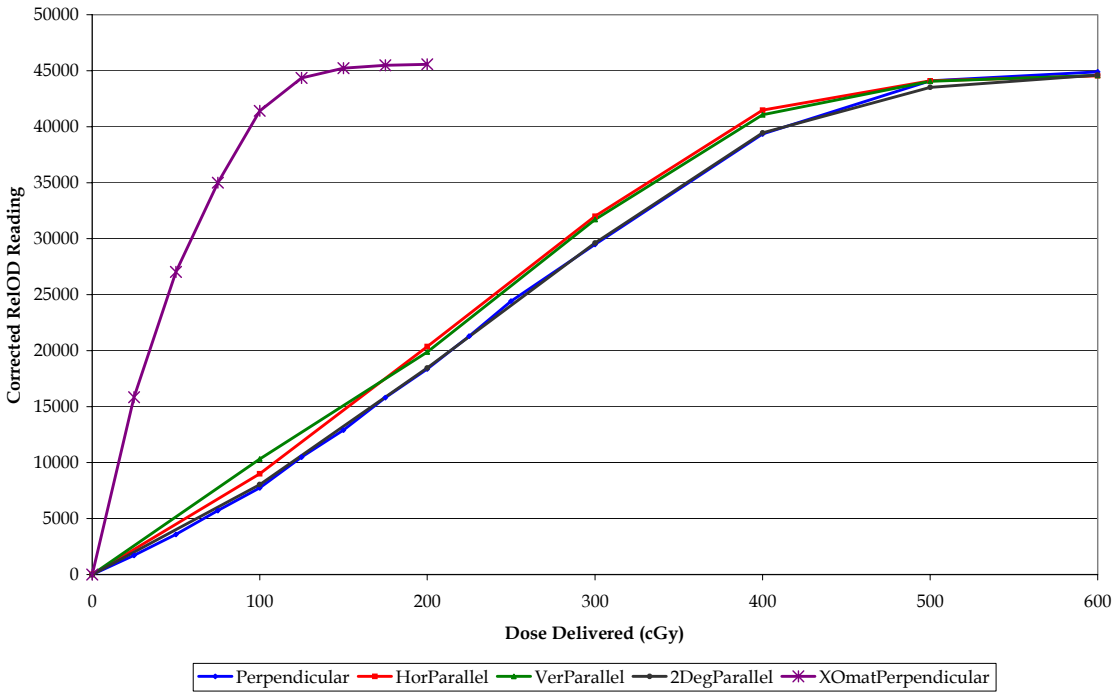

Figure 5.6. Plot of results for measurements of EDR2 and XV films, comparison of orientations at 15 cm depth.

5.3.5 Results - XV Film Calibration

Table 5.9 and Figure 5.7 show the calibration results of the XV film exposed in the perpendicular orientation at 15 cm depth. Figure 5.7 shows the plot of the corrected relOD versus the dose delivered, up to a dose of 125 cGy, as well as a computer-fitted quadratic curve. Table 5.9 gives the uncorrected and corrected relOD readings. An equation relating the dose to the corrected OD readings was formed from the plotted results, and the doses recalculated to this fit. The differences between the delivered and the calculated doses are given as dose differences and percentage values.

The table shows that the largest dose difference is –6.0 cGy for the 125 cGy dose value, which is equivalent to –5.1%. The next highest difference is 5.1 cGy or 4.9% for the 100 cGy dose point. The most important region for the potential measurement of a single IMRT beam is around the 5 to 25 cGy dose range, and the deviations for the 25 cGy dose point are average, with a difference of –3.8 cGy, or –17.8%.

Table 5.9. Results for calibration of XV film, perpendicular orientation, 15 cm depth.

Dose Delivered (cGy)	Raw RelOD Reading	Corrected RelOD Reading	Dose Calculated from Fit (cGy)	Dose Difference (cGy)	Percentage Difference (%)
0	2165.3	0.0	1.4	1.4	
25	18011.1	15845.8	21.2	-3.8	-17.8
50	29205.7	27040.4	50.1	0.1	0.2
75	37170.4	35005.2	78.1	3.1	4.0
100	43571.4	41406.1	105.1	5.1	4.9
125	46532.3	44367.0	119.0	-6.0	-5.1

Equation for curve of fit: $D = 4.9x10^{-8}R^2 + 4.8x10^{-4}R+1.38$

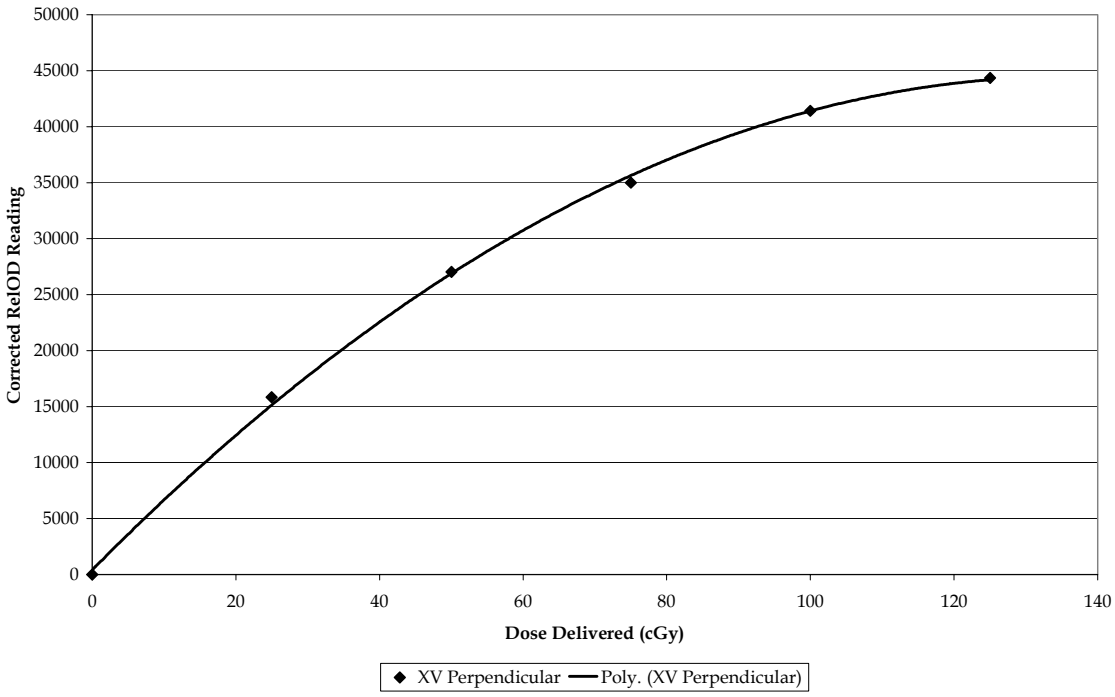

Figure 5.7. Plot of results for calibration of XV film, perpendicular orientation, 15 cm depth.

5.3.6 Results - EDR2 Film Calibration

Table 5.10 and Figure 5.8 show the calibration results for the EDR2 film exposed in the perpendicular orientation at 15 cm depth. Figure 5.8 shows the plot of the uncorrected relOD versus the dose delivered, up to a dose of 300 cGy, as well as a computer-fitted quadratic curve. Table 5.10 gives the uncorrected and corrected relOD readings. The equation relating the dose to the corrected OD readings is given in the table, and the doses were recalculated using this fit. The differences between the delivered and the calculated doses are given as dose differences and percentage values.

The plot appears to show a fairly good conformity of the measured results to a quadratic line of fit. This is demonstrated in the table, where the majority of deviations from the fit are acceptably low. The largest dose difference is 5.4 cGy for the zero dose value, which occurred because the line of fit was not set to an intercept of zero.

The next highest differences were -5.3 cGy or -5.6%, 4.9 cGy or 1.9%, and -4.9 cGy or -1.7% for the 100, 250, and 300 cGy dose points respectively. The most important region for the potential measurement of a full IMRT fraction is around the 200 cGy dose point, and the deviations there are good, with 2.4 cGy or 1.3%, 1.6 cGy or 0.8%, and 3.1 cGy or 1.3% for 175, 200, and 225 cGy respectively.

Table 5.10. Results for calibration of EDR2 film, perpendicular orientation, 15 cm depth.

Dose Delivered (cGy)	Raw RelOD Reading	Corrected RelOD Reading	Dose Calculated from Fit (cGy)	Dose Difference (cGy)	Percentage Difference (%)
0	2551.0	0.0	5.4	5.4	
25	4276.8	1725.8	26.1	1.1	4.2
50	6120.1	3569.1	47.7	-2.3	-4.9
75	8247.9	5697.0	71.9	-3.1	-4.3
100	10305.2	7754.2	94.7	-5.3	-5.6
125	13039.4	10488.4	124.0	-1.0	-0.8
150	15468.6	12917.7	149.0	-1.0	-0.7
175	18341.8	15790.8	177.4	2.4	1.3
200	20901.9	18350.9	201.6	1.6	0.8
225	23832.3	21281.3	228.1	3.1	1.3
250	26961.5	24410.5	254.9	4.9	1.9
300	32040.4	29489.4	295.1	-4.9	-1.7

Equation for curve of fit: $D = -7.8 \times 10^{-8} R^2 + 1.21 \times 10^{-2} R + 5.40$

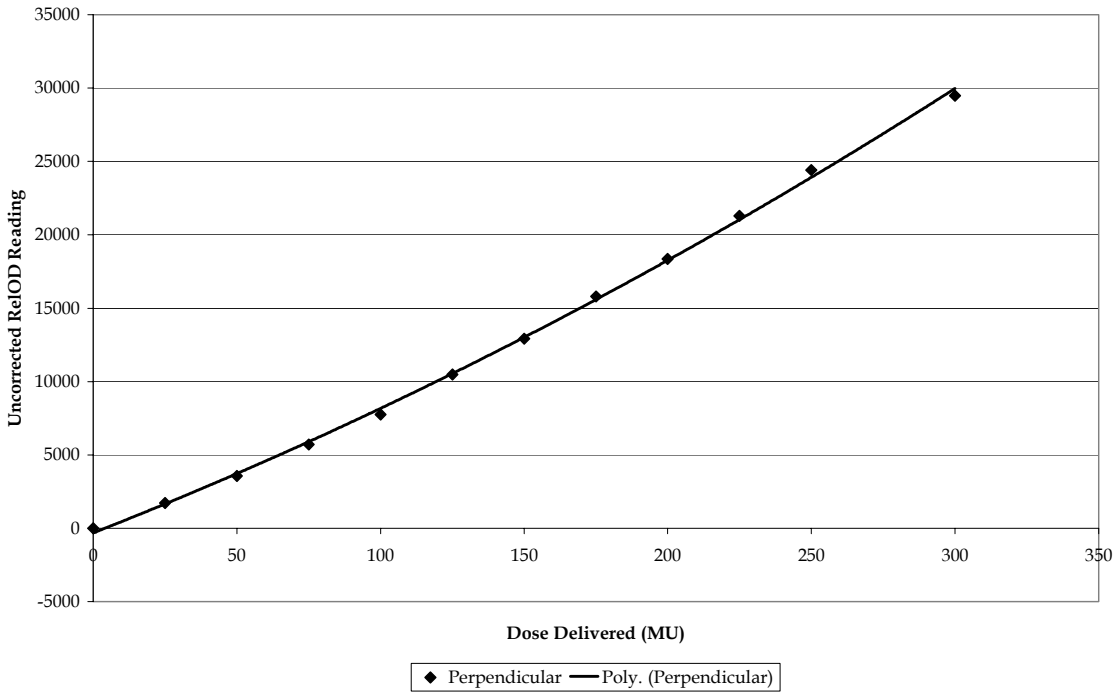

Figure 5.8. Plot of results for calibration of EDR2 film, perpendicular orientation, 15 cm depth.

5.3.7 Results - Scanner Exposure Tests

Figure 5.9 shows the results of adjusting the level, or length of time, of exposure of the film digitiser when scanning the EDR2 perpendicular film. The plot clearly shows that the lowest exposure of 10 (milliseconds) must be used in order to ensure that the lowest dose values will be reliably analysed, as the higher exposures pass too much light through the film, resulting in saturation or 'zero' relOD readings for the lower dose regions on the film.

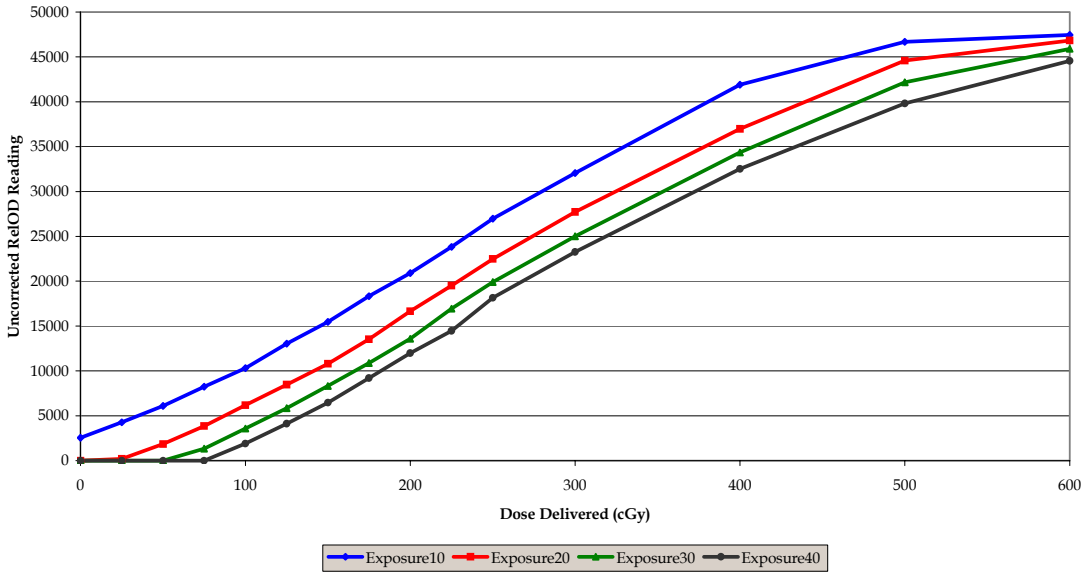

Figure 5.9. Results for measurements of EDR2 film with different scanner exposure times.

5.3.8 Results - Scanner Resolution Tests

Figure 5.10 show the results of scanning the EDR2 perpendicular film using different resolutions. From the plot, it appears that no single resolution produces a significantly different result. Although the plots do diverge slightly at the higher resolutions, there is no clear indication in smoothness of accuracy of a superior plot.

An increase in resolution leads to a very large increase in file size, resulting in slower digitising capabilities, and using up more disk space. Therefore, as there is no apparent advantage thus far of using a higher resolution scan, film scans should be performed at the lowest resolution of 60 dots-per-inch.

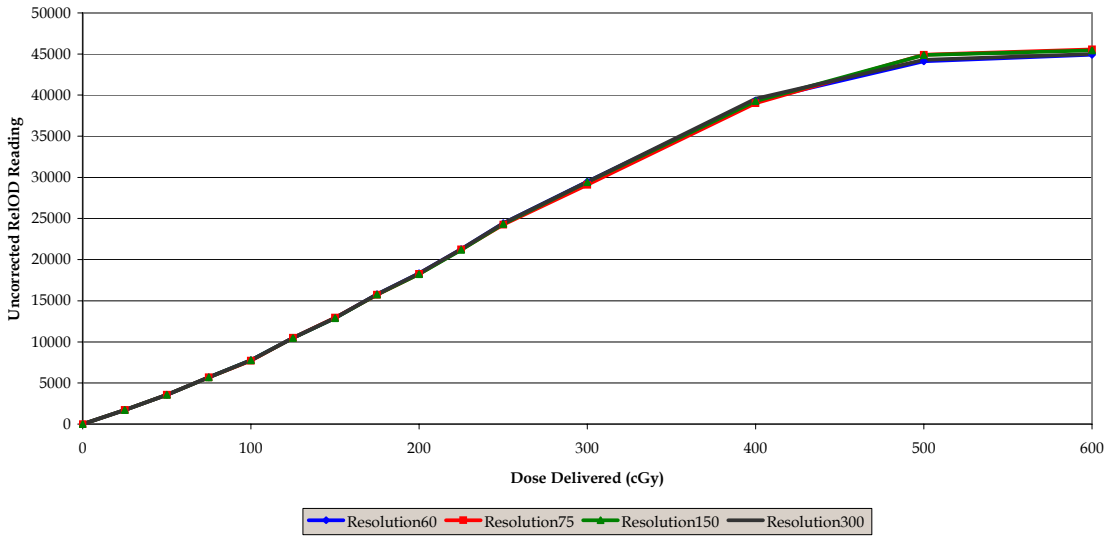

Figure 5.10. Results for measurements of EDR2 film with different scanner resolution settings.

5.4 Conclusion - Film Tests

The results of the step test film scan demonstrate that the film scanner and analysis software are capable of producing reliable scans.

The previously discussed results of the film tests demonstrate that EDR2 film is capable of a dose range appropriate to IMRT dosimetry, conforms acceptably to a computer-fit equation so that dose conversions can be easily calculated, measures low doses well, and is suitably stable enough to provide reproducible results. However compared to the ionisation chamber it is unreliable for inter-comparisons between different set-ups.

For all future calibrations the perpendicular set-up should be used whenever possible, as perpendicular film is simpler to cut and position, resulting in less chance of human error, and it provides more reliable results because the instances of air gaps are reduced, and the measurable area is larger than that for parallel film.

When scanning the film, the results show that a short exposure in this case should always be used in order to ensure the lower dose end of the film range is covered. Because adjusting the resolution did not appear to make much difference the lowest resolution should be used where possible to reduce the size of a scanned file and make it easier to use.

The results of the XV film calibrations indicate that it should have advantages similar to those of the EDR2 film. Because of the smaller dose range, it would not be suitable for the majority of full-fraction IMRT dosimetry checks, as these are typically in the 1 to 2 Gy range, which is beyond the point at which XV film saturates. However, XV film has the advantage of being less expensive than the EDR2 film, and therefore possibly more suitable for dosimetry of individual beams.

There was not a large difference between the two types of software except in ease of use, although calibrating film with Osiris with 12-bit depth did not provide acceptable results. Since there was no real difference between the 8-bit and 12-bit scans with ImageJ software, 12-bit depth was generally used because the larger greyscale range inherently provides better resolution in film scans.

Chapter 6: Patient Dosimetry

6.1 Aim - Patient Dosimetry

Because the IMRT treatment technique is a new technique for which plan checking cannot rely on simple hand calculations, a new quality assurance (QA) method had to be designed. The purpose of this part of the project was to find a suitable, economical, time-effective and feasible system of checking each patient plan using ionisation chambers and film.

Various combinations of film and ionisation chamber dosimetry were to be used and compared in an effort to find the best IMRT dosimetry technique. While ionisation chamber isocentre checks in a phantom for all fields were always done, not all fields were checked with every combination of dosimetry set-up for all case plans. Some form of qualitative, and perhaps quantitative, film check combination was always performed, and planar dose map checks were carried out for each case. Usually several fields only were selected for planar dose map checks because there were sometimes too many beams involved to make a full check possible in the tight time line between plan validation and patient treatment.

The dosimetry results for each case were individually assessed, and compared with Pinnacle calculated doses. The results for all cases were combined in various ways to provide comparisons between the techniques used.

A description of each of the techniques is given, followed by a summary of the individual plans, the techniques used to check them, and the results for each case. Finally, an overall discussion of the results is given.

6.2 Method - Patient Dosimetry

6.2.1 Method - Ionisation Chamber Calibration

The same technique was used for both the 0.03 cc (small) and 0.6 cc (regular) ionisation chambers.

Before setting up the IMRT treatment, the ionisation chamber was set into the solid water slab with 1.5 cm of solid water on top to place the centre of measurement of the chamber at d_{max}. The top of the solid water was set to 100 cm SSD. Following an initial warm-up of 200 MU, 100 MU was delivered with a 10 cm × 10 cm, field, which was known to give a dose of 100 cGy at d_{max}. The chamber reading was taken, and the measurement repeated three times to give an average chamber reading for 100 MU. It was shown in '4.4 Conclusion - Ionisation Chamber Tests' that the linearity of response of the ionisation chamber means that a single dose point could be used to calibrate the entire dose curve. However, to ensure the accuracy of the calibration three doses each of 25 MU and 50 MU (equivalent to 25 cGy and 50 cGy respectively) were also delivered. An average value of dose per unit charge reading was calculated and this value used as a simple conversion factor to calculate the dose from measurements of the patient plans.

The cubic solid water phantom was set up with the ionisation chamber at the centre of the block. The centre of the block (and therefore, the physical centre of the ionisation chamber) was positioned at the isocentre. It is acknowledged that the effective point of ionisation chamber measurement is 2 mm from this position but this was shown to have little appreciable effect on calibration measurements, as quantified in '4.4 – Conclusion - Ionisation Chamber Tests'.

Because the gantry would be rotated from the control room between beams, a quick rotation during set-up ensured it would not collide with the couch or

phantom, or drag on the cord connecting the chamber to the external electrometer.

Once the phantom had been set up the entire treatment could be carried out from the control room. All of the beam could be delivered by either using the dMLC file or by setting up a phantom treatment fraction. The output of each beam was measured and converted to a dose value using the calibration data. The overall dose was measured as an accumulated dose, and by adding the individual outputs of each beam. Because the ionisation chamber exhibits good reproducibility of results, and the time taken to carry out an entire set of treatment measurements was a limiting factor, usually only one set of measurements was taken, and additional sets of measurements were taken as required.

6.2.2 Method - Ionisation Chamber Zero Gantry Angle Measurements

The second form of ionisation chamber measurement tested was the zero gantry angle dose distribution. Each beam was recalculated for a gantry angle of zero, for a source-to-axis distance (SAD) of 100 cm.

This was to provide a back-up check of the dose calculation; when a physical dose check is carried out, this set-up should prove more accurate because it avoids the difficulties of dosimetry at an angle, through the couch, or through a non-smooth contour edge of the phantom.

To measure a zero gantry angle field dose the ionisation chamber was placed at the isocentre with 10 cm of solid water build-up on top, which put the SSD at 90 cm.

The beam delivery could be carried out from the external control room, in the same way as for the isocentric ionisation chamber measurements. It is acknowledged that zero gantry angle tests do not fully test all of the Varis beam parameter transfer process. So while zero gantry angle tests are useful a beam angle test is also recommended.

6.2.3 Method - Film Calibration

The same film dosimetry technique was used for both the XV and the EDR2 films. Because of the different dose ranges for the two types of film, generally the XV film was used to measure individual beam doses, and the EDR2 film was used to measure full treatment doses.

Before setting up an IMRT treatment a set of calibration films was exposed. A film packet, cut to size (so as not to waste too much film) was positioned at the centre of a 10 cm × 10 cm field, with the plane of the film perpendicular to the direction of the beam. 1.5 cm of solid water was placed on top of the film so that it was at d_{max} at 100 cm SSD.

The film was exposed to 10 MU, which was known to be 10 cGy at d_{max}. This was repeated for various dose values, as the dose response of film is not linear, so that a calibration curve could be created. The EDR2 film was usually calibrated up to 200 cGy in 25 cGy increments, and the XV film up to 100 cGy in 10 cGy increments.

The films from the same batch were developed in sequence to ensure consistency, and then digitised for analysis. Once digitised a rectangular ROI was selected in the centre of the field, and the analysis tools used to find the average relOD of the ROI. A plot was formed of the dose delivered versus the relOD, and a quadratic curve was fitted to give an equation for the dose represented by a particular relOD.

6.2.4 Method - Film Axial Cross-Section Measurements

To check the IMRT plan in the axial cross-section using film the cubic solid water phantom was placed so that the film could be positioned parallel in relation to the gantry at any angle. In an effort to reduce the air gaps caused by the solid water slabs 'fanning' outwards, heavy blocks were placed at either end of the phantom and micropore tape wrapped around the top. However, the air gaps could not be completely removed. This was especially difficult for the IMRT treatments because to allow the beam through at all angles a phantom had to be set up on the 'tennis racquet' part of the couch, which sags slightly. In future custom clamps or a dedicated IMRT phantom will provide better film pressure consistency.

An uncut film packet was fitted into the centre of the solid water phantom, and the phantom positioned at the isocentre. The gantry was rotated to ensure no collision with the couch or the phantom would occur, and set to the correct position for the first beam.

Once the phantom had been set up the entire treatment could be carried out from the control room, in the same way as for the axial ionisation chamber measurements. A fresh film XV was inserted for each beam, and an EDR2 film to carry out an entire dose fraction.

The films were developed in the same batch as the calibration films to ensure consistency, and then digitised for analysis. A very small rectangular ROI was positioned on the point of interest, to find the relOD. The equation fitted to the calibration curve for the relevant film type was used to calculate the dose to that point, which could then be compared to the expected dose as predicted by Pinnacle.

6.2.5 Method - Film Planar Measurements

To expose a planar film the film packet was placed on top of some solid water, perpendicular to the beam axis and at 100 cm SAD. 10 cm of solid water build-up was placed on top.

The beam was delivered, and a fresh film used for each beam. The films were developed in the same batch as the calibration films to ensure consistency, and then digitised for analysis. A small ROI was positioned on the point of interest, to find the relOD. The equation fitted to the calibration curve was used to calculate the dose to that point, which could then be compared to the expected dose as predicted by Pinnacle.

6.3 Case 1 Dosimetry

6.3.1 Aim - Case 1

The 'Case 1' (P1) plan was designed for an axilla (neck) treatment. It consisted of two beams, AP (antero posterior) and PA (postero anterior), which are directly opposite each other at gantry angles of 0° and 180°. The beams have been split into segments to improve the dose to the axilla.

Although it makes use of the dMLC controller, Case 1 is not actually an inverse-planned IMRT plan, but was used as an extremely simple trial plan as it has few high-dose gradients, and measurements can be repeated many times with minimal time and film usage.

This is a plan that uses three segments in the AP beam and two in the PA beam to improve dose homogeneity in the axilla. These treatments may be known variously as 'forward-planned IMRT' or more appropriately as fields with 'in-field segmentation'.

6.3.2 Method - Case 1

The Case 1 plan was checked for both beams separately and for a whole treatment using the regular ionisation chamber and the EDR2 film.

The ionisation chamber was used to check each beam and the whole dose distribution in each set-up. Although the chamber showed a linear dose response above 25 cGy, it was also used with the MUs tripled, in an attempt to compare the results with measurements of future plans, which might require the MUs to be tripled.

The films were exposed in two set-ups:

- Parallel, where the film was set upright in the solid water phantom so that the plane of the film was always parallel to the beam axis;
- Perpendicular, where the film was placed so that it was perpendicular to the axis of the beam.

The parallel set-up would result in the film being exposed in a position to obtain an image of the axial cross-section dose distribution, which is most commonly used angle in which to compare dose distributions calculated by Pinnacle.

The perpendicular film set-up could be used for the entire treatment delivery of the Case 1 plan without having to reposition the film because the plan involves just two opposing beams. Normally the perpendicular set-up would be used for checking beams that have been recalculated for the zero gantry angle position.

6.3.3 Results - Case 1

The results for the individual beam measurements of the Case 1 plan are given in Table 6.1 for the regular ionisation chamber and Table 6.2 for the EDR2 film. The results for the whole treatment measured with each dosimeter are given in Table 6.3.

The results show the dose delivered, as predicted by Pinnacle, compared with the dose measured by each dosimetry method. The differences between the predicted and measured results are given as dose (cGy) and percentage values.

Most of the dosimeters show close matches for the Case 1 plan. The regular ionisation chamber gave very good results for the whole treatment with a difference between measured and predicted dose of –0.4 cGy, or –0.2% (expected 175.0 cGy, measured 174.6 cGy). Similarly, the individual beam measurements were acceptable, with Beam1 giving a dose of 90.6 cGy compared to an expected 87.5 cGy (a difference of 3.1 cGy or 3.4%) and Beam2 giving a dose of 84.1 cGy compared to an expected 87.5 cGy (a difference of –3.5 cGy or –4.1%).

The measurements made with the increased dose did not improve the results, with an overall measured dose of 514.6 cGy, compared to a predicted dose of 525 cGy, giving a difference of –10.4 cGy or –2.0%. The individual beam measurements were poor, with Beam1 measuring a dose of 268.0 cGy compared to an expected 262.5 cGy (a difference of 5.5 cGy or 2.1%) and Beam2 giving a dose of 246.5 cGy compared to an expected 262.5 cGy (a difference of –16.0 cGy or –6.5%). This indicates that tripling the dose delivered provided absolutely no dose collection advantage for the regular ionisation chamber.

Most of the film dosimetry techniques gave good results for the whole treatment measurements, with the exception being 19.6 cGy or 10.1% for the EDR2 film exposed in the horizontal parallel set-up (expected 175.0 cGy and measured 194.6 cGy). Since the Case 1 plan was the only plan in which it was possible to carry out the full treatment in this set-up, this was not a significant problem.

The next highest discrepancy for the film results was 5.7 cGy or 3.2% for the EDR2 film exposed in the perpendicular set-up (expected 175.0 cGy and measured 180.7 cGy).

The standard set-up for future film measurements will be parallel to the beam, with any calibration exposures to be done perpendicular to the beam. This showed good results for both types of software used. Because of the infeasibility of phantom setup with multiple beams 2 degree offsets were not practised. The worst result was for the film analysed with ImageJ in the 12-bit depth mode, with a measured dose of 176.5 cGy compared to an expected dose of 175.0 cGy giving a difference of 1.5 cGy, or 0.8%.

Figure 6.1. The axial dose distribution for Case 1 measured on EDR2 film and digitised.

The films were also used to qualitatively check the dose distribution in the cross-section of the whole fraction treatment, and each planar beam distribution. The developed films were checked by eye and with a ruler on a light box to ensure the correct orientation of the dose distribution, and to compare the dimensions of the fields to the dimensions predicted by Pinnacle.

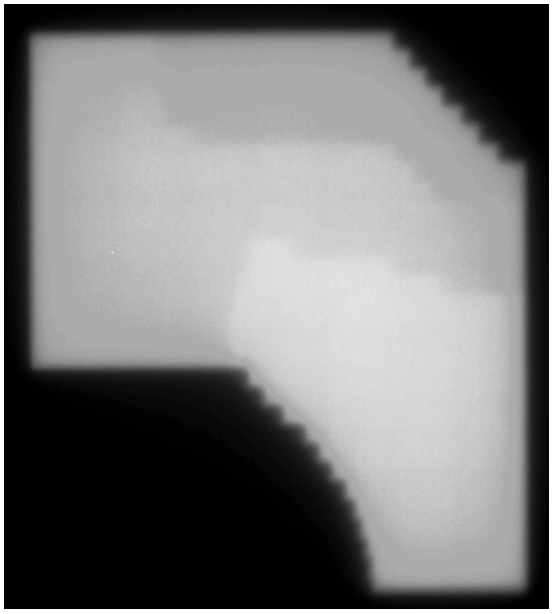

Figure 6.2. The planar dose distribution for Case 1, Beam1 measured on XV film and digitised.

All of the qualitative films showed very good results. The axial film for the whole treatment (see Figure 6.1) clearly showed the relative distribution was similar to the isodose map (not shown). Similarly the planar dose distributions (see Figure 6.2) showed a very good match to the Pinnacle-predicted distributions. This is important because it shows that the treatment was planned and delivered with the correct orientation, position and scaling.

Table 6.1. Case 1 individual beams measured with regular ionisation chamber for (a) normal MU delivery and (b) tripled MU delivery.

Regular Ionisation Chamber					
Beam	**MU**	**Predicted Dose (cGy)**	**Measured Dose (cGy)**	**Dose Difference (cGy)**	**Percent Difference (%)**
Beam1	134	87.5	90.6	3.1	3.4
Beam2	124	87.5	84.1	-3.5	-4.1
Whole	258	175	174.6	-0.4	-0.3

Regular Ionisation Chamber - Triple Dose					
Beam	**MU**	**Predicted Dose (cGy)**	**Measured Dose (cGy)**	**Dose Difference (cGy)**	**Percent Difference (%)**
Beam1	402	262.5	268	5.5	2.1
Beam2	373	262.5	246.5	-16.0	-6.5
Whole	775	525	514.6	-10.4	-2.0

Table 6.2. Case 1 individual beams measured with EDR2 film for (a) perpendicular set-up and (b) parallel set-up.

EDR2 Film Osiris 12D - Perpendicular					
Beam	**MU**	**Predicted Dose (cGy)**	**Measured Dose (cGy)**	**Dose Difference (cGy)**	**Percent Difference (%)**
Beam1	134	87.5	90.5	3.0	3.3
Beam2	124	87.5	81.9	-5.6	-6.8
Whole	258	175	180.7	5.7	3.2

EDR2 Film Osiris 12D - Vertical Parallel					
Beam	**MU**	**Predicted Dose (cGy)**	**Measured Dose (cGy)**	**Dose Difference (cGy)**	**Percent Difference (%)**
Beam1	134	87.5	102.0	14.5	14.2
Beam2	124	87.5	90.0	2.5	2.8
Whole	258	175	209.6	34.6	16.5

Table 6.3. Case 1 full treatment results for ionisation chambers and EDR2 film.

Dosimetry Method	Dose (cGy)	Dose Relative to Pinnacle	cGy Diff	%Diff
Pinnacle	175.0	1.000	0.0	0.0
IMRT Check				
Reg Ion	174.6	0.998	-0.4	-0.2
X3 Reg Ion	514.6	0.980	-10.4	-2.0
Small Ion				
X3 Small Ion				
Osiris 8D	174.2	0.996	-0.8	-0.4
Osiris 12D	209.6	1.198	34.6	16.5
ImageJ 8D	174.2	0.995	-0.8	-0.5
ImageJ 12D	176.5	1.008	1.5	0.8
O 12D H Par	194.6	1.112	19.6	10.1
O 12D Perp	180.7	1.033	5.7	3.2

6.3.4 Conclusion - Case 1

Good results were obtained for the Case 1 plan. It is acknowledged that this was a simple case because it had few segments with few high dose gradient regions. The dose calculation point was positioned at the isocentre where there was a reasonably large region of uniform dose, which meant that errors in positioning the point of measurement should not have much of an effect on the dose measurement. Only two beams were used, which reduced the potential for multiple sources of error. Also, the two beams were directly opposing each other, both passing through the flat part of the phantom, and the PA beam through the tennis racquet part of the couch (avoiding attenuating factors such as the metal sides of the couch).

All of the films proved very useful for qualitatively checking the cross-sectional dose distribution of the whole fraction treatment, and the planar beam dose distributions. Performing a comparative check between the films and the predicted dose distributions was very quick, and provided adequate reassurance of the correctness of the physical jaw and leaf parameters used in the treatment.

As was expected from the film tests, using Osiris with 12-bit depth did not provide good quantitative results. Using Osiris with 8-bit depth and ImageJ gave good results, and little advantage can be seen with ImageJ scanned with 12-bit over 8-bit depth. This implies that the 8-bit depth is adequate over the film contrast ranges tested, although it must be noted that most film analysis tools currently available only provide 12-bit or 16-bit depth scans.

6.4 Case 2 Dosimetry

6.4.1 Aim - Case 2

The 'Case 2' plan was designed to treat a basal cell carcinoma (BCC) of the forehead. In an effort to avoid delivering excessive dose to the eye and brain, and especially the lacrimal gland of the eye, an IMRT plan involving 10 beams was developed.

An unusual aspect of this plan was that one beam was non-coplanar as the couch was set to 90-deg for Beam1, which might affect the accuracy of the detectors used because of their orientations relative to the beam being changed.

According to the ionisation chamber orientation tests carried out in '4.3.2 Results - Regular Ionisation Chamber Calibration', a change in the direction of the beam relative to the axis of the ionisation chamber from perpendicular to parallel should not significantly affect the measured results. However according to the tests carried out on film in '5.3.3 Results - EDR2 Film Set-Ups', up to a 25% difference was found between films exposed in the perpendicular and parallel orientations. So the non-coplanar beam might adversely affect the accuracy of the film dosimetry results; however this beam was just one of 10 beams so the combined results would only be affected approximately in proportion to this beam weight.

6.4.2 Method - Case 2

The Case 2 plan was tested for a whole treatment using the calibrated regular ionisation chamber, the small ionisation chamber, and the EDR2 film. The EDR2 film was digitised and analysed using both Osiris and ImageJ software. The regular ionisation chamber was also used to measure individual beams. All of the beams were also measured with the regular ionisation chamber with triple the number of MUs delivered for each beam,

in order to see if the increased dose could improve the sensitivity. Two individual beams – Beam4 and Beam10 – were checked using calibrated XV film.

To ensure that the plan had been delivered correctly to the treatment computer it was decided that at least one full IMRT check would be carried out by adding an extra fraction to a phantom treatment file. The solid water phantom was treated in clinical mode as if it were the patient, replanned so that the MUs were retained but the dose was recalculated to the isocentric position at the centre of the phantom.

The set-up of the film necessarily resulted in Beam1 passing through the plane of the film, while all of the other beams passed parallel to the plane of the film. Shifting the phantom to realign the film between beams was not a feasible option because the film was also used to provide a qualitative visual check of the overall dose distribution, and this option would be unavailable if the film were moved during treatment. Besides, the phantom is heavy and awkward, so moving it during treatment whilst maintaining the precision of the set-up would be too difficult.

6.4.3 Results - Case 2

The original Case 2 plan suffered a few initial problems. For several fields, the dose to one or more beamlets was planned at less than 1 MU, which cannot be delivered by the Varian Clinac 2100C. To overcome this during the tests, the MUs for these beams were doubled; bringing the dose deliveries to a level the linac was capable of. To rectify this problem for the actual patient plan, the very low MU segments were simply removed (an option available in the Pinnacle software); considering the planed MUs were less than 1 this did not significantly alter the overall dose distribution.

Due to the nature of IMRT plans the dose gradients at the isocentre can be steeper than in conventional plans, therefore an important test was to compare the dose outputs measured using the regular chamber as well as the small chamber. Although the small chamber has better spatial resolution, the smaller volume makes it less sensitive to the low doses per field that are being delivered. To intensify the problem with IMRT the dose at the isocentre may be measured in a low intensity region of the low dose weighted field.

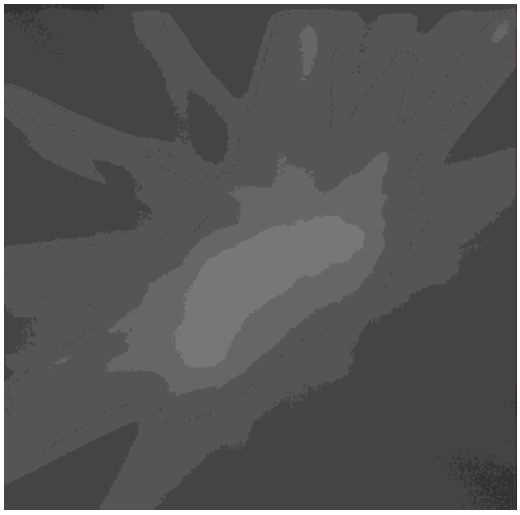

Figure 6.3. The axial dose distribution for Case 2 measured on EDR2 film and digitised.

The results for the individual beam measurements of the Case 2 plan are given in Table 6.4 for the regular ionisation chamber and Table 6.5 for the XV film. The results for the whole treatment measured with each dosimeter are given in Table 6.6.

The maximum dose error measured for an individual beam using the regular ionisation chamber was –26.1% for Beam10. However this error was for a very small dose value, which means just a couple of cGy difference could result in a large and somewhat distorted percentage error. The dose

difference for Beam10 was –2.3 cGy (expected dose 11.1 cGy and measured dose 8.8 cGy). It should be noted that because of the set-up of the phantom on the racquet frame Beam10 had to pass through the couch and part of the metal bar on the side of the couch. Such attenuation would not occur with the patient because they would be set up at the other end of the couch away from the metal bar. The next highest dose discrepancy was 1.4 cGy for Beam9 (expected 21.7 cGy, measured 20.3 cGy), which is a –6.9% difference. The small measured differences indicate that using the regular ionisation chamber as a dosimeter for individual beams was adequate.

The sum of the individual beam measurements using the regular ionisation chamber resulted in a measured dose of 134.5 cGy compared to an expected value of 134.5 cGy. This is a difference for the combined beams of zero. When the whole treatment was remeasured in a repeated delivery the dose was measured at 134.8 cGy, which is a dose difference of 0.3 cGy, and a percentage difference of 0.2%. Both of these results indicate the regular ionisation chamber was successfully reproducible when used to measure this IMRT treatment.

Because the ionisation chamber is relatively insensitive to small doses the individual beam measurements were repeated with three times the dose delivered, to see if the results could be improved. The results were at best only marginally improved, with Beam10 measured at 25.3 cGy when 33.3 cGy was expected, which is a dose difference of –8.0 cGy or a percentage difference of –31.8%. The sum of the beams showed a dose difference of –14.7 cGy or a percentage difference of –3.8% (expected dose 403.5 cGy and measured dose 388.8 cGy), which was not as good as either of the original measurements. For this case scaling up the dose to enhance the charge collection of the ionisation chamber did not improve the match to the planning computer.

The small ionisation chamber gave a good result for the whole treatment of 134.5 cGy, which is a difference of zero. This would appear to demonstrate that either chamber is suitable as a dosimeter for an IMRT treatment measurement.

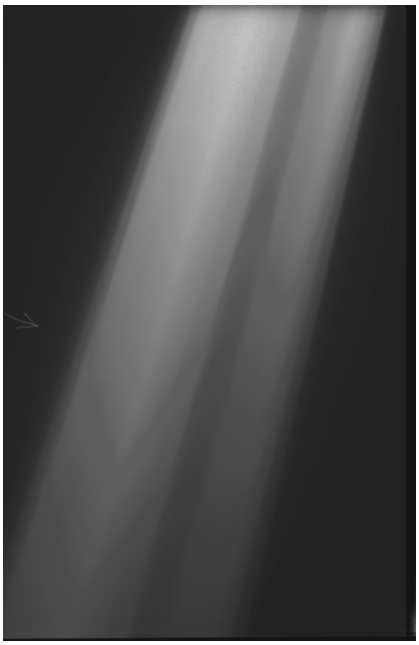

Figure 6.4. The parallel dose distribution for Case 2, Beam4 measured on XV film and digitised.

The measurements of the whole treatment using EDR2 film showed acceptable results. When analysed with the Osiris software with 8-bit depth a dose of 137.6 cGy was measured, compared to an expected 134.5 cGy, which is a difference of 3.1 cGy or 2.3%. Osiris software with 12-bit depth gave a dose of 139.1 cGy, which is a difference of 4.6 cGy or 3.3%.

Using the ImageJ software to analyse the film resulted in dose measurements of 137.9 cGy for 8-bit depth and 136.9 cGy for 12-bit depth, which is a percentage difference of 2.5% and 1.7% respectively.

An appreciable difference cannot be seen between using 8-bit or 12-bit depth to perform the scans. Using the 12-bit depth mode did take up a lot more disc space, and took longer to scan.

There was also not a large difference found between using Osiris or ImageJ software to analyse the film. If this is the case for all of the IMRT checks, the advantage of ImageJ is that it is easier to use because of its additional analysis tools.

The two individual beams that were measured parallel to the beam axis with the XV film (Table 6.5) and analysed using ImageJ with 12-bit depth did not show satisfactory results. Beam4 gave a measured dose of 31.8 cGy compared to an expected 26.4 cGy, which is a difference of 5.4 cGy or 17.0%. Beam10 gave a measured dose of 9.0 cGy compared to an expected 11.1 cGy, which is a difference of –2.1 cGy or –23.3%. Such poor results were to be expected because the individual beams contained some high dose gradients. It is possible that the tape and blocks used to hold the phantom together did not provide adequate pressure to avoid air bubbles in the film wrap. This was an inadequacy in the phantom construction and the new ART IMRT phantom, which has nylon screw thread clamping, may be better for these parallel film measurements. Figure 6.4 shows the parallel image of Beam4 in which a cool spot in the centre is apparent, and Figure 6.5 shows the planar images of Beam8 and Beam4 in which the dose gradients can be seen.

All of the films showed reasonable qualitative results. The axial film for the whole treatment (Figure 6.3) clearly showed that the orientation, relative dose distribution, and dimensions of the treatment were correct. Similarly the planar dose distributions (Figure 6.5) showed a good match to the Pinnacle-predicted distribution.

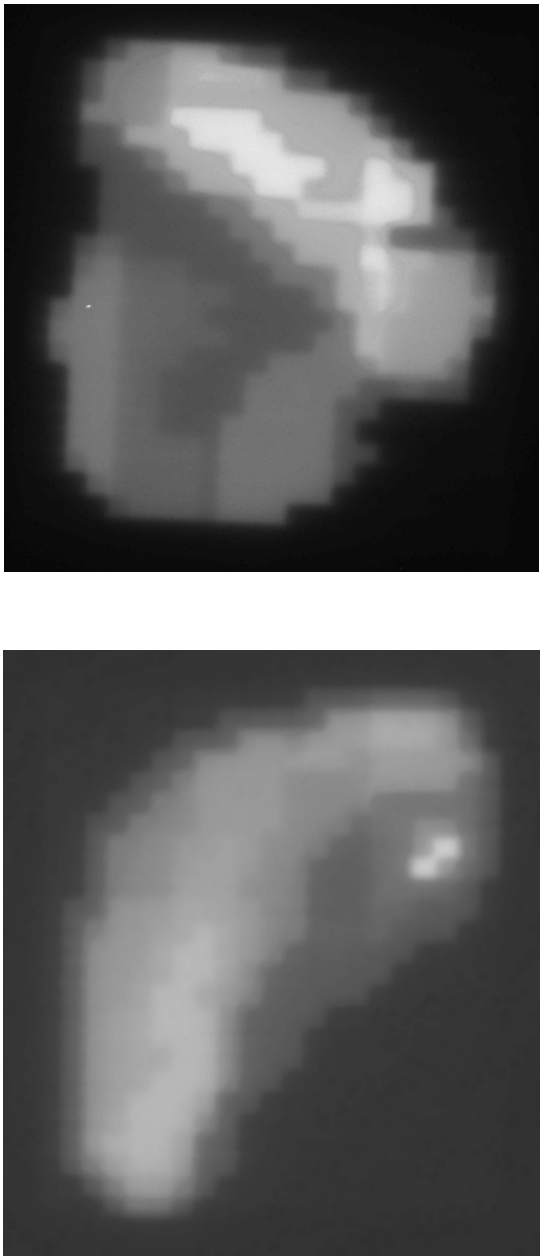

Figure 6.5. The planar dose distribution for Case 2 (a) Beam8 and (b) Beam4 measured on XV film and digitised.

Table 6.4. Case 2 individual beams measured with regular ionisation chamber for (a) normal MU delivery and (b) tripled MU delivery.

Regular Ionisation Chamber					
Beam	**MU**	**Predicted Dose (cGy)**	**Measured Dose (cGy)**	**Dose Difference (cGy)**	**Percent Difference (%)**
Beam1	35.4	7.8	8.8	1.0	11.4
Beam2	81.2	13.9	14.4	0.5	3.5
Beam3	52.9	14.5	14.9	0.4	2.7
Beam4	116.1	26.4	27.5	1.1	4.0
Beam5	38.8	6.4	6.6	0.2	3.0
Beam6	98.3	3.7	3.6	-0.1	-2.8
Beam7	109.7	7.7	7.6	-0.1	-1.3
Beam8	61.5	21.3	22	0.7	3.2
Beam9	68.4	21.7	20.3	-1.4	-6.9
Beam10	30.8	11.1	8.8	-2.3	-26.1
Whole	693.1	134.5	134.5	0.0	0.0

Regular Ionisation Chamber - Triple Dose					
Beam	**MU**	**Predicted Dose (cGy)**	**Measured Dose (cGy)**	**Dose Difference (cGy)**	**Percent Difference (%)**
Beam1	106.2	23.4	24.7	1.3	5.3
Beam2	243.6	41.7	40.3	-1.4	-3.5
Beam3	158.7	43.5	43.2	-0.3	-0.7
Beam4	348.3	79.2	79.6	0.4	0.5
Beam5	116.4	19.2	19.6	0.4	2.0
Beam6	294.9	11.1	9.2	-1.9	-20.7
Beam7	329.1	23.1	25.2	2.1	8.3
Beam8	184.5	63.9	62.3	-1.6	-2.6
Beam9	205.2	65.1	59.5	-5.6	-9.4
Beam10	92.4	33.3	25.3	-8.0	-31.6
Whole	2079.3	403.5	388.8	-14.7	-3.8

Table 6.5. Case 2 individual beams measured with parallel XV film.

XV Film - Osiris 12D - Parallel					
Beam	**MU**	**Predicted Dose (cGy)**	**Measured Dose (cGy)**	**Dose Difference (cGy)**	**Percent Difference (%)**
Beam4	116.1	26.4	31.8	5.4	17.0
Beam10	30.8	11.1	9	-2.1	-23.3

Table 6.6. Case 2 full treatment results for ionisation chambers and EDR2 film.

Case 2 Whole Dose				
Method	**Dose (cGy)**	**Relative Dose**	**cGy Diff**	**%Diff**
Pinnacle	134.5	1.00	0.0	0.0
IMRT Check	134.8	1.00	0.3	0.2
Reg Ion	134.5	1.00	0.0	0.0
X3 Reg Ion	388.8	0.96	-14.7	-3.8
Small Ion	134.5	1.00	0.0	0.0
X3 Small Ion				
Osiris 8D	137.6	1.02	3.1	2.3
Osiris 12D	139.1	1.03	4.6	3.3
ImageJ 8D	137.9	1.03	3.4	2.5
ImageJ 12D	136.9	1.02	2.4	1.7

6.4.4 Conclusion - Case 2

The measurements of the individual beams using the regular ionisation chamber show no advantage in increasing the MUs delivered in order to overcome the insensitivity of the chamber. This would not be a desirable technique anyway as it is not the actual treatment delivered to the patient. Besides, the regular ionisation chamber gave good results in the normal treatment mode, as did the small ionisation chamber, and both would be suitable for checking an IMRT treatment fraction. The regular chamber performed adequately while checking individual IMRT beams as well.

The second time a check was carried out as a clinical treatment, the delivery went very smoothly. After calibration data was acquired and the phantom set up, the patient 'treatment' itself took about 20 minutes.

The calibrated film results for the whole treatment were satisfactory enough to be used dosimetrically, although they were not ideal. The individual parallel film beam results were not good enough to use. Little difference could be seen between the results analysed using ImageJ software with 8-bit and 12-bit depth.

The qualitative film results provided very useful checks for both the axial and the planar distributions, and they definitely played a valuable role in the IMRT plan check, in particular as registration and alignment check tools.

6.5 Case 3 Dosimetry

6.5.1 Aim - Case 3

The Case 3 plan was the second IMRT plan to be tested. As with Case 2, Case 3 had a basal cell carcinoma (BCC) on the side of the face and neck, so it was important to try to irradiate the tumour while avoiding as much of the eye and brain as possible. A treatment was planned with ten coplanar beams.

6.5.2 Method - Case 3

The dose rate problems (UDRS) that occurred with the Case 2 plan were avoided this time by ensuring sufficient MUs were delivered per segment.

Checking the Case 3 plan involved calibrating the regular ionisation chamber, and using it to measure the dose delivered during a complete treatment fraction. The reading for each beam was noted, as well as the total. The regular ionisation chamber measurements were also carried out with the MUs tripled to see if this could improve the collection efficiency of the chamber. All of the measurements were repeated with the small ionisation chamber.

EDR2 film was exposed to a full treatment at the isocentre and calibration films were exposed. The film was analysed using both Osiris and ImageJ software. XV films were calibrated and exposed parallel to the axis of the beam for Beam3 and Beam10.

In order to check the orientation and dimensions of each dose distribution planar films were exposed at a depth of 7.5 cm in solid water, at 100 cm SSD. The Pinnacle planar map tool was used to recalculate the dose distribution at this depth and gantry angle.

6.5.3 Results - Case 3

The dose measured using the regular ionisation chamber for the whole treatment was 124.1 cGy, compared to an expected value of 121.1 cGy, which is a percentage difference of 2.4% and a dose difference of 3.0 cGy. This is a satisfactory result. However, when the measurements were repeated the overall dose was calculated to be 127.6 cGy, which is a difference of 5.1% or 6.5 cGy, which showed that a significant amount of variation could occur between measurements. The criticality of phantom set-up and alignment was highlighted as the likely cause of the difference.

Although large percentage differences were observed between the individual beam measurements, this was due to the small doses involved. For example Beam2 showed a percentage difference of 38.8%, which equated to a dose difference of 0.2 cGy (measured dose 0.5 cGy and expected dose 0.3 cGy). The largest dose difference in cGy was for Beam6 (measured dose 58.4 cGy and expected dose 56.5 cGy), which was a difference of 1.9 cGy or 3.2%. This was a satisfactory result.

Each beam output was also measured at the isocentre using the small ionisation chamber. The measured dose for the whole treatment was 126.9 cGy compared to an expected 121.1 cGy, which is a percentage difference of 4.6% and a dose difference of 5.8 cGy. This result was comparable to that obtained during the second ionisation chamber check.

Individually the highest dose difference found using the small ionisation chamber was 2.4 cGy for Beam1 (expected dose 17.6 cGy and measured dose 20 cGy, which is a difference of 11.9%). The highest percentage difference was –60.9% for Beam2 (expected dose 0.3 cGy and measured dose 0.8 cGy, which is a dose difference of 5.0 cGy). These results were comparable (and slightly worse) to those for the regular ionisation chamber.

In an attempt to compensate for the relative insensitivity of the small ionisation chamber doses of three times the magnitude were delivered by tripling the MUs (Varis automatically accounts for the change in MUs by adjusting the delivery time for each segment accordingly). The overall dose was measured to be 378.8 cGy (expected dose 363.3 cGy), which is a dose difference of 15.5 cGy or a percentage difference of 4.1%. The largest difference for an individual beam was 5.6 cGy for Beam6 (expected dose 169.5 and measured dose 175.1, which is a percentage difference of 3.2%). The results are slightly improved over the original small ionisation chamber measurements.

For purposes of proper comparison the regular ionisation chamber was also used to measure triple doses. The overall dose was measured to be 368.6 cGy (expected dose 363.3 cGy), which is a dose difference of 5.3 cGy or a percentage difference of 1.4%. The largest difference for an individual beam was 3.5 cGy for Beam1 (expected dose 52.8 cGy and measured dose 56.3 cGy), which is a percentage difference of 6.3%. These results are clearly better than those for the small ionisation chamber.

The qualitative planar films were compared to the dose distributions calculated by Pinnacle to check that the beam was delivered in the right orientation and with the correct dimensions. The first batch of films was accidentally exposed at the wrong depth in the solid water phantom, which affected the dimensions of the dose distribution. This demonstrated the importance of being careful with both the set-up of the film, and the printing of the Pinnacle calculated planar dose map distributions, although a correction factor could be applied to account for the error. A second batch of films was exposed and this time the dose distribution dimensions matched

the expected Pinnacle planar dose map dimensions well when compared using a ruler.

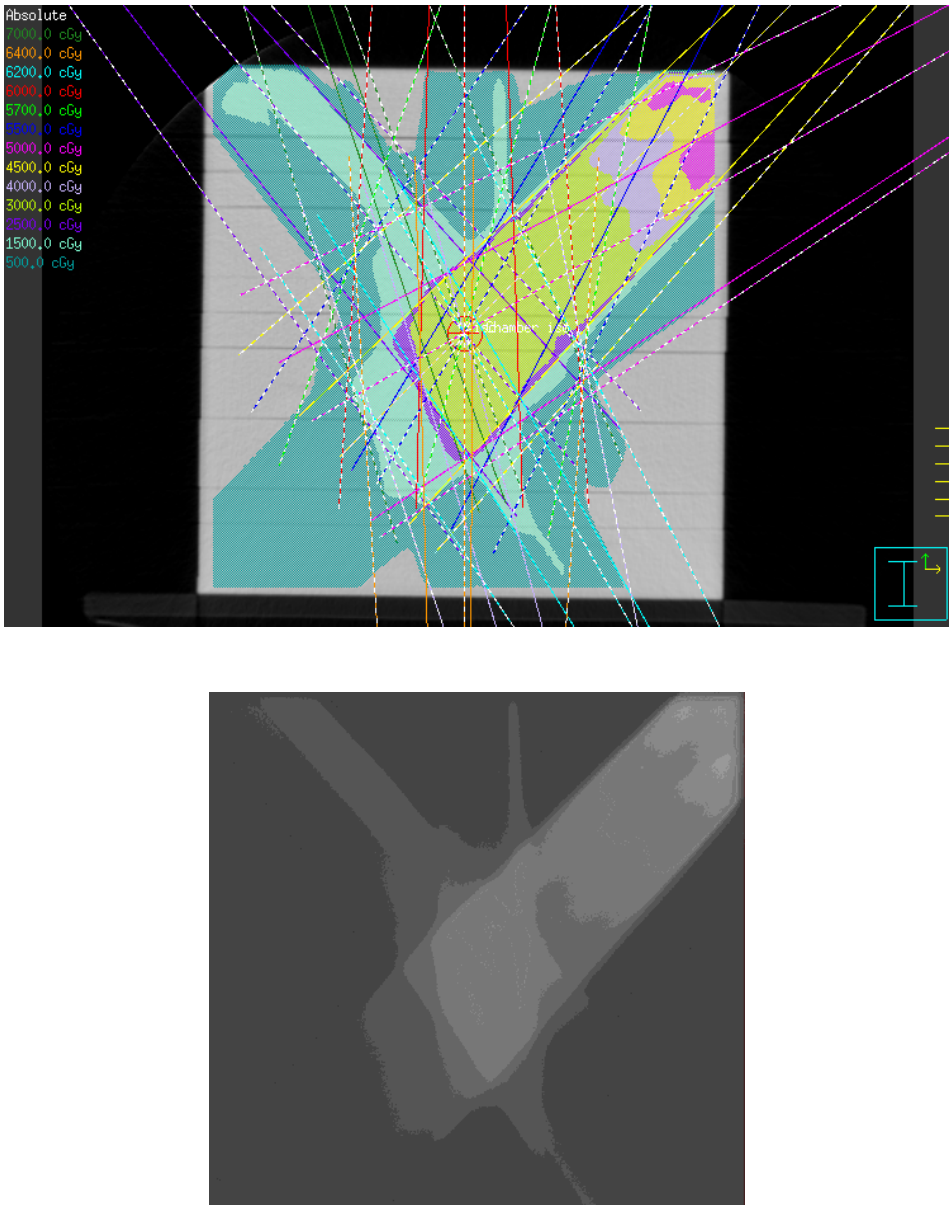

Figure 6.6. The axial dose distribution for Case 3 (a) predicted by Pinnacle, showing the beam angle distribution and (b) measured on EDR2 film and digitised.

Using the Osiris software the planar film measured a dose of 132.4 cGy compared to an expected of 121.1 cGy (difference 8.5% or 11.3 cGy) for the 8-bit depth and 133.2 cGy (difference 12.1% or 12.1 cGy) for the 12-bit depth. Using the ImageJ software the planar film measured a dose of 132.4

(difference 8.6% or 11.3 cGy) for the 8-bit depth and 131.6 cGy (difference 8.0% or 10.5 cGy) for the 12-bit depth.

The quantitative film measurements were not satisfactory, and this can be largely attributed to the steep dose gradients present around the isocentre, where the measurement was taken. The film can be difficult to accurately set up, and therefore the ImageJ, with its easier-to-use features, could be used to more exactly measure the point. There is not a large difference between any of the scans, which indicates the bigger problem was with pinpointing the centre of the dose distribution, and with the overall film analysis process, than with the type of software used.

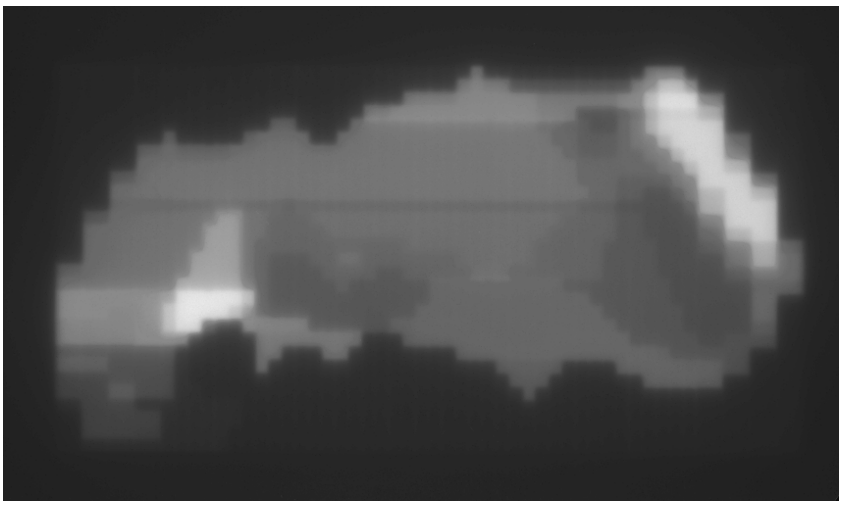

Figure 6.7. The planar dose distribution for Case 3, Beam7 measured on XV film and digitised.

Figure 6.7 shows a digitised planar distribution film for Beam7. The digitised image gives a very clear picture of the complex dose distribution for Beam7, with the regions receiving higher doses appearing as lighter regions on the image. This provides a very good visual comparison with the Pinnacle-predicted dose distribution. The image also shows a dark horizontal line of lower dose running across the middle of the field. This is a matchline (see '1.2.1 Matchlines'), which was not predicted by Pinnacle. The image can be

analysed to determine whether the matchline still provides a dose relatively close to the surrounding areas, or whether it is too large to be acceptable, in which case the beam must be replanned or the leaves offset to eliminate the fault. Tangboonduangjit *et al*.[110] carried out analysis on matchlines and found the dose difference when combined with the beam weight contribution to be acceptable for this case.

Table 6.7. Case 3 individual beams measured with regular ionisation chamber for (a) normal MU delivery and (b) tripled MU delivery.

Regular Ionisation Chamber					
Beam	**MU**	**Predicted Dose (cGy)**	**Measured Dose (cGy)**	**Dose Difference (cGy)**	**Percent Difference (%)**
Beam1	48	17.6	18.9	1.3	6.9
Beam2	9	0.3	0.4	0.1	25.0
Beam3	54	15.7	15.9	0.2	1.3
Beam4	81	1.8	1.4	-0.4	-28.6
Beam5	30	5.1	5	-0.1	-2.0
Beam6	115	56.5	56.7	0.2	0.4
Beam7	58	8.1	8.3	0.2	2.4
Beam8	30	10	11	1.0	9.1
Beam9	6	2.8	3.1	0.3	9.7
Beam10	20	3.2	3.4	0.2	5.9
Whole	450	121.1	124.1	3.0	2.4

Regular Ionisation Chamber - Triple Dose					
Beam	**MU**	**Predicted Dose (cGy)**	**Measured Dose (cGy)**	**Dose Difference (cGy)**	**Percent Difference (%)**
Beam1	144	52.8	56.3	3.5	6.2
Beam2	27	0.9	1.3	0.4	30.8
Beam3	162	47.1	47.0	-0.1	-0.2
Beam4	243	5.4	4.2	-1.2	-28.6
Beam5	90	15.3	14.6	-0.7	-4.8
Beam6	345	169.5	170.2	0.7	0.4
Beam7	174	24.3	24.5	0.2	0.8
Beam8	90	30	32.3	2.3	7.1
Beam9	18	8.4	9	0.6	6.7
Beam10	60	9.6	9.3	-0.3	-3.2
Whole	1350	363.3	368.6	5.3	1.4

Table 6.8. Case 3 individual beams measured with small ionisation chamber for (a) normal MU delivery and (b) tripled MU delivery.

Small Ionisation Chamber					
Beam	**MU**	**Predicted Dose (cGy)**	**Measured Dose (cGy)**	**Dose Difference (cGy)**	**Percent Difference (%)**
Beam1	48	17.6	20.0	2.4	12.0
Beam2	9	0.3	0.8	0.5	62.5
Beam3	54	15.7	16.8	1.1	6.5
Beam4	81	1.8	1.8	0.0	0.0
Beam5	30	5.1	5.7	0.6	10.5
Beam6	115	56.5	58.4	1.9	3.3
Beam7	58	8.1	9.1	1.0	11.0
Beam8	30	10	11.5	1.5	13.0
Beam9	6	2.8	3.8	1.0	26.3
Beam10	20	3.2	3.8	0.6	15.8
Whole	450	121.1	127.8	6.7	5.2

Small Ionisation Chamber - Triple Dose					
Beam	**MU**	**Predicted Dose (cGy)**	**Measured Dose (cGy)**	**Dose Difference (cGy)**	**Percent Difference (%)**
Beam1	144	52.8	58.0	5.2	9.0
Beam2	27	0.9	1.5	0.6	40.0
Beam3	162	47.1	48.9	1.8	3.7
Beam4	243	5.4	4.8	-0.6	-12.5
Beam5	90	15.3	15.8	0.5	3.2
Beam6	345	169.5	175.1	5.6	3.2
Beam7	174	24.3	25.6	1.3	5.1
Beam8	90	30	32.9	2.9	8.8
Beam9	18	8.4	9.5	1.1	11.6
Beam10	60	9.6	9.9	0.3	3.0
Whole	1350	363.3	378.8	15.5	4.1

Table 6.9. Case 3 individual beams measured with parallel XV film.

XV Film - Osiris 12D					
Beam	**MU**	**Predicted Dose (cGy)**	**Measured Dose (cGy)**	**Dose Difference (cGy)**	**Percent Difference (%)**
Beam3	54	15.7	17.3	1.6	9.2
Beam10	20	3.2	4	0.8	20.0

Table 6.10. Case 3 full treatment results for ionisation chambers and EDR2 film.

Whole Dose Measurements				
Method	**Dose (cGy)**	**Relative Dose**	**cGy Diff**	**%Diff**
Pinnacle	121.1	1.00	0.0	0.0
IMRT Check	127.6	1.05	6.5	5.1
Reg Ion	124.1	1.02	3.0	2.4
X3 Reg Ion	368.6	1.01	5.3	1.4
Small Ion	127.8	1.06	6.7	5.2
X3 Small Ion	378.8	1.04	15.5	4.1
Osiris 8D	132.4	1.09	11.3	8.5
Osiris 12D	133.2	1.10	12.1	9.1
ImageJ 8D	132.4	1.09	11.3	8.5
ImageJ 12D	131.6	1.09	10.5	8.0

6.5.4 Conclusion - Case 3

Including the time it took to calibrate the ionisation chamber, to set up the 'treatment' phantom, and to perform and measure one complete fraction as a Varis treatment, evaluating the Case 3 plan took a little longer than half an hour.

Exposing planar and parallel films took longer – approximately one to one-and-a-half hours, including development and visual comparison. However, the ionisation chamber measurement is the most important and immediate quantitative test, and the ability to do it in half an hour meant that if necessary that part of the plan check could be fitted into a treatment time slot during the day.

Exposing the planar films proved to be a convenient and effective method of qualitatively checking the dose distribution

The small ionisation chamber gave a comparable result to the regular ionisation chamber, however it was no better, and the small ionisation chamber would not be convenient for measuring some small magnitude individual beam doses because it's collection sensitivity would be inadequate. Even when the dose delivered was increased the small chamber showed no significant improvement. Therefore the regular ionisation chamber would be the preferred dosimeter for this check.

The quantitative film results were not good, and as with the previous cases digitising the film with 8-bit resolution proved no worse than with 12-bit, indicating that the limited dose contrast resolution that 8-bit resolution provides (see '5.1.4 Aim - Film Scanner Tests') did not seem to be a disadvantage with these films. The good ionisation chamber results indicated that the poor film results were due to the use of film itself, rather than the

high dose gradients at the isocentre that can be seen on the dose distribution for Case 3.

All of the measurements made of the whole treatment fraction resulted in measured doses higher than expected. One possible explanation is that the Pinnacle model for the asymmetric fields may possible contribute to the dose at the isocentre being different to that calculated. This effect would perhaps not be predicted by the Pinnacle model. However, the result of a 2.4% match, which is just above the nominal 2.0% aimed for, may equally be within the set-up/dosimetry tolerance. More cases will be needed to achieve a final standard deviation estimate of the differences expected between Pinnacle and the dosimetry check.

6.6 Case 4 Dosimetry

6.6.1 Aim - Case 4

The Case 4 plan was a larynx treatment consisting of 15 beams at 9 gantry angles. It was of particular interest for two reasons, as follows.

First, the plan was designed to minimise dose to the spinal cord, leaving a dose void in the dose distribution. Although a relatively large region of dose around the point of the measurement at the isocentre was quite regular for an IMRT plan, the dose void was only about 2 cm from isocentre, so the very steep dose gradient might affect measurements.

Secondly, the length of a field in the leaf drive axis is more limited with a Varian MLC than without because the leaves can only drive 14.5 cm out from each carriage. Fortunately the Varian MLC carriages can move to any location provided they are shielded by a jaw during beam on, hence a way around this is to create overlapping fields. Six fields had to be split into two for this case. In a normal treatment the field would be split along the central axis of the beam in order to reduce the effect of beam spread. The under- or overlap of the two 'subfields' depends on the positional accuracy of the jaws and generally a small cold or hot spot is unavoidable. With the IMRT treatment the fields could be overlapped and modulation within the overlap was used to decrease the total dose. The implication for each of these fields is that the magnitude of dose and hence the charge per MU is about half for each overlapping region than it would be for the usual incident IMRT field[79].

6.6.2 Method - Case 4

As the plan checking technique became more established less dosimetry was carried out. The use of the small ionisation chamber was not continued, as it had not shown any advantage over the regular ionisation chamber.

The calibrated regular ionisation chamber was used in the cubic solid water phantom to measure the dose at the isocentre of each beam and of the overall treatment.

EDR2 film was positioned at the isocentre and parallel to the axis of the beam. It was exposed to a whole treatment fraction. Calibration films were exposed perpendicular to the axis of the beam at d_{max} (1.5 cm) in solid water. The calibrated film was analysed using both Osiris and ImageJ software.

XV films were calibrated and exposed in the parallel orientation for two beam angles, both of which comprised two overlapped beams each: Beam1 with Beam2 and Beam6 with Beam7. These films were analysed with ImageJ software with 12-bit depth.

Planar XV films were exposed at 7.5 cm in water at 100 cm SAD for each beam. These were not dose calibrated, but they were compared for registration and alignment with the planar dose maps.

6.6.3 Results - Case 4

The regular ionisation chamber results for Case 4 were good. The highest dose difference recorded for the individual beams was 0.8 cGy for Beam9 (expected 7.7 cGy, measured 8.5 cGy, 9.4% difference) and –0.8 cGy for Beam15 (expected 10.3 cGy, measured 9.5 cGy, -8.4% difference). The highest percentage difference was 9.5% for Beam9, which is acceptable considering the small dose values involved.

Overall the regular ionisation chamber measured a dose of 136.4 cGy, compared to an expected 135.2 cGy. This is a very small difference of 1.2 cGy or 0.9%, which is within the 2% nominal difference aimed for.

The region of reduced dose around the spine appears not to have adversely affected the dosimetry at the isocentre.

The individual overlapped beams measured using the XV film gave adequate dose results, according to Table 6.12. Beam1 and Beam2 gave a combined dose of 17.7 cGy compared to an expected dose of 18.1 cGy, which is a difference of -0.4 cGy of -2.3%. Beam6 and Beam7 gave a combined dose of 14.6 cGy compared to an expected dose of 12.6 cGy, which is a difference of 2.0 cGy or 13.7%. The digitised image for the Beam6 and Beam7 film is shown in Figure 6.9. It shows a clear dose gap where the beam was designed to avoid the spinal cord, indicating a steep dose gradient.

Figure 6.8. The axial dose distribution for Case 4 (a) predicted by Pinnacle (b) measured on EDR2 film and digitised and (c) coloured.

The parallel axial dose distribution film was calibrated and analysed using both Osiris and ImageJ software, and similar results were obtained for each. The Osiris software measured a dose of 127.0 cGy compared to an expected dose of 135.2 cGy, which is a difference of –8.2 cGy or -6.5%. The ImageJ software gave a result of 126.6 cGy, which is a difference of –8.6 cGy or -6.8%. Both of these results are similar to film measurements of other plans, and they are poor in comparison with the ionisation chamber measurements. Once again a phantom with a better clamping system such as the ART IMRT phantom will be recommended to be tested in future cases.

Figure 6.9. The parallel dose distribution for Case 4, Beam6 and Beam7 measured on XV film and digitised.

The qualitative dose distribution film came out very well. It was digitised and this time a colour wash was placed on the image to make it easier to interpret and compare. The results are shown in Figure 6.8 along with the original Pinnacle-planned dose distribution, and it can be seen that the colour wash of the film is much easier to compare to the Pinnacle image than the greyscale image is.

Table 6.11. Case 4 individual beams measured with regular ionisation chamber for normal MU delivery.

Regular Ionisation Chamber					
Beam	**MU**	**Predicted Dose (cGy)**	**Measured Dose (cGy)**	**Dose Difference (cGy)**	**Percent Difference (%)**
Beam1	56	9.1	9.3	0.2	2.2
Beam2	69	9	9.1	0.1	1.1
Beam3	79	10.6	10.8	0.2	1.9
Beam4	55	9.8	9.8	0.0	0.0
Beam5	90	9.8	10	0.2	2.0
Beam6	76	6	6.4	0.4	6.3
Beam7	54	6.6	7.2	0.6	8.3
Beam8	103	6.7	6.8	0.1	1.5
Beam9	48	7.7	8.5	0.8	9.4
Beam10	87	8.4	8.5	0.1	1.2
Beam11	78	10	9.9	-0.1	-1.0
Beam12	57	10	10	0.0	0.0
Beam13	75	11.1	11.1	0.0	0.0
Beam14	55	10.1	9.7	-0.4	-4.1
Beam15	77	10.3	9.5	-0.8	-8.4
Whole	1059	135.2	136.4	1.2	0.9

Table 6.12. Case 4 overlapped beams measured with parallel XV film.

XV Film - Osiris 12D					
Beam	**MU**	**Predicted Dose (cGy)**	**Measured Dose (cGy)**	**Dose Difference (cGy)**	**Percent Difference (%)**
Beam1 & Beam 2	125	18.1	17.7	-0.4	-2.3
Beam6 & Beam7	130	12.6	14.6	2.0	13.7

Table 6.13. Case 4 full treatment results for ionisation chambers and EDR2 film.

Whole Dose Measurements				
Method	**Dose (cGy)**	**Relative Dose**	**cGy Diff**	**%Diff**
Pinnacle	135.2	1.00	0.0	0.0
IMRT Check	136.4	1.01	1.2	0.9
Reg Ion	136.4	1.01	1.2	0.9
X3 Reg Ion	363.0	0.89	-42.6	-11.7
Small Ion				
X3 Small Ion				
Osiris 8D	127.0	0.94	-8.2	-6.5
Osiris 12D	127.6	0.94	-7.6	-6.0
ImageJ 8D	126.6	0.94	-8.6	-6.8
ImageJ 12D	127.4	0.94	-7.8	-6.1

6.6.4 Conclusion - Case 4

The results for this case confirm the success of using the ionisation chamber as the main dosimeter for checking IMRT plans. For this case the film gave a reasonably satisfactory result for assessing dose at the isocentre. The results for the parallel film dosimetry of the overlapping beams were good, and this may prove a useful method of measuring individual beams with film, as well as for checking the dose distribution in the axial plane. A potential disadvantage is the amount of time required in making such measurements.

The uncalibrated films have proved a valuable method of qualitative plan checking for registration and alignment. Digitising and colouring the film enabled much easier visual comparison of dose distributions.

6.7 Case 4 Boost Dosimetry

6.7.1 Aim - Case 4 Boost

The Case 4 Boost plan was a boost treatment for the head and neck Case 4 plan to deliver an extra dose to the main part of the tumour. The treatment was planned with 12 coplanar beams.

Being a boost to a smaller region than the original treatment, less low dose modulation to shield structures within the beam were required, so the dose distribution for this treatment was much more regular than for the other IMRT treatments. This should make the dosimetry measurements of the plan more accurate because large dose gradients and hot or cold dose spots were avoided at the isocentre.

6.7.2 Method - Case 4 Boost

By the time the Case 4 Boost plan was checked the dosimetry system was better established than for the first three cases. All of the individual beams and the whole treatment plan were checked with the regular ionisation chamber. The measurements were repeated with triple the dose delivered.

No quantitative film measurements were carried out on individual beams. However the whole treatment dose was measured with calibrated EDR2 film and scanned and analysed with Osiris and ImageJ software with both 8-bit and 120-bit depth.

The same axial dose distribution films were analysed qualitatively using visual comparison and a ruler, and one of the digitised images was coloured to provide an easier dose distribution comparison.

6.7.3 Results - Case 4 Boost

The results for the individual beam measurements of the Case 4 Boost plan are given in Table 6.14 for the regular ionisation chamber. The results for the whole treatment measured with each dosimeter are given in Table 6.15.

The checks on the individual beams using the regular ionisation chamber produced good results. The highest dose difference is -2.5 cGy for Beam12, which measured 8.1 cGy compared to an expected 10.6 cGy. The percentage difference is -30.9%, but the reason this percentage value is so high is because small dose values are being compared. Beam1 and Beam7 approach this difference with -26.7% and 26.5% respectively, but these equate to just -2.3 cGy and 2.2 cGy dose differences. The sum of the individual beam measurements is 130.3 cGy compared to a Pinnacle-predicted value of 129.5 cGy, which is a dose difference of 0.8 cGy or a percentage difference of 0.6%, which is a good dosimetry result.

The regular ionisation chamber checks on the individual beams with the doses tripled are comparable to the measurements done with the normal doses. The dose measured for Beam12 is 24.2 cGy compared to an expected 31.8 cGy, which is a dose difference of -7.6 cGy or a percentage difference of -31.4%. The total treatment measurement is 385.6 cGy, compared to an expected dose of 388.5 cGy, which is a dose difference of -2.9 cGy or a percentage difference of -0.8%.

The measurements of the treatment with the doses tripled were much better than for previous patients, indicating that it was the uniformity of the dose distribution at the centre of the treatment rather than the dosimetry technique that was improved.

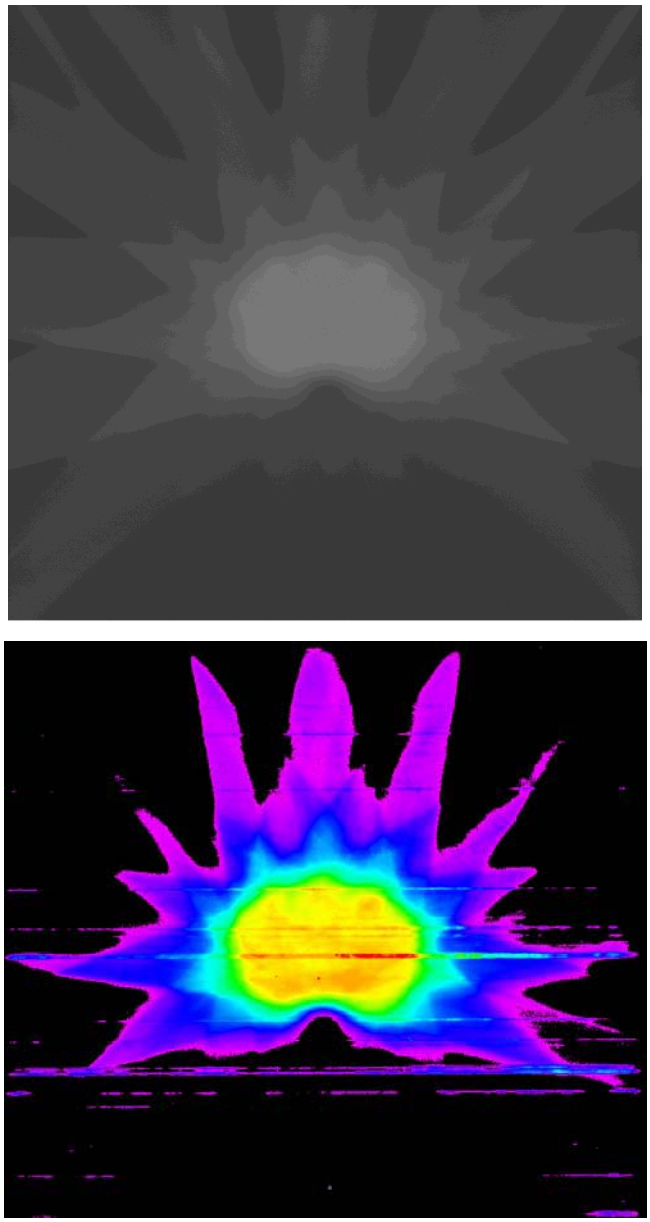

Figure 6.10. The axial dose distribution for Case 4 Boost measured on EDR2 film (a) digitised and (b) coloured. The streaks in the coloured image are actually due to a problem in the development process.

Table 6.15 shows results for the film dosimetry techniques. All four of the analysis methods gave similar results, the worst being ImageJ with 12-bit depth, which gives a measured dose of 136.9 cGy compared to an expected dose of 129.5 cGy, which is a difference of 5.4 cGy and 7.4%. The best film result is for Osiris with 12-bit depth with a measured dose of 136.5 cGy, which is a dose difference of 7.0 cGy or a percentage difference of 5.1%.

These results are very good in comparison to film measurements for previous patient plans, and again this is probably due to the more regular dose distribution at the isocentre than an improvement in dosimetry techniques.

The axial dose distribution measured at the isocentre using the EDR2 film was digitised and coloured to make comparison of the dose distribution easier. The digitised film is shown in original form and with a colour wash in Figure 6.10. This made it much easier to check the dose was delivered correctly. The coloured image shows streaks that were obvious on the film but not obvious on the greyscale image; these are actually due to the poor quality of the development process for this film. This is a good demonstration of how adding colour to the image can increase the amount of detail that can be distinguished.

Table 6.14. Case 4 Boost individual beams measured with regular ionisation chamber for (a) normal MU delivery and (b) tripled MU delivery.

Regular Ionisation Chamber					
Beam	**MU**	**Predicted Dose (cGy)**	**Measured Dose (cGy)**	**Dose Difference (cGy)**	**Percent Difference (%)**
Beam1	63	10.9	8.6	-2.3	-26.7
Beam2	55	12.3	13.2	0.9	6.8
Beam3	56	12.6	13.5	0.9	6.7
Beam4	68	11	11.9	0.9	7.6
Beam5	74	12.2	12	-0.2	-1.7
Beam6	93	6.1	8.3	2.2	26.5
Beam7	91	5.6	6.1	0.5	8.2
Beam8	74	11.5	11.4	-0.1	-0.9
Beam9	58	12	12.4	0.4	3.2
Beam10	59	12.9	13.3	0.4	3.0
Beam11	55	11.8	11.6	-0.2	-1.7
Beam12	61	10.6	8.1	-2.5	-30.9
Whole	807	129.5	130.3	0.8	0.6

Regular Ionisation Chamber - Triple Dose					
Beam	**MU**	**Predicted Dose (cGy)**	**Measured Dose (cGy)**	**Dose Difference (cGy)**	**Percent Difference (%)**
Beam1	189	32.7	25.8	-6.9	-26.7
Beam2	165	36.9	39.0	2.1	5.4
Beam3	168	37.8	40.1	2.3	5.7
Beam4	204	33	34.7	1.7	4.9
Beam5	222	36.6	35.6	-1.0	-2.8
Beam6	279	18.3	24.5	6.2	25.3
Beam7	273	16.8	17.9	1.1	6.1
Beam8	222	34.5	33.5	-1.0	-3.0
Beam9	174	36	36.6	0.6	1.6
Beam10	177	38.7	38.8	0.1	0.3
Beam11	165	35.4	34.9	-0.5	-1.4
Beam12	183	31.8	24.2	-7.6	-31.4
Whole	2421	388.5	385.6	-2.9	-0.8

Table 6.15. Case 4 Boost full treatment results for ionisation chambers and EDR2 film.

Whole Dose Measurements				
Method	**Dose (cGy)**	**Relative Dose**	**cGy Diff**	**%Diff**
Pinnacle	129.5	1.00	0.0	0.0
IMRT Check	130.3	1.01	0.8	0.6
Reg Ion	130.3	1.01	0.8	0.6
X3 Reg Ion	385.6	0.99	-2.9	-0.8
Small Ion				
X3 Small Ion				
Osiris 8D	136.8	1.06	7.3	5.3
Osiris 12D	136.5	1.05	7.0	5.1
ImageJ 8D	136.8	1.06	7.3	5.3
ImageJ 12D	136.9	1.06	7.4	5.4

6.7.4 Conclusion - Case 4 Boost

All of the dosimetry techniques gave very good results for the Case 4 Boost plan. This is largely due to the more regular dose distribution of the boost plan around the isocentre helping to eliminate set-up errors, which are critical when high dose gradients occur.

Again the regular ionisation chamber has proved to be the most effective dosimeter for checking IMRT plans. The EDR2 film is most effective for qualitatively checking dose distributions. Now it has also been found that digitising and colouring the film provides an even more comprehensive comparative check. The films themselves provide a valuable check straight after development, which can help to pick up obvious errors immediately. However, when given the time to digitise and colour the film, this would be more effective for finding subtle errors in the dose distribution, and fortunately this process does not take long for one film.

6.8 Case 5 Dosimetry

6.8.1 Aim - Case 5

The Case 5 plan was a scalp treatment consisting of 9 coplanar beams. The treatment was designed to conform to the curved shape of the skull in an attempt to avoid the brain. As a result the planned dose distribution was relatively small in area (see Figure 6.11), but large enough to position a regular ionisation chamber at the centre.

6.8.2 Method - Case 5

All of the individual beams and the whole treatment plan were checked with the regular ionisation chamber, which was calibrated at d_{max} in a solid water phantom at 100 cm SSD.

The whole treatment dose was also measured with calibrated EDR2 film and analysed using Osiris and ImageJ software. The axial films were also used to qualitatively evaluate the dimensions of the axial dose distribution. One film was digitised and coloured to provide a more accurate visual comparison.

6.8.3 Results - Case 5

The results for the individual beam measurements of the Case 5 plan with the regular ionisation chamber are given in Table 6.16. The results for the whole treatment measured with each dosimeter are given in Table 6.17.

The individual beam checks using the regular ionisation chamber gave good results. The highest dose difference found was 3.6 cGy for Beam3, with a measured dose of 11.3 cGy compared to a predicted dose of 7.7 cGy, which equates to 31.9%. All of the other results gave much lower differences, with the next highest dose difference being for Beam8 with a measured dose of

19.5 cGy compared to an expected 21.2 cGy, which is a difference of -1.7 cGy or -8.7%.

The whole treatment dose check with the regular ionisation chamber gave good results with a measured dose of 130.9 cGy compared to a predicted dose of 130.8 cGy, which is a dose difference of 0.1 cGy or 0.1%.

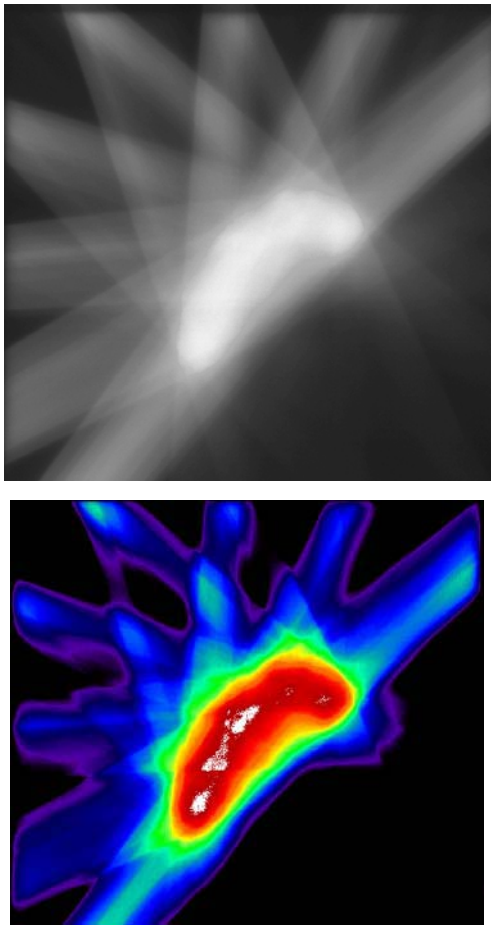

Figure 6.11. EDR2 film axial dose distributions for Case 5 (a) digitised and (b) coloured.

The calibrated EDR2 film did not produce very satisfactory results for the whole treatment dose measurements. The best result was using the Osiris software with 8-bit depth, which gave a measured dose of 138.4 cGy compared to an expected dose of 130.8 cGy, which is a dose difference of 7.6 cGy or 5.5%. The other three film results were slightly worse, with the ImageJ

software with 12-bit depth giving a measured dose of 138.9 cGy, which is a difference of 8.1 cGy or 5.8%.

Figure 6.11 shows the digitised images of the measured axial dose distribution, in both grayscale and with a colourwash. The coloured image made a comparison with the Pinnacle-predicted distribution much easier than the uncoloured image did, and indicated a good agreement between the predicted and the delivered dose.

The planar film exposed for Beam 7 is shown in Figure 6.12. Again, the planar film maps provided a good visual verification check using a ruler that the dose delivery was the correct position, orientation and dimensions. Commercial software was not available at the ICCC to do further film analysis such as dose difference maps.

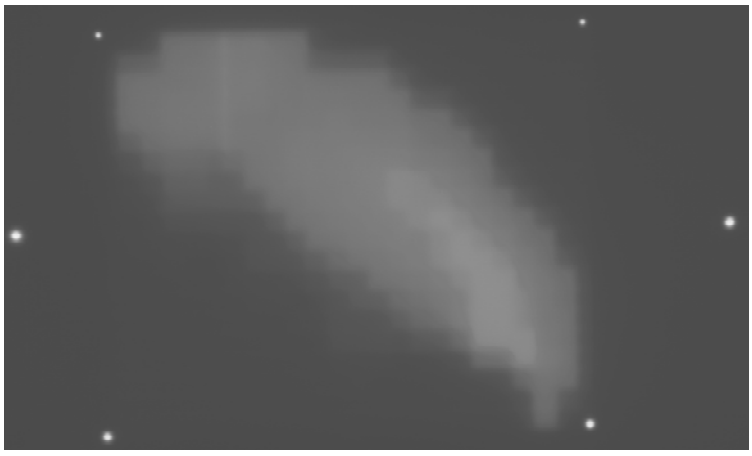

Figure 6.12. Beam 7 for Case 5 planar dose distribution (courtesy Puangpen Tangboonduangjit).

Table 6.16. Case 5 individual beams measured with regular ionisation chamber.

Regular Ionisation Chamber					
Beam	**MU**	**Predicted Dose (cGy)**	**Measured Dose (cGy)**	**Dose Difference (cGy)**	**Percent Difference (%)**
Beam1	70	17.7	18.2	0.5	2.7
Beam2	54	23.1	22.3	-0.8	-3.6
Beam3	64	7.7	11.3	3.6	31.9
Beam4	70	6.7	6.5	-0.2	-3.1
Beam5	71	3.7	3.7	0.0	0.0
Beam6	68	9.1	9.2	0.1	1.1
Beam7	62	20.5	20.3	-0.2	-1.0
Beam8	61	21.2	19.5	-1.7	-8.7
Beam9	56	21.1	19.9	-1.2	-6.0
Whole	576	130.8	130.9	0.1	0.1

Table 6.17. Case 5 full treatment results for ionisation chambers and EDR2 film.

Whole Dose Measurements				
Method	**Dose (cGy)**	**Relative Dose**	**cGy Diff**	**%Diff**
Pinnacle	130.8	1.00	0.0	0.0
Reg Ion	130.9	1.00	0.1	0.1
Reg Ion 2				
X3 Reg Ion				
Small Ion				
X3 Small Ion				
Osiris 8-bit	138.4	1.06	7.6	5.5
Osiris 12-bit	142.0	1.09	11.2	7.9
ImageJ 8-bit	139.7	1.07	8.9	6.4
ImageJ 12bit	138.9	1.06	8.1	5.8

6.8.4 Conclusion - Case 5

The regular ionisation chamber gave a very good result for Case 5, reaffirming its usefulness as a dosimetry tool. The overall dose distribution did not prove to be too small to provide adequate coverage for the regular chamber.

Using the EDR2 film as a dosimeter was not so successful. The qualitative dose distribution films, however, were very useful, and all future films should be coloured to provide simple, fast validation of dose deliveries.

6.9 Case 6 Dosimetry

6.9.1 Aim - Case 6

The Case 6 plan was designed with eleven beams. This time the treatment was also replanned for beam down deliveries, with the MUs retained and the doses recalculated.

Because beam down tests are used at other institutions this was tested as an option to see if better alignment and not traversing the steep angles of the cube phantom or the table bars would produce a better dose match between the ionisation chamber and the Pinnacle plan.

6.9.2 Method - Case 6

It was now a well-established IMRT dosimetry method within the clinic to use the regular ionisation chamber to check each of the individual beams and the whole treatment in the cubic solid water phantom. For Case 6 this was performed in the manner anticipated for future treatments. The regular ionisation chamber was calibrated at 1.5 cm depth and 100 cm SSD, and then set to isocentre in the cubic phantom. An entire treatment was delivered as a patient fraction on Varis, with no entry to the room between beams. The cumulative dose for the whole treatment was measured on the electrometer, and the charge readings were noted for each beam. The calibration values were used to calculate the dose delivered for each beam and for the entire treatment and this was compared to the Pinnacle-predicted values.

The planar beams were calculated at 15 cm depth in the phantom with an SSD of 85 cm, which placed the measurements at the isocentre. The MUs remained the same, so the predicted doses changed. The calibrated chamber was positioned in the same set-up as for the normal treatment. Each beam was delivered with the gantry at zero and the calibration value used to

calculate the dose delivered from the charge readings. To obtain a result for the whole treatment the values for each beam were summed.

Calibrated EDR2 film was also exposed in the parallel set-up to obtain an axial dose distribution, and the results were analysed using Osiris and ImageJ software. EDR2 films were exposed to the planar doses, but not calibrated, to qualitatively check the dose distributions of each beam.

6.9.3 Results - Case 6

The results for the individual beam measurements of the Case 6 plan are given in Table 6.18 for the regular ionisation chamber measured with the original gantry angles and in the planar beam down dose configuration. The results for the whole treatment measured with each dosimeter are given in Table 6.19.

The individual beam measurements show two beams with unusually high dose differences. Beam1 measured 6.3 cGy compared to an expected 10.8 cGy, which is a dose difference of -4.5 cGy or a percentage difference of -71.4%. Beam11 measured 6.1 cGy compared to an expected dose of 11.2 cGy, which is a dose difference of -5.1 cGy or a percentage difference of -83.6%. Beam1 and Beam11 were delivered at gantry angles of 130° and 230° respectively, which meant they had to pass through the corner of the phantom and the bar on the side of the couch. As a secondary effect sharp contours at the corner of the phantom may affect the accuracy of the dose prediction, and would not be present when calculating the dose distribution for a patient. Passing the beam through the bar on the couch could not be avoided because the phantom had to be placed on the tennis racquet part of the couch (the patient would be positioned on the carbon fibre part of the couch where the bars can be avoided). On the new Exact couch tops with

movable bars, one of which is to be installed with a new linac at ICCC, this will not be an issue. The other beams gave good results, with Beam3 and Beam7 giving the next highest dose difference of 0.7 cGy, or 5.1% and 4.9% respectively.

The results for the original Case 6 plan are not as good as was expected for the regular ionisation chamber measurements, based on previous cases. The whole treatment measured 129.5 cGy compared to an expected 137.6 cGy, which is a dose difference of -8.1 cGy or a percentage difference of -6.3%. Previously the worst results were for the Case 3 plan (see '6.5.3 Results - Case 3'), which gave a difference of 3.0 cGy or 2.4% for the whole treatment.

The planar dose results show a clear improvement over the original results. Beam1 measured 14.0 cGy compared to an expected dose of 13.2 cGy, which is a dose difference of 0.8 cGy or a percentage difference of 5.9%. Beam11 measured a dose of 14.0 cGy compared to an expected dose of 13.7 cGy, which is a dose difference of 0.3 cGy or a percentage difference of 2.2%. The sum of the beams is 152.2 cGy compared to an expected dose of 150.2 cGy, which is a dose difference of 2.0 cGy or a percentage difference of 1.3%. This is a very satisfactory result, and shows that measuring the planar distribution can give a more accurate dosimetry result than isocentric measurements.

Table 6.17 gives the results for the full patient treatment measured by the regular ionisation chamber and by the film. Figure 6.11 shows the digitised film with and without a colourwash. Unexpectedly, the EDR2 film gave a good dosimetric response with the largest dose difference being for the film analysed using Osiris software with 12-bit depth, which gave a measurement of 138.3 cGy compared to an expected 137.6 cGy (a dose difference of just 0.7 cGy or a percentage difference of 0.5%). As all of the other EDR2 film results were high (apart from Case 4) it is likely that the film was giving a high

reading for a dose that had been reduced by attenuation by the bars on the couch.

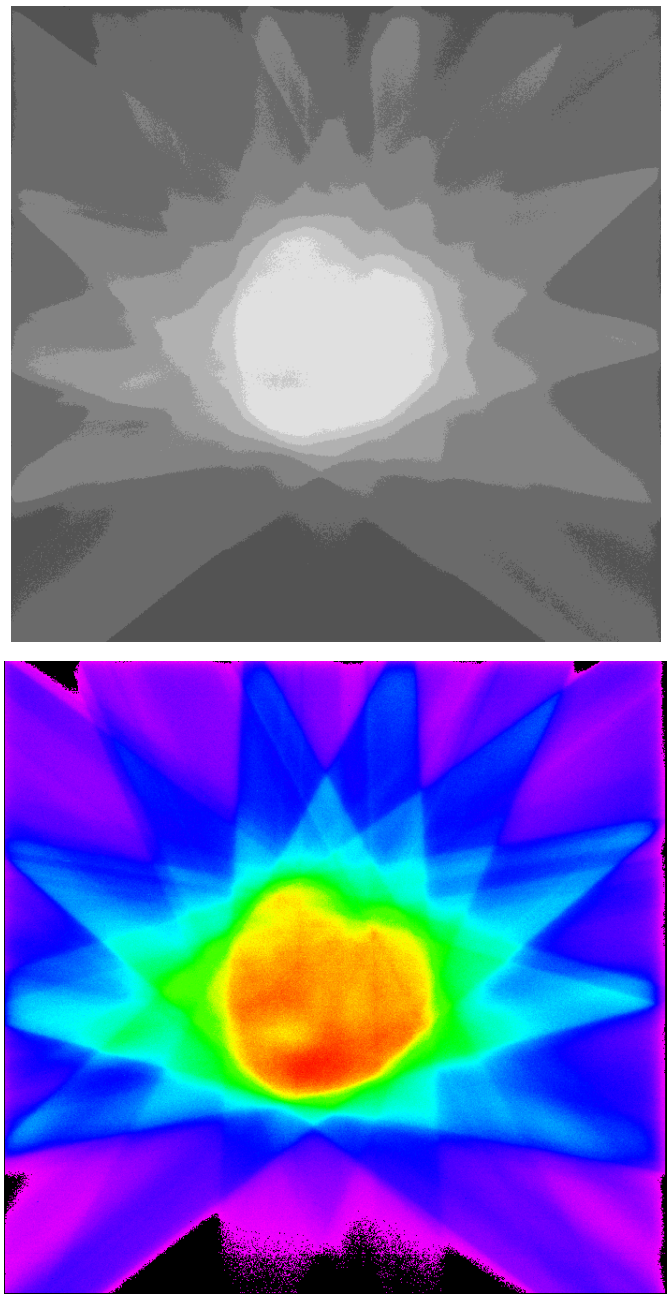

Figure 6.13. The axial dose distribution for Case 6 measured on EDR2 film (a) digitised and (b) coloured.

Figure 6.14 shows the digitised image of the planar film for Beam6. The matchline effect can be seen as the three brighter vertical lines. The white spots are caused by pinpricks made in the film packet to align the film with

the light field and to enable better positional accuracy during analysis. Because this dose distribution had three matchlines it was used as a reference step-and-shoot sequence for subsequent studies with an EPID dosimeter and with Monte Carlo models (Puangpen Tangboonduangjit, private communication, 2005).

As was expected, the film also gave very good qualitative results for both the axial and the planar beam dose distributions. Again, adding colour to the digitised film made a qualitative comparison between the predicted and the measured distributions much easier.

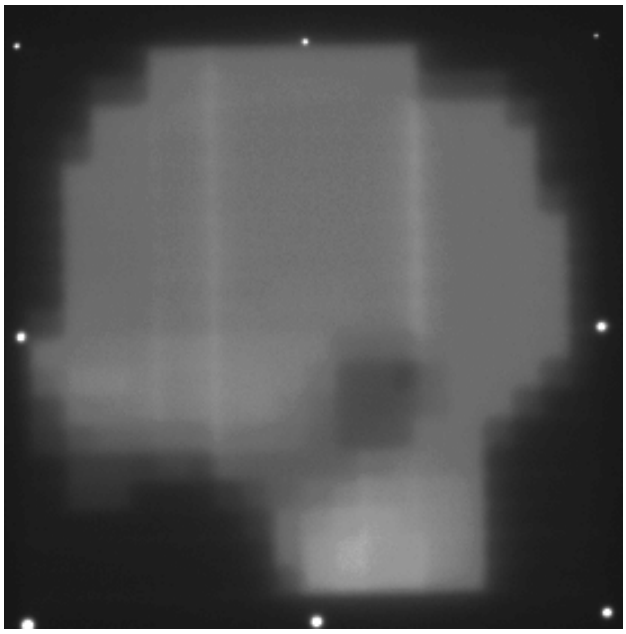

Figure 6.14. The planar dose distribution for Case 6, Beam6 measured on XV film and digitised.

Table 6.18. Case 6 individual beams measured with regular ionisation chamber for (a) normal MU delivery and (b) planar MU delivery.

Regular Ionisation Chamber					
Beam	**MU**	**Predicted Dose (cGy)**	**Measured Dose (cGy)**	**Dose Difference (cGy)**	**Percent Difference (%)**
Beam1	52	10.8	6.3	-4.5	-71.4
Beam2	67	13.9	14.0	0.1	0.7
Beam3	60	12.9	13.6	0.7	5.1
Beam4	48	10.9	11.1	0.2	1.8
Beam5	56	11.4	11	-0.4	-3.6
Beam6	67	14.1	14	-0.1	-0.7
Beam7	67	13.5	14.2	0.7	4.9
Beam8	54	10.7	10.8	0.1	0.9
Beam9	65	14	13.8	-0.2	-1.4
Beam10	43	14.2	14.6	0.4	2.7
Beam11	48	11.2	6.1	-5.1	-83.6
Whole	627	137.6	129.5	-8.1	-6.3

Regular Ionisation Chamber - PLANAR DOSES					
Beam	**MU**	**Predicted Dose (cGy)**	**Measured Dose (cGy)**	**Dose Difference (cGy)**	**Percent Difference (%)**
Beam1	52	13.2	14.0	0.8	5.9
Beam2	67	14.2	14.6	0.4	2.6
Beam3	60	13.3	13.7	0.4	2.9
Beam4	48	13.4	13.5	0.1	0.9
Beam5	56	12.9	12.6	-0.3	-2.0
Beam6	67	14.1	13.1	-1.0	-7.4
Beam7	67	14.5	15.0	0.5	3.5
Beam8	54	12.8	13.0	0.2	1.2
Beam9	65	13.8	14.0	0.2	1.1
Beam10	43	14.3	14.7	0.4	2.5
Beam11	48	13.7	14.0	0.3	2.2
Whole	627	150.2	152.2	2.0	1.3

Table 6.19. Case 6 full treatment results for ionisation chambers and EDR2 film.

Whole Dose Measurements				
Method	**Dose (cGy)**	**Relative Dose**	**cGy Diff**	**%Diff**
Pinnacle	137.6	1.00	0.0	0.0
IMRT Check	129.6	0.94	-8.0	-6.2
Reg Ion	129.6	0.94	-8.0	-6.2
X3 Reg Ion				
Small Ion				
X3 Small Ion				
Osiris 8D	137.5	1.00	-0.1	-0.1
Osiris 12D	138.3	1.01	0.7	0.5
ImageJ 8D	137.7	1.00	0.1	0.1
ImageJ 12D	137.5	1.00	-0.1	-0.1

6.9.4 Conclusion - Case 6

The poor results for the regular ionisation chamber measurements were not typical of the measurements made for previous plans. Measuring the dose delivered by the original plan with the correct gantry angles is essential to properly ensure the accuracy of the entire treatment. However, measuring the planar doses gave added confidence that the correct dose has been calculated, and proved a valuable secondary check. Beam1 and Beam11 were the main contributors to the -6.3% difference, probably due to the couch rails, or misalignment of the sharp corner of the phantom.

Although the film dosimetry gave good results, previous film measurements indicate these results were not typical. Great care in calibration and processor maintenance is required if film is to be relied upon as a dosimetry technique.

Chapter 7: IMRT Dosimetry Conclusion

7.1 IMRT Dosimetry

Table 7.1 displays a list of all the physics duties involved in verifying a regular and an IMRT plan, and the estimated times for each. The IMRT plan times represent those achieved for Case 6 after much practice with previous cases. As can be seen from the table, IMRT verification takes longer to complete than regular radiotherapy verification, which could have an impact on the number of patients who can be feasibly planned and verified for treatment using IMRT in a given time period. However, the verification times are improving with each patient, indicating an increase in efficiency.

Table 7.1. Comparison of the physics time required to check a regular radiotherapy plan and an IMRT plan.

Dosimetry Process	Regular Plan (hrs)	IMRT Plan (hrs)
dose calculation check	0.25	
ionisation chamber check		0.50
uncalibrated axial film		0.30
uncalibrated planar films		0.50
film developing, analysing etc.		0.75
dosimetry report		0.25
TOTAL	0.25	2.30

As the ICCC is a small clinic with pressing time commitments, it has been decided to allow only two IMRT patients to be on treatment at any one time. As the number of IMRT patients treated at the centre is increased it is anticipated that more advanced plan checking techniques, such as dedicated dose calculation software, will become available.

Table 7.2 gives the results for the regular ionisation chamber measurements of the full deliveries for each IMRT case. Table 7.3 gives the results for the

EDR2 film analysed with ImageJ 12-bit depth measurements of the full deliveries for each IMRT case.

It can be seen that the regular ionisation chamber gave good results for full isocentric dose checks. The exception was for Case 6, which gave a dose difference of -8.1 cGy, or -6.3%. The error may have been due to a misalignment or possibly bed rails interfering with the beam, but the actual cause was not tracked down. Carrying out planar dose measurements on a recalculated plan for Case 6 increased the total plan check time but did provide valuable secondary validation information for this plan, with a final dose difference of 2.0 cGy, or 1.3%.

The film gave less satisfactory results. Cases 1, 2 and 6 gave good results of 0.8%, 1.8% and -0.1% respectively. However, the other cases gave poor results ranging from 5.4% to 8.0%. These results show that EDR2 film can be used as a dosimeter for IMRT checks, but care must be taken when using this method that a backup dosimetry technique is available, and this test remains most useful as an alignment check.

The small ionisation chamber did not show any real advantage over the regular ionisation chamber, and in most cases provided inferior results. Similarly poor results were found for measurements performed with triple the MUs delivered. Hence, there should be no need to perform further trials of these techniques for the types of IMRT treatment currently planned at the ICCC.

Several of the large differences between measured and planned doses may have been due to a steep dose gradient. This was not confirmed in this thesis. But the results led to the position of dose gradients in patient fields versus ionisation chamber position being looked at using beams eye views, and an

extra measurement is now routinely taken in a different position if the original ionisation chamber position is deemed to be in a high dose gradient region.

Table 7.2. All patient dosimetry results, regular ionisation chamber.

Case	Predicted Dose (cGy)	Measured Dose (cGy)	Dose Difference (cGy)	Percentage Difference (%)
Case 1	175.0	174.6	-0.4	-0.3
Case 2	134.5	134.5	0.0	0.0
Case 3	121.1	124.1	3.0	2.4
Case 4	135.2	136.4	1.2	0.9
Case 4 Boost	129.5	130.3	0.8	0.6
Case 5	130.8	130.9	0.1	0.1
Case 6	137.6	129.5	-8.1	-6.3
Case 6 - Beam Down	150.2	152.2	2.0	1.3

Table 7.3. All patient dosimetry results, EDR2 film ImageJ 12-bit depth.

Patient	Predicted Dose (cGy)	Measured Dose (cGy)	Dose Difference (cGy)	Percentage Difference (%)
Case1	175.0	176.5	1.5	0.8
Case2	134.5	136.9	2.4	1.8
Case3	121.1	131.6	10.5	8.0
Case4	135.2	127.4	-7.8	-6.1
Case4Boost	129.5	136.9	7.4	5.4
Case5	130.8	138.9	8.1	5.8
Case6	137.6	137.5	-0.1	-0.1

Based on the ease and speed of set-up and the accuracy of each dosimetry method, as tested on the first IMRT plans, the procedure for checking each IMRT plan currently exists as follows.

When the planning radiotherapist has finished planning the treatment and the doctor has approved it, the plan details are transferred to the linear accelerator verification computer. The desired number of fractions is set to prevent accidentally over-treating a patient, so the radiotherapist adds two or three extra fractions to a different identification file to allow the tests to be carried out. The first fraction is delivered in clinical mode to the calibrated 0.6 cc Farmer-type thimble ionisation chamber at the isocentre and each beam dose is measured. While the larger volume was a disadvantage in spatial resolution the extra sensitivity at low dose levels (of the order of 10 cGy per field) seemed a more important feature.

The second fraction is delivered in clinical mode to EDR2 film placed in the axial orientation parallel to all beam exposures at the isocentre. The film is digitised and coloured to enable evaluation of the axial dose distribution and to check alignment. The third fraction is reserved in case a set of measurements needs to be repeated.

The plan is recalculated for planar measurements, and to avoid confusion this is not added as a treatment fraction, instead the treatment is delivered in service mode (which is a non-treatment mode that doesn't require verification of beam set-ups). Usually just one or two planar XV films are exposed for qualitative visual comparison of one or two Pinnacle-calculated beam dose distributions. Tangboonduangjit *et al*.[116] carried out quantitative dose profile comparisons of the films. It is assumed that if the randomly selected beams have been calculated in the correct orientation and dimensions then so have the rest of the beams. It would be better to compare

each planar dose map from Pinnacle with each planar film but this takes too long to be practical.

If the results of the isocentric ionisation chamber measurements are not satisfactory the measurements may be repeated in the planar orientation to eliminate errors caused by the sharp contours of the phantom or by passing the beam through the couch (for example see '6.9.3 Results - Case 6').

Usually the planning radiotherapist is present for the phantom dosimetry checks, which allows them to check that their plan can be safely delivered. The radiotherapist checks:

- The shape of the MLC for the first segment of each beam using the light field projector and a Pinnacle template.
- That gantry angles won't cause the beam to traverse the couch side rails in the patient set-up.
- That the automatic set-up of the treatment won't cause a collision with the couch or the patient.
- That the set MUs don't cause interlocks, for example that sufficient time has been set.

Any difficulties with delivering the plan can therefore be corrected before the patient is involved.

A form has been developed that provides the ionisation chamber measurements for each beam and for the whole treatment, along with the calculated dose and percentage differences. The form also contains a checklist for confirmation of an accurate axial dose distribution film being collected and, if desired, planar dose distribution films. It is a dynamic document, allowing for additions such as the quantitative planar dose calculations carried out for Case 6. The form is signed by the responsible physicist and verified by a second physicist. The treating oncologist uses the

information provided to make a final decision on whether to proceed with the IMRT treatment. An example of the layout of the dosimetry form for Case 6 is shown in Figure 7.1.

Currently only head and neck patients are treated with IMRT at ICCC. This site was selected because head cast fixation causes minimal movement. There is little doubt head and neck IMRT, particularly with overlapping fields and the sparing of multiple structures, presents the most complex IMRT distributions and more segments (10 to 20) per beam than other sites (6 to 10 for prostate). It is fair to say every new IMRT patient has provided a major challenge to oncologists defining volumes and dose objectives, to radiotherapy planners devising plans to meet these objectives, and to physicists providing dosimetry validation. An IMRT program requires a lot of planning and cooperation and is not to be entered into lightly.

In future the ICCC may or may not extend the program to prostate treatments, which are considered more difficult to target because of tumour-positioning and patient immobilisation considerations. This would also depend on the radiation oncologists, as there are issues with the clinical evidence of dose escalation studies.

As the number of patients treated with IMRT increases time considerations will become a priority. When this happens the current dosimetry process may have to be reviewed, but until then the procedure is considered satisfactory for checking all IMRT patient plans.

IMRT Physics Dosimetry - Summary Sheet

Patient: CASE 6 **Date:**

1. Ion chamber check vs. Pinnacle planning

Beam (no.)		Planned cGy	Measured cGy	cGy diff	% diff
1	B130	10.8	6.3	-4.5	-71.7
2	B104	13.9	14.0	0.1	0.8
3	B78	12.9	13.6	0.7	5.4
4	B52	10.9	11.1	0.2	1.9
5	B26	11.4	11.0	-0.4	-3.8
6	B0	14.1	14.0	-0.1	-0.6
7	B334	13.5	14.2	0.7	5.1
8	B308	10.7	10.8	0.1	1.0
9	B282	14	13.8	-0.2	-1.3
10	B256	14.2	14.6	0.4	3.0
11	B230	11.2	6.1	-5.1	-84.8
total treatment		137.6	129.6	-8.0	-6.2

2. Film axial check vs. Pinnacle planning

Registration (qualitative)	

3. Film planar dose maps vs. Pinnacle planning

Beam (no.)		Registration
1	B130	
2	B104	
3	B78	
4	B52	
5	B26	
6	B0	
7	B334	
8	B308	
9	B282	
10	B256	
11	B230	

Signed physicist:_____

Checked physicist:_____

Figure 7.1. An example of the IMRT Phyics Dosimetry form developed for ICCC.

References

01. *Adenocarcinoma of the Prostate* [Online]. (No date). Available: http://www.virtualcancercentre.com/ [Accessed 2003].
02. Agazaryan N, Solberg TD, DeMarco JJ. Patient specific quality assurance for the delivery of intensity modulated radiotherapy. *J Applied Clinical Med Phys* 2003; **4**: 40-50.
03. Ahnesjo A. Collapsed cone convolution of radiant energy for photon dose calculation in heterogeneous media. *Med Phys* 1989; **16**: 577-592.
04. Attix FH. *Introduction to Radiological Physics and Radiation Dosimetry*. Wiley-Interscience, New York, USA. 1986.
05. Australian Health Technology Advisory Committee. *Beam and isotope radiotherapy*. Australian Government Publishing Service, Australia. 1997.
06. Australian Institute of Health and Welfare. (2001). Cancer in Australia 2000 [Online]. Available: www.aihw.gov.au/publications [Accessed 2004, Apr. 04].
07. Azcona JD, Siochi RAC, Azinovic I. Quality assurance in IMRT: Importance of the transmission through the jaws for an accurate calculation of absolute doses and relative distributions. *Med Phys* 2002; **29**: 269-274.
08. Baird CT, Starkschall G, Liu HH *et al*. Verification of tangential breast treatment dose calculations in a commercial 3D treatment planning system. *J Applied Clinical Med Phys* 2001; **2**: 73-84.
09. *Benefits of SmartBeam IMRT to the Patient* [Online]. (No date). Available: www.varian.com [Accessed 2003].
10. Bortfeld T, Schlegel W. Optimization of beam orientations in radiation therapy: some theoretical considerations. *Phys Med Biol* 1993; **38**: 291-304.
11. Boyer AL, Ochran TG, Nyerick CE *et al*. Clinical dosimetry for implementation of a multileaf collimator. *Med Phys* 1992; **19**: 1255-1261.

12. Boyer A, Xing L, C-M. Ma CM *et al*. Theoretical considerations of monitor unit calculations for intensity modulated beam treatment planning. *Med Phys* 1999; **26**: 187-195.
13. *Breast Cancer* [Online]. (No date). Available: http://cancer.gov/cancerinfo/pdq/treatment/breast/ [Accessed 2003].
14. Budrukkar AN, Hope G, Cramb J *et al*. Dosimetric study of optimal beam number and arrangement for treatment of nasopharyngeal carcinoma with intensity-modulated radiation therapy. *Aust Rad* 2004; **48**: 45-50.
15. Cadman P, Bassalow R, Sidhu NPS *et al*. Dosimetric considerations for validation of a sequential IMRT process with a commercial treatment planning system. *Phys Med Biol* 2002; **47**: 3001-3010.
16. *CancerBACUP: helping people live with cancer* [Online]. (No date). Available: http://www.cancerbacup.org.uk [Accessed 2004, Apr. 14].
17. Carol MP. IMRT: Where We Are Today. In: Sternick, ES (ed). *The Theory & Practice of Intensity Modulated Radiation Therapy*. Advanced Medical Publishing, Wisconsin, USA. 1997; 17-33.
18. Chan J, Russell D, Peters VG, Farrell TJ. Comparison of monitor unit calculations performed with a 3D computerized planning system and independent "hand" calculations: Results of three years clinical experience. *J Applied Clinical Med Phys* 2002; **3**: 293-301.
19. Chapman A, Butson M, Quach K, Rozenfeld A, Metcalfe P. Verification of CT number to density conversion for a simulator-CT attachment. *Aust Phys Eng Sci Med* 2002; **25**: 78-80.
20. Charlan PM, Chetty IJ, Yokoyama S, Fraass BA. Dosimetric comparison of extended dose range film with ionization measurements in water and lung equivalent heterogeneous media exposed to megavoltage photons. *J Applied Clinical Med Phys* 2003; **4**: 25-39.

21. Cheung KY, Choi PHK, Chau RMC *et al*. The roles of multileaf collimators and micro-multileaf collimators in conformal and conventional nasopharyngeal carcinoma radiotherapy treatments. *Med Phys* 1999; **26**: 2077-2085.
22. Childress NL, Dong L, Rosen II. Rapid radiographic film calibration for IMRT verification using automated MLC fields. *Med Phys* 2002; **29**: 2384-2390.
23. Chong LM, Hunt M. Intensity-Modulated Radiation Therapy For Head And Neck Cancer. In: *A Practical Guide To Intensity-Modulated Radiation Therapy*. Medical Physics Publishing, Madison, Wisconsin, USA. 2003: 191-218.
24. Chui CS, Chan MF, Yorke E *et al*. Delivery of intensity-modulated radiation therapy with a conventional multileaf collimator: Comparison of dynamic and segmental methods. *Med Phys* 2001; **28**: 2441-2449.
25. Constantinou C, Attix FH, Paliwal BR. A solid water phantom material for radiotherapy x-ray and 'gamma'-ray beam calibrations. *Med Phys* 1982; **9**: 436-441.
26. Convery DJ, Rosenbloom ME. Treatment delivery accuracy in intensity-modulated conformal radiotherapy. *Phys Med Biol* 1995; **40**: 979-999.
27. Das IJ, Akber SF. Ion recombination and polarity effect of ionization chambers in kilovoltage x-ray exposure measurements. *Med Phys* 1998; **25**: 1751-1757.
28. Deng J, Pawlicki T, Chen Y *et al*. The MLC tongue-and-groove effect on IMRT dose distributions. *Phys Med Biol* 2001; **46**: 1039-1060.
29. Dogan N, Leybovich LB, Sethi A. Comparitive evaluation of Kodak EDR2 and XV2 films for verification of intensity modulated radiation therapy. *Phys Med Biol* 2002; **47**: 4121-4130.

30. Doler W, Rassow S, Jager A, Vosshenrich R. Investigation of the imaging properties of an x-ray film scanner. *Phys Med Biol* 1994; **39**: 917-922.
31. Dunscombe PB, Nieminen JM. On the field-size dependence of relative output from a linear accelerator. *Med Phys* 1992; **19**: 1441-1444.
32. El-Khatib E, Antolak J, Scrimger J. Evaluation of film and thermoluminescent dosimetry of high-energy electron beams in heterogeneous phantoms. *Med Phys* 1992; **19**: 317-323.
33. Ezzell GA, Chungbin S. The overshoot phenomenon in step-and-shoot IMRT delivery. *J Applied Clinical Med Phys* 2001; **2**: 138-148.
34. *Farmer chamber geometry* [Online]. (No date). Available: http://www.additec.de/medtec/PRODUCTS/PHYSICS/EXRADIN.HTM [Accessed 2005].
35. Fiveash JB, Murshed H, Duan J *et al*. Effect of multileaf collimator leaf width on physical dose distributions in the treatment of CNS and head and neck neoplasms with intensity modulated radiation therapy. *Med Phys* 2002; **29**: 1116-1119.
36. Fontenla DP, Napoli JJ, Chui CS. Beam characteristics of a new model of 6-MV linear accelerator. *Med Phys* 1992; **19**: 343-349.
37. Fraass BA. The development of conformal radiation therapy. *Med Phys* 1995; **22**: 1911-1918.
38. Grant WH. Commissioning & Quality Assurance of an IMRT System. In: Sternick, ES (ed). *The Theory & Practice of Intensity Modulated Radiation Therapy*. Advanced Medical Publishing, Wisconsin, USA. 1997; 121-125.
39. Hansen VN, Evans PM, Budgell GJ *et al*. Quality assurance of the dose delivered by small radiation segments. *Phys Med Biol* 1998; **43**: 2665-2675.
40. Hong LX, McCormick B, Chui CS, Hunt MA. IMRT Of Cancer Of The Breast. In: *A Practical Guide To Intensity-Modulated Radiation Therapy*. Medical Physics Publishing, Madison, Wisconsin, USA. 2003: 233-250.

41. Horton JL. *Handbook of Radiation Therapy Physics*. Prentice-Hall, Inc., New Jersey, USA. 1987.
42. Hounsell AR. Monitor chamber backscatter for intensity modulated radiation therapy using multileaf collimators. *Phys Med Biol* 1998; **43**: 445-454
43. Hounsell AR, Wilkinson JM. Head scatter modelling for irregular field shaping and beam intensity modulation. *Phys Med Biol* 1997; **42**: 1737-1749.
44. IAEA Technical Report Series No. 277. *Absorbed Dose Determination in Photon and Electron Beams. An International Code of Practice*. IAEA, Vienna. 1987.
45. IAEA Technical Report Series No. 398. *Absorbed Dose Determination in Photon and Electron Beams An International Code of Practice for Dosimetry based on Standards of Absorbed Dose to Water*. IAEA, Vienna. 2000.
46. ICRU Report 42. *Use of Computers in External Beam Radiotherapy Procedures with High-Energy Photons and Electrons*. Maryland, USA. 1987.
47. ICRU Report 44. *Tissue Substitutes in Radiation Dosimetry and Measurement*. Maryland, USA. 1989.
48. ICRU Report 50. *Prescribing, Recording, and Reporting Photon Beam Therapy*. Maryland, USA. 1993.
49. ICRU Report 62. Prescribing, Recording and Reporting Photon Beam Therapy (Supplement to ICRU Report 50). Maryland, USA. 1993.
50. *Intensity Modulated Radiation Therapy: An Introduction for Patients and Clinicians* [Online]. (No date). Available: http://cancer.med.upenn.edu/treatment/[Accessed 2003].
51. Jeraj R, Keall P. The effect of statistical uncertainty on inverse treatment planning based on Monte Carlo dose calculation. *Phys Med Biol* 2000; **45**: 3601-3613.
52. Jones L, Hoban P. A comparison of physically and radiobiologically based optimization for IMRT. *Med Phys* 2002; **29**: 1447-1455.

53. Ju SG, Ahn YC, Huh SJ, Yeo IJ. Film dosimetry for intensity modulated radiation therapy: Dosimetric evaluation. *Med Phys* 2002; **29**: 351-355.
54. Karzmark CJ, Morton RJ. *A Primer on Theory and Operation of Linear Accelerators in Radiation Therapy*. Medical Physics Publishing, Wisconsin, USA. 1998.
55. Keall P, Wu Q, Wu Y, Kim JO. Dynamic MLC IMRT. In: Palta JR, Mackie TR (ed). *Intensity-Modulated Radiation Therapy: The State of the Art. Medical Physics Publishing*, Wisconsin, USA. 2003; 319-372.
56. Kirsner SM, Prado KL, Tailor RC, Bencomo JA. Verification of the accuracy of 3D calculations of breast dose during tangential irradiation: measurements in a breast phantom. *J Applied Clinical Med Phys* 2001; **2**: 149-156.
57. Laub WU, Wong T. The volume effect of detectors in the dosimetry of small fields used in IMRT. *Med Phys* 2003; **30**: 341-347.
58. Leybovich LB, Sethi A, Dogan N. Comparison of ionization chambers of various volumes for IMRT absolute dose verification. *Med Phys* 2003; **30**: 119-123.
59. Liu HH, Mackie TR, McCullough EC. A dual source photon beam model used in convolution /superposition dose calculations for clinical megavoltage x-ray beams. *Med Phys* 1997; **24**: 1960-1974.
60. Liu S, Lind BK, Brahme A. Two accurate algorithms for calculating the energy fluence profile in inverse radiation therapy planning. *Phys Med* Biol 1993; **38**: 1809-1824.
61. Lof J, Lind BK, Brahme A. An adaptive control algorithm for optimization of intensity modulated radiotherapy considering uncertainties in beam profiles, patient set-up and internal organ motion. *Phys Med Biol* 1998; **43**: 1605-1628.
62. Loi G, Pignoli E, Scorsetti M *et al*. Design and characterization of a dynamic multileaf collimator. *Phys Med Biol* 1998; **43**: 3149-3155.

63. LoSasso TJ. IMRT Delivery System QA. In: Palta JR, Mackie TR (ed). *Intensity-Modulated Radiation Therapy: The State of the Art. Medical Physics Publishing*, Wisconsin, USA. 2003; 561-592.
64. LoSasso T, Chui CS, Ling CC. Comprehensive quality assurance for the delivery of intensity modulated radiotherapy with a multileaf collimator used in the dynamic mode. *Med Phys* 2001; **28**: 2209-2219.
65. Low DA, Harms WB, Mutic S, Purdy JA. A technique for the quantitative evaluation of dose distributions. *Med Phys* 1998; **25**: 656-661.
66. Low DA, Mutic S. Abutment region dosimetry for sequential arc IMRT delivery. *Phys Med Biol* 1997; **42**: 1465-1470.
67. Low DA, Parikh P, Dempsey JF *et al*. Ionization chamber volume averaging effects in dynamic intensity modulated radiation therapy beams. *Med Phys* 2003; **30**: 1706-1711.
68. Ma CM, Ding M, Li JS *et al*. A comparative dosimetric study on tangential photon beams, intensity-modulated radiation therapy (IMRT) and modulated electron radiotherapy (MERT) for breast cancer treatment. *Phys Med Biol* 2003; **48**: 909-924.
69. Ma CM, Nahum AE. Effect of size and composition of the central electrode on the response of cylindrical ionization chambers in high-energy photon and electron beams. *Phys Med Biol* 1993; **38**: 267-290.
70. MacKenzie MA, Lachaine M, Murray B *et al*. Dosimetric verification of inverse planned step and shoot multileaf collimator fields from a commercial treatment planning system. *J Applied Clinical Med Phys* 2002; **3**: 97-109.
71. Mackie R. What Should the Ideal Planning & Delivery System Provide? In: Sternick, ES (ed). *The Theory & Practice of Intensity Modulated Radiation Therapy*. Advanced Medical Publishing, Wisconsin, USA. 1997; 143-144.

72. Mackie TR, Holmes T, Swerdloff S *et al*. Tomotherapy: A new concept for the delivery of dynamic conformal radiotherapy. Med Phys 1993; 20: 1709-1719
73. Mackie TR, Olivera GH, Kapatoes JM *et al*. Helical Tomotherapy. In: Palta JR, Mackie TR (ed). *Intensity-Modulated Radiation Therapy: The State of the Art*. Medical Physics Publishing, WI, USA. 2003; 247-284.
74. Mackie TR, Reckwerdt P, McNutt T *et al*. Photon Beam Dose Computations. In: Mackie TR, Palta JR ed). *Teletherapy: Present and Future*. Advanced Medical Publishing, Wisconsin, USA. 1996; 103-132.
75. Mageras GS, Podmaniczky KC, Mohan R. A model for computer-controlled delivery of 3-D conformal treatments. *Med Phys* 1992; **19**: 945-953.
76. Martini FH, Timmons M. *Human Anatomy*, 2nd edn. Prentice Hall, New Jersey, USA. 1997.
77. *Medical Linacs* [Online]. (No date). Available: http://www.cs.nsw.gov.au/ [Accessed 2003].
78. Mersseman B, Wagter CD. Characteristics of a commercially available film digitizer and their significance for film dosimetry. *Phys Med Biol* 1998; **43**: 1803-1812.
79. Metcalfe P, Chapman A, Arnold A *et al*. Intensity-modulated radiation therapy: Not a dry eye in the house. *Aust Radiol* 2004; **48**: 35-44.
80. Metcalfe P, Kron T, Hoban P. *The Physics of Radiotherapy X-Rays from Linear Accelerators*. Medical Physics Publishing, Wisconsin, USA. 1997.
81. Metcalfe P, Tangboonduangjit P, White P. Intensity-modulated radiation therapy: overlapping co-axial modulated fields. *Phys Med Biol* 2004; **49**: 3629-3637.
82. Millar M, Cramb J, Das R *et al*. APESM Supplement. ACPSEM Position Paper: Recommendations for the Safe Use of External Beams and Sealed Brachytherapy Sources in Radiation Oncology. *APESM* 1997; **20**.

83. Mohan R, Mageras GS, Baldwin B *et al*. Clinically relevant optimization of 3-D conformal treatments. *Med Phys* 1992; **19**: 933-943.
84. Morris S. *Radiotherapy and Physics Equipment*. Harcourt Publishers Limited, London UK. 2001.
85. Moss, WT. The Orbit. In: Cox JD (ed). *Moss' Radiation Oncology: Rationale, Technique, Results*, 7th edn. Mosby Publishers, St Louis, USA. 1994; 246-253.
86. National Council on Radiation Protection and Measurements. *Report 69: Dosimetry of X-Ray and Gamma-Ray Beams for Radiation Therapy in the Energy Range 10 keV to 50 MeV*. NCRP, Washington DC, USA. 1981. -
87. Olch AJ. Dosimetry performance of an enhanced dose range radiographic film for intensity-modulated radiation therapy quality assurance. *Med Phys* 2002; **29**: 2159-2168.
88. Palta JR, Kim S, Li JG, Liu C. Tolerance Limits And Action Levels For Planning And Delivery Of IMRT. In: Palta JR, Mackie TR (ed). *Intensity-Modulated Radiation Therapy: The State of the Art. Medical Physics Publishing*, Wisconsin, USA. 2003; 593-612.
89. Papatheodorou S, Rosenwald JC, Zefkili S *et al*. Dose calculation and verification of intensity modulation generated by dynamic multileaf collimators. *Med Phys* 2000; **27**: 960-971.
90. Partridge M, Ebert M, Hesse BM. IMRT verification by three-dimensional dose reconstruction from portal beam measurements. *Med Phys* 2002; **29**: 1847-1858.
91. Pasma KL, Dirkx MLP, Kroonwijk M *et al*. Dosimetric verification of intensity modulated beams produced with dynamic multileaf collimation using an electronic portal imaging device. *Med Phys* 1999; **26**: 2373-2378.
92. Pignoli E, Serretiello S, Somigliana A *et al*. Dosimetric verification of a commercial 3D treatment planning system for conformal radiotherapy

with a dynamic multileaf collimator. Phys Med Biol 2000; 45: N77-N84.

93. Ploeger LS, Smitsmans MHP, Gihuijs KGA, van Herk M. A method for geometrical verification of dynamic intensity modulated radiotherapy using a scanning electronic portal imaging device. *Med Phys* 2002; **29**: 1071-1079.
94. Podgorsak EB, Podgorsak MB. Special Procedures and Techniques in Radiotherapy. In: Podgorsak EB (ed). *Review of Radiation Oncology Physics: A Handbook for Teachers and Students*. International Atomic Energy Agency, Vienna, Austria. 2003: 413-446.
95. Porceddu S, Hope G, Wills J *et al*. Intensity-modulated radiotherapy: Examples of its utility in head and neck cancer. *Aust Rad* 2004; **48**: 51-57.
96. *Prodigy: Providing access to clinical knowledge about the common conditions and symptoms managed in primary care* [Online]. (No date). Available: http://www.prodigy.nhs.uk [Accessed 2004, Apr. 15].
97. *Prostate Cancer* [Online]. (No date). Available: http://cancer.gov/cancerinfo/pdq/treatment/prostate/ [Accessed 2003].
98. *Prostate Cancer: The Basics* [Online]. (No date). Available: http://cancer.med.upenn.edu/types/[Accessed 2003].
99. Purdy JA. The Development of Intensity Modulated Radiation Therapy. In: Sternick, ES (ed). *The Theory & Practice of Intensity Modulated Radiation Therapy*. Advanced Medical Publishing, Wisconsin, USA. 1997; 1-9.
100. Ramsey C, Dube S, Hendee WR. Point/Counterpoint: It is necessary to validate each individual IMRT treatment plan before delivery. Med Phys 2003; 30: 2271-2273.
101. Ramsey ML. (2004). *Basal Cell Carcinoma* [Online]. Available: http://www.emedicine.com/derm/topic47.htm [Accessed 2004, Dec 26].

102. Selman J. *The Basic Physics of Radiation Therapy*, 3rd edn. Charles C Thomas, Illinois, USA. 1990.

103. Sharpe MB, Miller BM, Yan D, Wong JW. Monitor unit settings for intensity modulated beams delivered using a step-and-shoot approach. *Med Phys* 2000; **27**: 2719-2725.

104. Sherwood L. *Human Physiology: From Cells to Systems*, 3rd edn. Wadsworth Publishing Company, California, USA. 1997.

105. *SmartBeam IMRT* [Online]. (No date). Available: www.varian.com [Available 2005].

106. Sodertrom S, Brahme A. Optimization of the dose delivery in a few field techniques using radiobiological objective functions. *Med Phys* 1993; **20**: 1201-1210.

107. Sontag MR, Cunningham JR. Clinical Application of a CT based treatment planning system. *Computerized Tomography* 1978; **2**: 117-130.

108. Starkschall G, Eifel PJ. An interactive beam-weight optimization tool for three-dimensional radiotherapy treatment planning. *Med Phys* 1992; **19**: 155-163.

109. Stern RL, Fraass BA, Gerhardsoon A *et al*. Generation and use of measurement-based 3-D dose distributions for 3-D dose calculation verification. *Med Phys* 1992; **19**: 165-173.

110. Suchoweska N, Davison A, Drew J, Metcalfe P. The Validity of Using Radiographic Film for Radiation Dosimetry. *Aust Phys Eng Sc Med* 1997; **20**: 20-26.

111. Suchowerska N, Hoban P, Davison A, Metcalfe P. Perturbation of radiotherapy beams by radiographic film: measurements and Monte Carlo simulations. *Phys Med Biol* 1999; **44**: 1755-1765.

112. Sultanem K, Shu H-K, Xia P *et al*. Three-dimensional intensity-modulated radiotherapy in the treatment of nasopharyngeal carcinoma: the University of California-San Francisco experience. *Int J Rad Onc Bio Phys* 2000; **48**: 711-722.

113. Symonds-Tayler JRN, Webb S. Gap-stepped MLC leaves with filler blades can eliminate tongue-and-groove underdoses when delivering IMRT with maximum efficiency. *Phys Med Biol* 1998; **43**: 2393-2395.

114. Tailor RC, Chu C, Followill DS, Hanson WF. Equilibration of air temperature inside the thimble of a Farmer-type ion chamber. *Med Phys* 1998; **25**: 496-502.

115. Tangboonduangjit P, Metcalfe P, Butson M *et al*. Matchline dosimetry in step and shoot IMRT fields: a film study. *Phys Med Biol* 2004; **49**: N287-N292.

116. Tangboonduangjit P, Wu I, Butson M *et al*. Intensity modulated radiation therapy: Film verification of planar dose maps. *Aust Phys Eng Sci Med* 2003; **26**: 194-199.

117. Task Group 50. *AAPM Report No. 72: Basic Applications of Multileaf Collimators*. Medical Physics Publishing, Madison, USA. 2001.

118. Turner AP, Wizenberg MJ. Resource Planning for IMRT. In: Sternick, ES (ed). *The Theory & Practice of Intensity Modulated Radiation Therapy*. Advanced Medical Publishing, Wisconsin, USA. 1997; 229-242.

119. van Dalen S, Keijzer M, Huizenga H, Storchi PRM. Optimization of multileaf collimator settings for radiotherapy treatment planning. *Phys Med Biol* 2000; **45**: 3615-3625.

120. van Santvoort JPC, Heijmen BJM. Dynamic multileaf collimation without 'tongue-and-groove' underdosage effects. *Phys Med Biol* 1996; **41**: 2091-2105.

121. Verhaegen F, Symonds-Tayler R, Liu HH, Nahum AE. Backscatter towards the monitor ion chamber in high-energy photon and electron beams: charge integration versus Monte Carlo simulation. *Phys Med Biol* 2000; **45**: 3159-3170.

122. Vidar Systems Corporation. *VIDAR VXR-12 plus Film Digitizer user's manual*. Virginia, USA, 2002.

123. Vieira SC, Dirkx MLP, Pasma KL, Heijmen BJM. Fast and accurate leaf verification for dynamic multileaf collimation using an electronic portal imaging device. *Med Phys* 2002; **29**: 2034-2040.

124. Wang X, Spirou S, LoSasso T *et al*. Dosimetric verification of intensity-modulated fields. *Med Phys* 1996; **23**: 317-327.

125. Webb S. The effect on tumour control probability of varying the setting of a multileaf collimator with respect to the planning target volume. *Phys Med Biol* 1993; **38**: 1923-1935.

126. Webb S. *Intensity-Modulated Radiation Therapy*. Institute of Physics Publishing, Bristol, UK. 2002.

127. Webb S. Optimizing the planning of intensity-modulated radiotherapy. *Phys Med Biol* 1994; **39**: 2229-2244.

128. Webb S. The physical basis of IMRT and inverse planning. *Brit J Radiol* 2003; **76**: 678-689.

129. Webb S. *The Physics of Three-Dimensional Radiation Therapy - Conformal Radiotherapy, Radiosurgery and Treatment Planning*. IOP Publishing Ltd, Bristol, UK. 1993.

130. Webb S, Convery DJ, Evans PM. Inverse planning with constraints to generate smoothed intensity-modulated beams. *Phys Med Biol* 1998; **43**: 2785-2805.

131. *What are the side effects of radiation therapy?* [Online]. (No date). Available: http://cancer.med.upenn.edu/treatment/ [Accessed 2003].

132. White DR. Tissue substitutes in experimental radiation physics. *Med Phys* 1978; **5**: 467-479.

133. White DR, Martin RJ, Darlison R. Epoxy resin based tissue substances. *British J Radiology* 1977; **50**: 814-821.

134. Williams MJ, Metcalfe P. Verification of a rounded leaf-end MLC model used in a radiotherapy treatment planning system. *Phys Med Biol* 2006; **51**: N65-N78.

135. Woodard HQ, White DR. The composition of body tissues. *British J Radiology* 1986; **59**: 1209-1219.

136. Wu Q, Arnfield A, Tong S *et al*. Dynamic splitting of large intensity-modulated fields. *Phys Med Biol* 2000; **45**: 1731-1740.

137. Xu T, Shikhaliev PM, Al-Ghazi M, Molloi S. Reshapable physical modulator for intensity modulated radiation therapy. *Med Phys* 2002; **29**: 2222-2229.

138. Yeo IJ, Wang CKC, Burch SE. A new approach to film dosimetry for high-energy photon beams using organic plastic scintillators. *Phys Med Biol* 1999; **44**: 3055-3069.

139. Yu CX. Intensity-modulated arc therapy with dynamic multileaf collimation: an alternative to tomotherapy. *Phys Med Biol* 1995; **40**: 1435-3069.

140. Yu CX, Jaffray DA, Wong JW. The effects of intra-fraction organ motion on the delivery of dynamic intensity modulation. *Phys Med Biol* 1998; **43**: 91-104.

141. Yu CX, Symons MJ, Du MN *et al*. A method for implementing dynamic photon beam intensity modulation using independent jaws and a multileaf collimator. *Phys Med Biol* 1995; **40**: 769-787.

142. Yu CX, Yan D, Du MN, Verhey SZLJ. Optmization of leaf positions when shaping a radiation field with a multileaf collimator. *Phys Med Biol* 1995; **40**: 305-308.

143. Yuen K, Al-Ghazi MSAL, Swift CL, White CA. A practical method for the calculation of multileaf collimator shaped fields output factors. *Med Phys* 1999; **26**: 2385-2389.

144. Zacarias AS, Lane RG, Rosen II. Assessment of a linear accelerator for segmented conformal radiation therapy. *Med Phys* 1993; **20**: 193-198.

145. Zhu XR, Jursinic PA, Grimm DF *et al*. Evaluation of Kodak EDR2 film for dose verification of intensity modulated radiation therapy delivered by a static multileaf collimator. Med Phys 2002; 29: 1687-1692.